Higher Twist Contributions to Charm and Light Gluino Production

BY

Thomas Dominic Gutierrez

B.S. (San Jose State University, San Jose) 1991

M.S. (San Jose State University, San Jose) 1994

DISSERTATION

Submitted in partial satisfaction of the requirements for the degree of

DOCTOR OF PHILOSOPHY

in

Physics

in the

OFFICE OF GRADUATE STUDIES

of the

UNIVERSITY OF CALIFORNIA

DAVIS

Approved:

_____

_____

_____

Committee in Charge

2000

Acknowledgments

I would like to thank my father for inspiring me throughout my life. This world was prematurely robbed of a genius. Live in the Moment; live in the Possibility; live in the Opportunity; live in the Question. I miss you, dad.

A deep and warm thanks to my mother, Arlene, my brothers, Vince and Leo, our dearest friend Joe, the Liccardos, and the love of my life, Jennifer, for supporting me over the years. I could not have finished without their ever present loving guidance and moral support.

I would like to thank my advisor, Ramona Vogt, for taking me under her wing, putting up with me, and pushing me to be my very best through all trials and tribulations. Many thanks go to Dan Cebra who always had the right inspiring words to rejuvenate me and who brought me into the fold, making me feel like part of the team.

Special acknowledgments go to Jack Gunion, the Nuclear Group at UCD, Joe Kiskis, Scott Johnson, Shannon Gomes, Bobby Lau, Tom Corboline, Joe Becker, Todd Sauke, and the untold numbers of friends, family, and colleagues at UCD, SJSU, and elsewhere who have intellectually and emotionally inspired me through vigorous discussions of physics and philosophy. Finally, a very special thanks goes to my extended family the Miliotos, the Klays, the Roesslers, and the Knorrs for being a part of my life and accepting me and my family as their own.

Illud Cetus Advenit.

Thomas Dominic Gutierrez
June 2000
Physics

Higher Twist Contributions to Charm and Light Gluino Production

Abstract

Two separate studies of particle production at higher twist are presented. Both studies are based upon a model developed to describe anomalous production of charm quarks. In this model, heavy quark states can briefly exist in the hadron wavefunction, leading to enhanced forward, or large x_F, production of charm. Although this model, known as the intrinsic charm model, was first applied to charm production, it can be applied quite generally to any strongly-interacting heavy particle in a QCD state. The first topic studied is the forward production of charm and charm-strange hadrons by pion, proton, and hyperon beams. The original intrinsic charm model is refined and expanded in this work and compared to recent data with hyperon beams on nuclear targets. The second topic is more speculative. If the mass of the gluino, the supersymmetric partner of the gluon, is light, of the same order as a charm or bottom quark mass, then the proposed R-hadrons may exhibit some of the same production characteristics as large x_F charm hadrons. R-hadron production is studied in an intrinsic gluino framework and the effects at large x_F are shown to be significant.

Contents

List of Figures

List of Tables

Chapter 1

Introduction

1.1 Overview

Quantum field theory has been very successful in describing scattering problems involving point particles. However, if scattering occurs between systems with complex structure, such as atoms, nuclei, or hadrons, the scattering formalism becomes richer and more intricate.

Quantum electrodynamics, QED, is the quantum theory describing the interactions between electromagnetically charged objects, such as electrons, and photons. In QED, constituents of the bound state and the bound states themselves can be studied separately. However, one does not have such a luxury when studying the structure of hadrons since the bound states interact via the strong force. These states are governed by quantum chromodynamics, QCD.

The QED Lagrangian is invariant under an Abelian U(1) local gauge transformation and thus has only one type of charge – the electric charge. With this gauge symmetry, the photons themselves are neutral. In addition, the coupling constant in QED is known to be intrinsically small, making weak coupling approximations very useful. Electric charge screening around a charge in vacuum conspires to very weakly increase the strength of the interactions at short distances. Moreover, electrically charged objects are routinely observed; they are not confined to bound states.

In contrast, QCD is a non-Abelian SU(3) gauge theory. The symmetries of the QCD Lagrangian under local SU(3) gauge transformations are more complicated than those in QED. The fundamental fermions for QCD are quarks. The quarks come in three color charges called red, green, and blue, implying an SU(3) gauge structure. By

demanding local SU(3) gauge invariance, the introduction of eight colored massless gauge boson fields, called gluons, is required. Unlike the photons of QED, these gluons carry the charge of the interaction. This makes the effective range of the force short, $\sim$ 1 fm, because the gluons can couple to each other. Also, aside from the gauge structure of QCD, the strength of the force is intrinsically very strong. This makes weak coupling approximations untenable except by exploiting asymptotic freedom, discussed below.

Both the strength of the coupling and the SU(3) gauge structure contribute to two of the most interesting properties of QCD: asymptotic freedom and confinement. Asymptotic freedom is a direct consequence of the non-Abelian gauge structure. The coupling constant, α_s, weakens as the distance between colored objects becomes small or if the momentum scale is large. A one loop QCD calculation gives [1]

$$\alpha_s(Q^2) = \frac{12\pi}{(33 - 2n_f)\ln(Q^2/\Lambda^2_{\rm QCD})} \tag{1.1}$$

where Q^2 is the momentum scale and n_f is the the number of quark flavors. What defines small may depend on the exact problem, but a rough lower limit is set by the momentum scale $\Lambda_{\rm QCD} \sim 200$ MeV, approximately the inverse size of a typical hadron, ~ 1 fm^{-1}.

In addition, all known particles composed of quarks and gluons appear macroscopically as color neutral hadrons. No free colored objects have been observed in the laboratory. This nonintuitive property of QCD is known as confinement: quarks and gluons are forever doomed to reside in color singlet bound states. Although not proven conclusively, there is considerable theoretical evidence that the confinement of

colored objects is a fundamental property of QCD. No free colored objects are then expected to be observed. For example, free quarks, which have fractional electromagnetic charge, have not been seen. Asymptotic freedom and confinement in QCD are opposite to the corresponding behavior found in QED.

1.2 Parton Model

Because of confinement, typical scattering in QCD will always involve complicated bound states. Therefore, to perform scattering calculations in QCD one must ultimately find a way to treat such states in a straightforward manner. For this reason, the parton model was developed. The parton model [1, 2] provides a simple picture of QCD bound states for the purpose of modeling scattering processes.

The QCD bound state is made up of a variety of objects called partons which are essentially quarks, antiquarks, and gluons. A distinction is made between the primary constituents, the valence quarks, and the short-lived fluctuations, the sea. For example, although the proton (uud) is primarily composed of up quarks and down quarks, bound together by the exchange of gluons, there is also a sizable population of anti-up, anti-down, strange, and anti-strange quarks residing in the proton's sea. The light quark contribution to the sea must be extracted experimentally, usually from deep inelastic scattering, described below.

However, there is considerable evidence that heavy quarks, such as charm and bottom, are also present in the hadronic sea – albeit at a very low level. This is a very intriguing possibility. The heavy quark pair has a mass considerably larger than

the proton itself, yet it may be present in the bound state as a virtual fluctuation. In principle, any allowed fluctuation is present. For example, exotica, such as supersymmetric particles like the gluino, can be considered. Unlike light quarks, contributions from heavy particles to the hadronic sea may be calculated. These heavy fluctuations have considerable phenomenological impact, to be discussed below.

When the system is viewed in the infinite momentum frame [1, 3], IMF, each parton is assumed massless and carries some fraction of the original hadron momentum. In the IMF frame, the hadron is boosted to a highly relativistic frame. The direction and size of the boost are usually chosen so that the momentum transfer from the virtual particle becomes transverse to the axis of motion. Because of this choice and because of length contraction along the boost direction, the problem reduces to a two dimensional one in the transverse direction. In our frame of observation, the bound state has been compressed so that the only important scales are transverse to the direction of motion.

More importantly, in our frame, because of time dilation, the timescales over which the interaction takes place between the sufficiently virtual probe ($Q^2 > k_\perp^2$) and projectile become short compared to the timescales over which the constituents of the bound state, the partons, interact with each other. This insures that the probe interacts incoherently with only a single parton. Also in our frame, there are a well defined number of partons at the moment of interaction. In contrast, if the timescales are comparable, then interactions between partons in the bound state will cause fluctuations in the number of partons over the timescale of the external interaction. In this case, the external interaction might coherently probe several

partons at once, greatly complicating the calculation.

Now, with a well defined number of partons in the bound state over the timescale of an interaction and with the ability to incoherently probe a single parton during the interaction, universal properties of the hadron itself can be studied. Although properties of the hadron are frame independent, the parton model in the infinite momentum frame provides a particularly convenient physical picture. Important properties include sea and valence quark momentum distributions. These distributions are intrinsic to the hadron and can be carried over to other calculations.

To calculate important physical quantities such as the cross section in a scattering process, an expression for the scattering matrix is required. In quantum field theory, using Feynman diagrams, quantum mechanical amplitudes are expressed as perturbative expansions in powers of the coupling constant. These perturbative tools have proven to be remarkably successful in the absence of analytical solutions for problems of interest in QED. QED is ideally suited for such a perturbative expansion because the coupling constant is quite small, ensuring accurate results with only a few terms.

Originally, it was natural to hope that perturbation theory could be universally applied to problems of interest in QCD. However, because of confinement, the QCD coupling constant is greater than one once the distance scale is larger than ~ 1 fm, the size of a typical hadron. Perturbative scattering in QCD must be approached carefully. Perturbation theory in QCD becomes a useful calculational tool only when the coupling constant is small.

QCD is then divided into two domains: perturbative and nonperturbative QCD. Nonperturbative QCD must be used when when the coupling constant is large for

a given problem. These processes often must be modeled nonrigorously, but there are exceptions. The most successful rigorous nonperturbative method is lattice QCD [4] which utilizes the path integral approach to quantum field theory. The technique does not typically use perturbative approximations in the coupling constant – although there are other kinds of approximations made. Lattice calculations have made great progress towards understanding the fundamental structure of quantum field theory. These calculations have also made numerical improvements in calculating quark and hadron masses as well as modeling finite temperature effects in quantum field theory. However, lattice techniques are notoriously computer intensive and are currently unable to to perform important phenomenological calculations of dynamic scattering problems.

Perturbative QCD, pQCD, has been successfully applied to a number of physical processes including electron-positron annihilation, quark leptoproduction, and large transverse momentum jets. However, two particular applications of pQCD are of interest here. Deep inelastic scattering, DIS, resolves the detailed structure of hadrons when high energy leptons emit virtual particles with a large momentum transfer. The momentum transfer from the lepton probe sets the scale for the perturbative expansion. When pQCD is applied to highly relativistic collisions between hadrons, producing particles with a large invariant mass, the invariant mass sets the scale.

In each case, the calculations become more reliable as the momentum scale – momentum transfer or invariant mass – grows larger. This occurs for two reasons. First, the coupling constant in QCD decreases as the momentum scale increases due to asymptotic freedom: the perturbative expansion in powers of the coupling constant

will converge more quickly. Also, a large momentum scale will promote only single particle scattering in the bound state. For example, if the momentum transfer is too small in DIS, the wavelength of the virtual particle is long, permitting coherent scattering off several constituents of the bound state.

1.2.1 Deep Inelastic Scattering

Deep inelastic scattering of leptons on hadronic targets provides a clean view of hadron structure. The large momentum transfer of the probe can produce virtual particles of small wavelengths which can then resolve individual components of the hadron structure. By analyzing scattering data over various kinematic variables, detailed information about the hadron target can be inferred.

In inelastic electron-proton scattering, using the notation of Ref. [1], the cross section is proportional to the contraction of the lepton tensor, $L^e_{\mu\nu}$, with the hadron tensor, $W^{\mu\nu}$,

$$d\sigma \sim L^e_{\mu\nu} W^{\mu\nu} \tag{1.2}$$

where the leptonic tensor is

$$L^e_{\mu\nu} = \frac{1}{2} \sum_{\text{spins}} [\bar{u}(k_{\text{out}})\gamma_\mu u(k_{\text{in}})][\bar{u}(k_{\text{out}})\gamma_\nu u(k_{\text{in}})]^*. \tag{1.3}$$

and $\overline{u}(k_{\text{out}})$ and $u(k_{\text{in}})$ represent the outgoing and incoming Dirac spinors with corresponding momentum k_{out} and k_{in}. The general symmetric form of the hadronic tensor is

$$W^{\mu\nu} = -W_1 g^{\mu\nu} + \frac{W_2}{M^2} p^\mu p^\nu + \frac{W_4}{M^2} q^\mu q^\nu + \frac{W_5}{M^2}(p^\mu q^\nu + q^\mu p^\nu) \tag{1.4}$$

where M is the mass of the proton. The term W_3 has been omitted because it is reserved for the parity violating portion of the structure function of the proton. The W_3 term is probed with neutrino beams rather than electron beams and is needed for a complete global analysis of the hadron structure. Using Ward identities to write W_5 and W_4 in terms of W_1 and W_2, the expression simplifies to

$$W^{\mu\nu} = W_1(-g^{\mu\nu} + \frac{q^\mu q^\nu}{q^2}) + \frac{W_2}{M^2}(p^\mu - \frac{p.q}{q^2}q^\mu)(p^\nu - \frac{p.q}{q^2}q^\nu). \tag{1.5}$$

The structure functions W_1 and W_2 depend on two independent variables: the four-momentum transfer between the electron and proton, $Q^2 = -q^2$, and the energy transfer in the target rest frame, $\nu = (p \cdot q)/M$. Neglecting the mass of the electron, the cross section can be written

$$\frac{d\sigma_{\rm lab}}{dE'd\Omega} = \frac{\alpha^2}{4E^2\sin^4(\theta/2)}[W_2(\nu, Q^2)\cos^2(\theta/2) + 2\mathrm{W}_1(\nu, \mathrm{Q}^2)\sin^2(\theta/2)] \tag{1.6}$$

where now W_1 and W_2 can be extracted experimentally by measuring the energy of the outgoing electron and its angle.

If the virtual photon is scattering off a point particle of unit charge in the proton, e.g. a parton of mass m, then W_1 and W_2 will take the form

$$2mW_1^{\rm point}(\nu, Q^2) = \frac{Q^2}{2m\nu}\delta(1 - \frac{Q^2}{2m\nu}) \tag{1.7}$$

$$\nu W_2^{\rm point}(\nu, Q^2) = \delta(1 - \frac{Q^2}{2m\nu}). \tag{1.8}$$

If, in the limit of large Q^2, W_1 and W_2 approach their elastic point-scattering limits and become a function of one variable, $\omega = 2M\nu/Q^2$, this is a signal that the virtual photon is probing an electrically charged pointlike constituent of the proton.

The proton structure functions F_1 and F_2, in the pointlike limit of large Q^2, are defined in terms of W_1^{point} and W_2^{point}

$$MW_1^{\text{point}}(\nu, Q^2) \to F_1(\omega) \tag{1.9}$$

$$\nu W_2^{\text{point}}(\nu, Q^2) \to F_2(\omega). \tag{1.10}$$

The kinematics of the parton model define the four-momentum of the struck parton as xP where P is the four-momentum of the proton and x is the momentum fraction carried by that parton. This implies $m = xM$, so the massless limit is taken assuming P is large. In this limit, substituting $m = xM$ into Eqs. (1.7) and (1.8), F_1 and F_2 become

$$F_1(\omega) = \frac{1}{2x^2\omega}\delta(1 - \frac{1}{x\omega}) \tag{1.11}$$

$$F_2(\omega) = \delta(1 - \frac{1}{x\omega}). \tag{1.12}$$

Eqs. (1.11) and (1.12) describe the proton structure functions for an electron scattering off of one parton carrying an exact momentum fraction x. If the i^{th} parton has a probability $f_i(x)$ of having momentum fraction x, the above expressions can be generalized by integrating over all momentum fractions and summing over all partons weighted by their respective distributions,

$$F_2(\omega) = \sum_i \int e_i^2 f_i(x) x\delta(1 - \frac{1}{x\omega}) \tag{1.13}$$

$$F_1(\omega) = \frac{\omega}{2}F_2(\omega). \tag{1.14}$$

This gives

$$F_2(x) = \sum_i e_i^2 x f_i(x) \tag{1.15}$$

$$F_1(x) = \frac{1}{2x} F_2 \tag{1.16}$$

where e_i is the fractional electric charge of the i^{th} parton and

$$x = \frac{1}{\omega} = \frac{Q^2}{2M\nu}. \tag{1.17}$$

The kinematics of the probe, Q^2 and ν, are directly related to the momentum fraction of the parton, x. The property that F_1 and F_2 only depend on x and not Q^2 is called Bjorken scaling. Although the above approach agrees with the data for $\omega \sim 4$, scaling violations were found experimentally when $\omega \neq 4$. These are explained by higher order corrections to the above treatment, where, for example, single partons radiate gluons. Gluon radiation drives the evolution of the parton distribution functions from one momentum scale to another. If the parton distributions are known at some low momentum scale, Q_0, they can be determined at higher scales through the coupled quark and gluon evolution equations, the Altarelli-Parisi (DGLAP) equations [1]

$$\frac{d}{d\ln Q^2} f_i(x, Q^2) = \frac{\alpha_s}{2\pi} \int_x^1 \frac{dy}{y} (f_i(y, Q^2) P_{qq}(\frac{x}{y}) + g(y, Q^2) P_{qg}(\frac{x}{y})) \tag{1.18}$$

$$\frac{d}{d\ln Q^2} g(x, Q^2) = \frac{\alpha_s}{2\pi} \int_x^1 \frac{dy}{y} (\sum_i f_i(y, Q^2) P_{gq}(\frac{x}{y}) + g(y, Q^2) P_{gg}(\frac{x}{y})) \tag{1.19}$$

where $f_i(x, Q^2)$ and $g(x, Q^2)$ are the parton distribution functions for quarks of flavor i and gluons respectively. The functions $P_{qq}(x/y)$, $P_{qg}(x/y)$, $P_{gq}(x/y)$, and $P_{gg}(x/y)$ are splitting functions which give the probability that a parton shifts from momentum fraction y to x by radiating a gluon with $y > x$.

The proton, although dominated by the uud valence quark configuration at high x, has fluctuations of $q\bar{q}$ pairs, the sea quarks, as well as gluons in its bound state. In fact, as mentioned previously, all possible fluctuations not expressly forbidden should be present to some degree. This includes heavy quarks, weak vector bosons, SUSY particles, and other exotica. In a QCD bound state, because of the strong coupling constant, sea fluctuations participating in the strong interaction can play a prominent role in bound state dynamics. QED bound states also have fluctuations of this kind, but they are less probable because of the small coupling constant. They tend to play only a small role in the bound state dynamics, but can contribute measurably to the energy spectrum of bound states as in the case of the celebrated Lamb shift in hydrogen.

The essence of the parton model in DIS is that a lepton scattering off a complex hadronic bound state can be reduced to point interactions in the large Q^2 limit. Further analysis demonstrates that the bound state can be understood through the structure functions which in turn are related to the parton distributions of the constituents. In the case above, electromagnetic properties of the proton can be fully characterized by the structure functions $F_1(x)$ and $F_2(x)$. These are ultimately related to the parton distribution functions, $f_i(x)$, through Eq. (1.15). Once measured, these distributions should be characteristic to the proton and usable in other calculations, such as hadron-hadron interactions, after evolution to the appropriate momentum scale as in Eqs. (1.18) and (1.19).

1.2.2 Hadron-Hadron Interactions

Treating hadron-hadron interactions presents a unique set of complications. In this case, two bound states of partons are colliding. If a calculation is to be accurate, this will necessarily involve both long scales, the partons in the confined QCD bound state, and short scales, the partons participating in hard interactions sufficient to produce a large invariant mass.

The cross section for a hadron-hadron process, $A+B \to Q+\bar{Q}$, producing a heavy quark pair is given by [5]

$$\sigma = \sum_{i,j} \int dx_1 dx_2 f_{i/A}(x_1, \mu_F^2) f_{j/B}(x_2, \mu_F^2) \hat{\sigma}_{ij}. \tag{1.20}$$

This form for the cross section is known as leading twist. The parton distribution functions for projectile and target, $f_{i/A}$ and $f_{j/B}$, are typically evaluated at the factorization scale $\mu_F = M$ where M is the invariant mass of the heavy quark pair. As discussed in the previous section, the parton distributions are related to the structure function F_2 through Eq. (1.15) and represent the probability of finding a particular parton with longitudinal momentum fraction x in the bound states of the initial hadrons. The parton level cross section $\hat{\sigma}_{ij}$ is related to the matrix elements of the particular subprocess contributing to the final state. It is evaluated at the renormalization scale μ_R, typically set equal to μ_F. The sum convolutes the parton densities with the short distance cross section for each participating parton pair from the projectile, i, and target, j.

The applicability of pQCD here depends on having a small coupling constant at the momentum scale set by the invariant mass of the produced particle. This will insure a

reliable perturbative expansion. However, the reliability of this method also depends on the ability to factorize the contributions of each scale in the calculation. The contributions from long and short scales must be independent; if they are entangled, the utility of this method may break down. This independence insures that only single partons are interacting from target and projectile – each is playing a well-defined role in its respective bound state but interacting as essentially free point-particles with the other. The ability to factorize each contribution depends on the hard scale involved. At softer scales, the long and short distance behaviors may mix. This indicates that multi-parton processes will begin to contribute in an essentially nonperturbative way, rendering Eq. (1.20) unreliable. If the cross section is dominated by parton-parton level processes and the long and short scales factorize, the leading twist cross section, Eq. (1.20), is reliable.

1.3 Anomalous Charm Production

In principle, heavy quark hadroproduction is ideally suited for pQCD applications as described in Eq. (1.20). The large mass sets a scale where $\alpha_s(M^2)$ is both less than one and sufficiently small for the perturbative expansion to converge with just a few terms. Also, a large mass reliably separates long and short distance contributions between the parton distribution functions and the matrix elements. These parton distribution functions can be extracted from experimental data, such as in DIS, described above.

Amongst the three heavy quarks – top, bottom, and charm – the charm quark

finds itself in a special position. At $m_c \sim 1.5$ GeV, it is light enough so that charm is produced and measured fairly easily. However, charm is heavy enough so that, using the one loop form for α_s given by Eq. (1.1), $\alpha_s \sim 0.24$. This is obtained using $n_f = 4$ with $Q = 3.0$ GeV, the charm pair mass scale. This value of α_s is small enough so that a perturbative expansion can be done with some confidence, but large enough so that nonperturbative effects can contribute nontrivially. In contrast, for the strange quark, the heaviest of the light quarks with $m_s \sim \Lambda_{\rm QCD}$, α_s becomes very large at the strange pair mass scale. This renders the use of Eq. (1.20) unworkable for strangeness production. Although $\alpha_s \sim 0.18$ at the bottom pair mass scale, with $Q \sim 2m_b \sim 9$ GeV and $n_f = 5$, and $\alpha_s \sim 0.09$ at the top pair mass scale, with $Q \sim 2m_t \sim 350$ GeV and $n_f = 6$, these particles are considerably less abundant than charm. All of these values of α_s should be compared to the small QED coupling constant $\alpha = 1/137 \sim 0.007$. With the above values of α_s, pQCD, as applied to quark hadroproduction, will never attain the same accuracy as QED.

Because the charm quark is easy to produce and its mass straddles the domain between hard and soft scales in QCD, charm hadroproduction offers a unique window into the transition between pQCD and nonperturbative QCD. The difference between charm production calculations and the experimental data gives a strong measure of nonperturbative contributions to hadroproduction. By studying the exact nature of anomalies observed in charm production, a more complete view of soft production processes emerges.

Many experiments have measured unexpected effects in charm production. For example, the types of anomalies observed include large J/ψ and J/ψ pair cross sec-

tions as $x_F \to 1$, leading particle effects, and nonlinear cross section dependence on the atomic number of the target, $A(x_F)$. Table 1.1 lists various experiments and the effects they observed. The list is not exhaustive, but gives strong support for the breakdown of leading twist pQCD.

Experiment	Energy	Process	Effect
NA3 [6, 7, 8]	150 GeV 280 GeV 400 GeV	$\pi^- A \to J/\psi J/\psi$ $\pi^- A \to J/\psi J/\psi$ $pA \to J/\psi J/\psi$	Anomalously high double J/ψ production at large x_F and $A(x_F)$ dependence
EMC [9]	280 GeV	$\mu\text{Fe} \to cX$	Anomalously large $c(x)$ at large x_{Bj}
E537 [10]	125 GeV	$\pi A \to J/\psi X$	Polarization flip of J/ψ at large x_F
WA82 [11]	340 GeV	$\pi^- A \to D^\pm X$	Leading/Nonleading $D^\pm$ asymmetry
E769 [12]	250 GeV	$\pi^\pm A \to D^\pm X$	
WA89 [13, 14]	330 GeV	$\Sigma^- A \to H_{cs} X$	Leading strange-charm hadrons and associated asymmetries
SELEX [15]	650 GeV	$\Sigma^- A$ and $\pi^- A$	

Table 1.1: Experimental evidence for anomalous charm production

As discussed above, although some nonperturbative contributions to charm production may be expected, their character cannot be easily be anticipated without guidance from experimental data. As illustrated in Table 1.1, anomalous charm pro-

duction is often seen at large x_F, where x_F is the longitudinal fraction of the available momentum carried by the final state hadron, $x_F = 2P_L/\sqrt{s}$. The deviation of experiments from pQCD calculations often grows as $x_F \to 1$. The reasons for anomalous production at large x_F are subtle and are discussed below.

Two important charm puzzles central to this work are the leading charm effect and the dependence of the cross section on the atomic number of the target as a function of x_F.

The leading charm effect describes a process whereby final state charm hadrons, which share valence quarks with the projectile, carry a larger fraction of the projectile momentum than charm hadrons which share no valence quarks. For example, with a $\pi^-(d\bar{u})$ projectile, a final state $D^-(d\bar{c})$ would be leading, due to the common d quark, while a $D^+(c\bar{d})$ would be nonleading. The next-to-leading order, NLO, corrections at leading twist can contribute to small production asymmetries between charm hadrons and their antiparticles. However, these effects are below the 10% level and cannot account for the factors of 3 to 10 enhancement seen in some experiments. Such strong initial-final state correlations are not predicted by leading twist pQCD. This implies some recombination mechanism may be at work. A breakdown of factorization must be occurring between long and short scale contributions of the cross section.

The effect is often measured by directly comparing leading twist $d\sigma/dx_F$ calculations with the data. However, the effect may become more obvious in particle ratios, e.g. $(d\sigma/dx_F)_{D^-}/(d\sigma/dx_F)_{D^+}$, or by some other measure like the leading/nonleading asymmetry

$$\mathcal{A}(x_F) = \frac{(d\sigma/dx_F)_{\rm L} - (d\sigma/dx_F)_{\rm NL}}{(d\sigma/dx_F)_{\rm L} + (d\sigma/dx_F)_{\rm NL}}. \tag{1.21}$$

Leading twist pQCD predicts a linear A dependence of the cross section in hA interactions, where h is any hadron. For $x_F < 0.6$, a linear dependence is observed in charm hadroproduction. However, as $x_F \to 1$, the dependence approaches $\sim A^{2/3}$ – proportional to the cross sectional area, since the nuclear volume scales like A. This implies the onset of long scale contributions, i.e. from the whole surface of the target, in charm production at large x_F. This is unexpected because the scale is supposedly set by the charm pair mass with $M_{c\bar{c}} \sim 3$ GeV. Intuitively, even if α_s is not small enough for a reliable perturbative expansion, the charm cross section would seem insensitive to large scale effects – such as the surface of the nucleus.

Both leading charm and the A dependence at large x_F point to multi-parton processes and thus cannot be adequately described by leading twist pQCD. Although some nonperturbative effects are expected in charm production, the breakdown of leading twist at large x_F is surprising. Also, the fact that higher twist terms contribute to the cross section at large x_F but not elsewhere requires explanation.

1.3.1 Higher Twist

To gain insight into some of the charm puzzles, the contributions of higher twist terms are explored. Higher twist terms are added to Eq. (1.20). A more formal treatment of hadron scattering uses the operator product expansion, OPE, on the light cone. Here, contributions to the hadronic tensor can be categorized in powers

of $1/Q^2$ where Q^2 is the momentum scale of the problem – this might represent the momentum transfer in DIS or the invariant mass, M, in hadron-hadron interactions. The suppression factor in the expansion of the hadronic tensor in powers of $1/Q^2$ is known as the twist. It is defined as the mass dimension of the field operator minus the spin. A calculation where the long and short scales are factorized and the scale is hard enough that a perturbative expansion is reliable is leading twist. As described above, this is the dominant term in the OPE. It insures that there are only single hard parton-parton interactions contributing to the cross section. Processes with minimal twist tend to dominate the QCD cross section at high momentum transfer but this is not always the case: in some regions of phase space there may be competing effects.

Multiparton processes in hadron-hadron interactions tend to be composed of higher twist operators and are usually suppressed by powers of $1/M^2$. Naively, they only seem to contribute when perturbative QCD is unreliable. This occurs when the momentum scale is small. Higher twist terms in the heavy quark hadroproduction cross section for a hadron-hadron process would emerge as higher order corrections to the leading twist cross section in Eq. (1.20),

$$\sigma = \sum_{i,j} \int dx_1 dx_2 f_{i/A}(x_1, \mu_F^2) f_{j/B}(x_2, \mu_F^2) \hat{\sigma}_{ij} + \mathcal{O}(\frac{\Lambda_{\rm QCD}^2}{\mu_H^2}). \tag{1.22}$$

The terms of $\mathcal{O}(\Lambda_{\rm QCD}^2/\mu_H^2)$ are usually suppressed compared to leading twist parton fusion. Therefore, the hard scale $\mu_H \sim M$ must be large for a leading twist perturbative expansion to be reliable in QCD. However, in certain regions of phase space, higher twist terms can contribute to the cross section as much as leading twist giving seemingly anomalous production rates. This is particularly interesting be-

cause, if such mechanisms can be understood, it may provide insight into some of the anomalies seen in charm production.

1.3.2 Intrinsic Charm

The anomalous charm production described previously seems independent of the parton structure of the target. Also, anomalous production occurs in regions of large x_F where the produced charm hadron carries a large fraction of the projectile momentum. This prompted the authors of Refs. [16, 17] to speculate on what role the projectile alone might play in producing charm. In this context, the intrinsic charm model was developed. Although the model was originally designed for charm hadroproduction, it can equally be applied to any strongly interacting heavy particle in a QCD bound state such as a bottom quark or even a gluino. The effects of intrinsic gluinos are the topic of Chapter 3.

The intrinsic charm model first seeks to characterize the x distribution of the charm in the sea of the projectile. These higher Fock states are fragile and, after a soft perturbation from the target, the coherence of the bound state is lost. The charm quarks can then coalesce with comoving spectator quarks. The charm quark, much more massive than the light quarks, tends to carry most of the momentum of the original bound state. After coalescence, charm hadrons carrying a large fraction of the projectile momentum are then produced.

Independent of projectile-target interactions, the projectile bound state wavefunc-

tion will be a superposition of all possible Fock state configurations

$$|\Psi\rangle = n_V|q_V\rangle + n_g|q_V g\rangle + \cdots + n_{q\bar{q}}|q_V q\bar{q}\rangle + \cdots + n_{Q\bar{Q}}|q_V Q\bar{Q}\rangle + \cdots . \qquad (1.23)$$

Most of these fluctuations are short-lived and the Fock expansion is dominated by the valence quarks, q_V, and lighter fluctuations. Some fleeting Fock states include heavy quarks, Q, "produced" internally through higher twist intrinsic mechanisms. In the limit where the heavy quark fluctuations carry a large fraction of the projectile's longitudinal momentum, intrinsic fluctuations can actually dominate and contribute nontrivially to heavy quark production [18, 19, 20].

A particularly interesting kinematic limit exists where higher twist terms can contribute to the cross section as much as leading twist at a new hard scale $\mu_H^2 = M^2(1-x)$. This occurs in the limit where $x \to 1$, $M \to \infty$, and $\mu_H = \Lambda_{\rm QCD}$. Here x is the momentum fraction of the projectile carried by the heavy quark pair. This limit is consistent with charm data where some final state charm hadrons are observed carrying a large fraction of the projectile momentum. This limit is in contrast to the typical leading twist limit of $M \to \infty$ and x =constant, giving $\mu_H = M \to \infty$.

In the limit $x \to 1$ and $M \to \infty$ and with the new hard scale $\mu_H^2 = \Lambda_{\rm QCD}^2 = M^2(1-x)$, we now expect that the corrections to leading twist, $\mathcal{O}(\Lambda_{\rm QCD}^2/\mu_H^2)$, contribute nontrivially to the cross section. This is a very interesting result.

In this limit, the Fock state is fragile and can easily be broken up by a soft gluon coming from the surface of the target. As the heavy quarks are created with $x \sim 1$, the entire bound system has a small transverse size, $r_\perp \sim 1/M$. After creation, the heavy quarks maintain this size while the rest of the system transversely expands to

$R_\perp \sim 1/\Lambda_{\rm QCD}$.

The spectator quarks can then be resolved by a soft perturbation with the modest transverse momentum $k_\perp \sim \Lambda_{\rm QCD} \sim 200$ MeV. The system can now easily be brought on shell, breaking up the coherence of the state and releasing the charm quarks. These quarks are now free to coalesce with spectator quarks.

A feature of this model is that to "produce" heavy quarks from the bound state in this limit, the resolving power does not have to be $\sim 1/M$. Because constituents of the bound state tend to minimize their invariant mass and move with the same velocity, intrinsic heavy quarks tend to carry most of the momentum of the state during its brief lifetime. Therefore, the heavy quarks, if liberated, can contribute, even dominate, the leading twist production at large x.

Although the heavy quarks themselves have been created at a hard scale set by M, the system as a whole, from genesis to coalescence, is still dominated by nonperturbative processes and the behavior of the system will be sensitive to the shape of the bound state wavefunction. Therefore, a tractable calculational method must be developed which characterizes the wavefunction. The form of the wavefunction for an n-particle Fock state can be approximated using the Bethe-Salpeter equation on the light cone [21]

$$(M_h^2 - \Sigma_{i=1}^n \frac{\hat{m}_i^2}{x_i})\Psi(x_i, k_{T_i}) = \int_0^1 [dy] \int \frac{[d^2 l_T]}{16\pi^2} \tilde{K}(x_i, k_{T_i}; y_i, l_{T_i}; M_h^2)\Psi(y_i, l_{T_i}). \quad (1.24)$$

Here, M_h is the mass of the parent hadron and $\hat{m}_i^2 = k_{T_i}^2 + m_i^2$ is the square of the effective transverse mass of the $i^{\rm th}$ parton in the bound state. The interaction kernel, $\tilde{K}$, is related to the vertex function. In perturbation theory, $\tilde{K}$ is proportional to

the sum of all irreducible amplitudes between two valence quark configurations. As a first approximation, the right hand side of Eq. (1.24) is constant and the transverse momentum of each parton, k_{T_i}, is evaluated at its RMS value $\sqrt{\langle k_{T_i}^2 \rangle}$. Now, the wavefunction for the n-particle Fock state takes the simple form

$$\Psi^{(n)}(x_i) \propto \frac{1}{(M_h^2 - \Sigma_{i=1}^n \frac{\langle \hat{m}_i^2 \rangle}{x_i})}. \tag{1.25}$$

Higher Fock states of the projectile containing heavy quarks have a number of phenomenological and experimental consequences. For example, such states allow for diffractive charm production. This may occur when a probe scatters off a pre-existing charm quark in the hadron bound state. Another interesting consequence is the leading particle effect, one of the charm puzzles already discussed.

Such initial-final state flavor correlations imply a breakdown of factorization. To illustrate how leading twist is altered, Eq. (1.20) can be modified to describe the production cross section for a final state hadron rather than heavy quarks. At leading twist, we have

$$\sigma_H = \sum_{i,j} \int dz_Q dx_1 dx_2 f_{i/A}(x_1, \mu_F^2) f_{j/B}(x_2, \mu_F^2) \frac{D_{H/Q}(z_Q)}{z_Q} \hat{\sigma}_{ij}. \tag{1.26}$$

Hadronization is included in the parton model by introducing a fragmentation function, $D_{H/Q}(z_Q)$, which describes the probability for the heavy quark, Q, to redistribute its momentum to a final state hadron, H. The fraction of the heavy quark momentum retained by the final state hadron is z_Q. Like the parton distribution functions, the fragmentation function factorizes at leading twist. This fact assumes that the fragmentation function is process independent and thus does not depend on the details of the initial or final state. It also implies that fragmentation must begin occurring over

timescales long compared to the interaction time over which the heavy quarks were generated. This insures that hadronization occurs "far away" from the interaction region.

As in the case of all leading twist assumptions, one expects factorization to break down when the scales involved are nonperturbative – i.e. when M is small. However, as described above, at fixed scale, higher twist terms can dominate at large x for heavy quarks. With this reasoning one would expect higher Fock states containing heavy quarks, which carry a large fraction of the hadron momentum, to contribute to the breakdown of factorization. This is a surprising result because pQCD makes no predictions about the breakdown of leading twist under these conditions.

Initial-final state correlations obtained from Fock state wavefunctions can be modeled by an initial state coalescence process. With the approximation for the wavefunction given in Eq. (1.25) the probability distribution is

$$\frac{d^n P}{\prod_i^n dx_i^n} = |\Psi^{(n)}|^2 = \frac{N_n \delta(1 - \sum_{j=1}^n x_j)}{(M_h^2 - \sum_{i=1}^n \frac{\langle \hat{m}_i^2 \rangle}{x_i})^2} \tag{1.27}$$

where N_n is the normalization constant for the particular n-particle Fock state and the delta function conserves momentum.

Eq. (1.27) can be modified to include the function $C(x_H, x_{H_1}, x_{H_2}, ..., x_{H_j})$, which describes the coalescence of the partons, j, in the initial state into the final state hadron, H. Here, x_H is the momentum fraction of the initial state carried by the final state hadron while x_{H_j} is the momentum fraction of parton j which is in the initial state and appears as a valence quark in the final state. With the coalescence function and a delta function to enforce momentum conservation over all x in the

bound state, the n-particle Fock state wavefunction becomes

$$\frac{dP}{dx_H} \approx \int \prod_{l=1}^{n} dx_l \frac{N_n \delta(1-\sum_{k=1}^{n} x_k) C(x_H, x_{H_1}, x_{H_2}, ..., x_{H_j})}{(M_h^2 - \Sigma_{i=1}^{n} \frac{\langle \hat{m}_i^2 \rangle}{x_i})^2}. \tag{1.28}$$

Particles in a bound state tend to move with the same velocity on the light cone. Particles with similar velocities in the initial bound state will tend to coalesce into bound states themselves after being brought on shell, motivating the use of the simplest coalescence function,

$$C(x_H, x_{H_1}, x_{H_2}, ..., x_{H_j}) \propto \delta(x_H - \sum_j x_{H_j}). \tag{1.29}$$

The details of how the leading and higher twist x_F distributions are combined are discussed extensively in chapters 2 and 3 in the context of the respective systems studied. The simplest approach is to use a two component model whereby the leading and higher twist contributions are added together. The leading twist cross section for a particular process is calculated using Eq. (1.20). The higher twist contribution for a specific final state, H, is obtained by multiplying the probability distribution, calculated using Eq. (1.28), by an appropriate weight, W. This gives

$$\frac{d\sigma}{dx_F} = \frac{d\sigma^{LT}}{dx_F} + W \frac{dP^{HT}}{dx_F}. \tag{1.30}$$

The form of W is based on various reasonable physical assumptions. For example, in charm production by pp interactions

$$W = \frac{\Lambda_{\rm QCD}^2}{m_{c\bar{c}}^2} \sigma_{pp}^{\rm in} \tag{1.31}$$

where the first factor is the expected higher twist contribution $\mathcal{O}(\Lambda_{\rm QCD}^2/\mu_H^2)$ in Eq. (1.22). The inelastic proton-proton cross section provides a standard from which

the higher twist cross section is scaled. The only remaining unknown is the normalization of the state itself, represented by N_n in Eq. (1.28). The normalization of a particular n-particle Fock state must be approximated based on empirical data. For example, an upper limit on the normalization of the 5-particle Fock state can be estimated by assuming it provides the dominant contribution to diffractive charm production. Particular normalization assumptions are covered in more detail in Chapters 2 and 3.

1.4 Intrinsic Gluinos

As discussed, the data supporting anomalous charm production are quite extensive. The intrinsic charm model was developed primarily to address these puzzles. It explains why anomalous charm production occurs primarily in the large x_F region of phase space. Specifically, it addresses leading charm and the coalescence mechanism by which initial-final state flavor correlations occur. It also describes how the nuclear target dependence approaches $A^{2/3}$ at large x_F.

The charm mass range is ideally suited for testing the predictions of the intrinsic charm model. It is natural to ask if the model might apply to other heavy particle systems. For example, in anticipation that similar "bottom puzzles" might exist, intrinsic bottom was studied in Ref. [22]. Leading bottom is predicted, but the probability of finding such a state in a hadron projectile drops rapidly, $\sim 1/m_b^2$, compared to charm. No data are yet available on leading bottom. "Intrinsic strangeness" certainly exists, but the leading twist production mechanism in Eq. (1.20) will give

spurious results because α_s is so close to unity. A leading strangeness model should be explored, but through a different avenue for leading twist production.

Having exhausted the options presented by the Standard Model, we turn to supersymmetry in order to seek new particles with the right sensitivity to the predictions made by the intrinsic charm model. Supersymmetry, SUSY, offers a rich new spectrum of as yet undetected particles.

There are a number of reasons why SUSY is an attractive theory. For example, the coupling constants of the SU(3) strong and the SU(2)×U(1) electroweak gauge theories in the Standard Model all change, to different degrees, with momentum scale. When the momentum scale is near 10^{15} GeV, all three constants nearly converge, but ultimately diverge. This is tantalizing as it alludes to a grand unified theory, GUT, where the strong and electroweak forces merge into one force with one coupling constant. Amazingly, by introducing SUSY into the Standard Model, the coupling constants converge exactly. SUSY also provides a natural means by which to break the electroweak symmetry, currently achieved "by hand".

In the minimal supersymmetric model, MSSM, each Standard Model particle has a supersymmetric counterpart. Naively, to find the quantum numbers of the SUSY counterparts to the Standard Model, subtract 1/2 from the spin but otherwise retain all other quantum numbers. This has the effect of creating fermion/boson partners for each boson/fermion in the Standard Model. However, the predicted mass scale for the SUSY counterparts is quite large, on the order of 1 TeV. Thus far, the large predicted mass of these particles has made confirmation of SUSY prohibitive.

However, there has been some speculation that some SUSY particles are light but

have as yet escaped detection [23, 24]. One such particle is the SUSY partner to the gluon, known as the gluino. The gluino is an electromagnetically neutral fermion with the same color structure as a gluon. The gluino is generally thought to have a mass of hundreds of GeV. Others have explored the possibility that the gluino is very light compared the the SUSY scale, lying in the mass range $0 < m_{\tilde{g}} < 5$ GeV. When the gluino mass is so small, bound states of gluinos and other strongly interacting particles are predicted to form, known collectively as R-hadrons. Although many experiments are potentially sensitive to light gluino masses and lifetimes, the resulting constraints are strongly model dependent. R-hadron search results have so far been negative [25, 26, 27]. Figure 1.1 from Ref. [28] shows the most current "optimistic" model dependent limits on the light gluino in the mass range $0 < m_{\tilde{g}} < 5$ GeV as a function of the squark mass, the SUSY partner to the light quark.

If the gluino mass is between $1 < m_{\tilde{g}} < 5$ GeV, it is natural to ask if R-hadrons would possess some of the same anomalous production observed in charm. If so, then the tools of the intrinsic charm model can be brought to bear on making appropriate predictions.

1.5 Organization

The remander of this dissertation is organized as follows:

Chapter 2 is a paper published in Nuclear Physics **B** [29]. Here, using an advanced two component intrinsic charm model, calculations are performed for $\Sigma^- A$ interactions. The $d\sigma/dx_F$ distributions for final state D^-, Σ_c^0, Ξ_c^+, and Λ_c^+ are studied and

compared to 330 GeV WA89 data. Also studied are D^-/D^+, D_s^-/D_s^+, and $\Lambda_c^+/\bar{\Lambda}_c^+$ asymmetries at WA89. In addition, predictions are made for 650 GeV $\Sigma^- A$ and $\pi^- A$ interactions for the SELEX detector at Fermilab as well as 800 GeV pA interactions.

Chapter 3 is a paper submitted to Nuclear Physics **B** [30] discussing the possibility of intrinsic gluinos in the proton bound state. This work uses the two component intrinsic charm model modified for intrinsic gluinos. The $d\sigma/dx_F$ distributions are calculated for hypothetical R^+, S^0, and R^0 hadrons, bound states of gluinos with quarks and gluons, in 800 GeV pA interactions.

Chapter 4 contains brief closing remarks regarding future prospects for the measurement and modeling of intrinsic states.

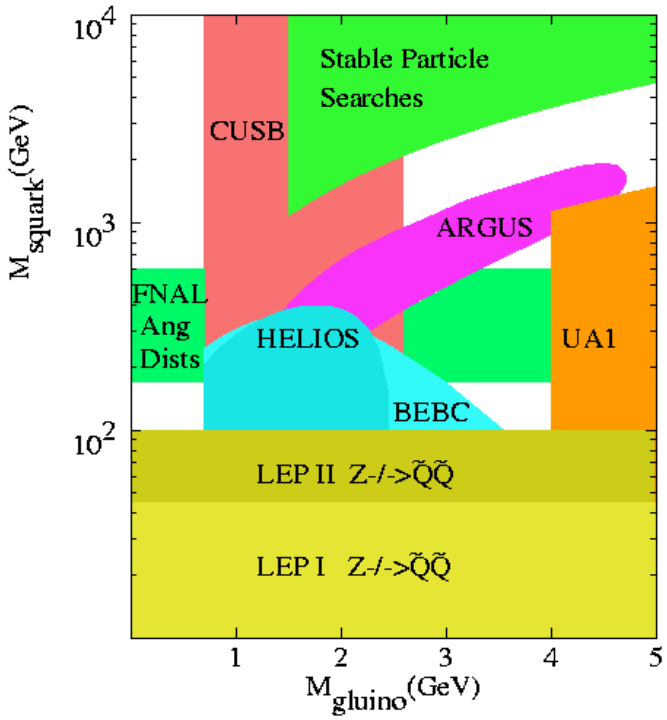

Figure 1.1: Regions of excluded light gluino masses in the $M_{\rm squark} - M_{\rm gluino}$ plane.

Chapter 2

Leading Charm in Hadron-Nucleus Interactions in the Intrinsic Charm Model

Leading Charm in Hadron-Nucleus Interactions in the Intrinsic Charm Model [1]

T. Gutierrez[a] and R. Vogt[a,b]

[a]Physics Department
University of California at Davis
Davis, California 95616
and
[b]Nuclear Science Division
Lawrence Berkeley National Laboratory
Berkeley, California 94720

ABSTRACT

Leading charm hadrons produced in hadron-nucleus interactions cannot be adequately described within the parton fusion model. Recent results on charm baryon production in $\Sigma^- A$ interactions at 330 GeV with the WA89 detector disagree with fusion predictions. Intrinsic heavy quark pairs in the $\Sigma^-(dds)$ wavefunction provide a simple mechanism for producing fast charm hadrons. We calculate leading charm baryon production from Σ^-, π^- and p projectiles in a two component model combining parton fusion with intrinsic charm. Final state D^-, Σ_c^0, Ξ_c^+, and Λ_c^+ $d\sigma/dx_F$ distributions and D^-/D^+, D_s^-/D_s^+ and $\Lambda_c^+/\overline{\Lambda}_c^+$ asymmetries are compared to WA89 data. Predictions are made for 650 GeV $\Sigma^- A$ and $\pi^- A$ interactions in the SELEX detector at Fermilab and for 800 GeV pA interactions.

PACS numbers: 12.38.Bx, 13.75.Ev, 14.20.Lg, 14.40.Lb

[1]This work was supported in part by the Director, Office of Energy Research, Division of Nuclear Physics of the Office of High Energy and Nuclear Physics of the U. S. Department of Energy under Contract Number DE-AC03-76SF00098.

2.1 Introduction

One of the most striking features of charm hadroproduction is the leading particle effect: the strong correlation between the quantum numbers of the projectile and the final-state charm hadron. For example, more D^- than D^+ are produced at large x_F in $\pi^- A \to D^{\pm} X$ interactions [31, 32, 33, 11, 12]. Such correlations are remarkable because they explicitly contradict the perturbative QCD factorization theorem [34] which predicts that heavy quarks hadronize through jet fragmentation functions independent of the initial state.

While leading charm effects are well established for D mesons, observations of charm baryons are more rare [35]. Two experiments with $\Sigma^-(dds)$ beams promise to clarify the situation in the baryon sector. The hyperon beam, with a strange valence quark, presents a unique opportunity to study the flavor dependence of leading charm hadroproduction since both charm and charm-strange baryons can be leading. The first, WA89, which directs a 330 GeV hyperon beam on carbon and copper targets, has reported the x_F distributions of $D^-(d\overline{c})$, $\Sigma_c^0(ddc)$, $\Xi_c^+(usc)$, and $\Lambda_c^+(udc)$ [13] as well as the D^-/D^+, D_s^-/D_s^+ and $\Lambda_c/\overline{\Lambda}_c$ production asymmetries [14]. The second, SELEX [15], has a large acceptance for forward charm production, enhancing the charm baryon yield. Their 650 GeV beam, approximately half $\pi^-(\overline{u}d)$ and Σ^-, promises to improve current samples from both beams by up to an order of magnitude. They also plan to study the A dependence of leading charm.

In previous work [22, 36], a QCD mechanism which produces leading charm at large x_F was introduced. An important feature of the model is coalescence, the

process through which a charm quark hadronizes by combining with quarks of similar rapidities, such as projectile spectator valence quarks. In a gauge theory the strongest attraction is expected to occur when the spectators and the produced quarks have equal velocities [16]. Thus the coalescence probability should be largest at small relative rapidity and rather low transverse momentum where the invariant mass of the $\overline{Q}q$ system is minimized, enhancing the binding amplitude.

This coalescence occurs in the initial state where the projectile wavefunctions of *e.g.* the π^-, p and Σ^- can fluctuate into Fock configurations containing a $c\overline{c}$ pair such as $|\overline{u}dc\overline{c}\rangle$, $|uudc\overline{c}\rangle$ or $|ddsc\overline{c}\rangle$ respectively. In these states, two or more gluons are attached to the charm quarks, reducing the amplitude by $\mathcal{O}(\alpha_s^2)$ relative to parton fusion [22]. The longest-lived fluctuations in states with invariant mass M have a lifetime of $\mathcal{O}(2P_{\rm lab}/M^2)$ in the target rest frame where $P_{\rm lab}$ is the projectile momentum. Since the comoving charm and valence quarks have the same rapidity in these states, the heavy quarks carry a large fraction of the projectile momentum and can thus readily combine to produce charm hadrons with large longitudinal momentum. Such a mechanism can then dominate the hadroproduction rate at large x_F. This is the underlying assumption of the intrinsic charm model [17] in which the wavefunction fluctuations are initially far off shell. However, they materialize as charm hadrons when light spectator quarks in the projectile Fock state interact with the target [18]. Since such interactions are strong, charm production will occur primarily on the front face of the nucleus in the case of a nuclear target. Thus the intrinsic charm mechanism has a stronger A dependence than charm production by leading-twist fusion.

In this work, we concentrate on the charm hadrons studied by WA89 and SELEX

in order to further examine the relationship between fragmentation and coalescence mechanisms. The calculations are made within a two-component model: leading-twist fusion and intrinsic charm [22, 36, 37, 38].

Leading particle correlations are also an integral part of the Monte Carlo program PYTHIA [39] based on the Lund string fragmentation model. In this model it is assumed that the heavy quarks are produced in the initial state with relatively small longitudinal momentum fractions by the leading twist fusion processes. In order to produce a strong leading particle effect at large x_F, the string has to accelerate the heavy quark as it fragments into the final-state heavy hadron. Such a mechanism demands that large changes of the heavy quark momentum take place in the final state. Other models of leading charm production by recombination in the final-state have been suggested [40, 41]. However, in this work we will only compare our results with the commonly used PYTHIA Monte Carlo.

In this paper, we first discuss the conventional mechanism for charm production at leading twist, parton fusion, and how the hyperon beam is taken into account in the model. Section 3 reviews the intrinsic charm model and describes the extension of the model used in this work. In section 4, we compare our results on $\Sigma^- A$ interactions with the WA89 data and make predictions for SELEX with Σ^- and π^- beams as well as pA interactions. Finally, we summarize our results.

2.2 Leading-Twist Charm Production

In this section we briefly review the conventional leading-twist model for the production of charm hadrons in $\Sigma^- p$, pp and $\pi^- p$ interactions. In leading-twist QCD, heavy quarks are produced by the fusion subprocesses $gg \to Q\overline{Q}$ and $q\overline{q} \to Q\overline{Q}$. The factorization theorem [34] predicts that fragmentation is independent of the quantum numbers of both the projectile and target. We will also show the corresponding distributions of charm hadrons predicted by the PYTHIA model [39].

Our calculations are at lowest order in α_s. A constant factor $K \sim 2-3$ is included in the fusion cross section since the next-to-leading order x_F distribution is larger than the leading order distribution by an approximately constant factor [42]. An additional factor of two is included to obtain the single charm distribution, twice the $c\overline{c}$ cross section. Note that neither leading order production nor the next-to-leading order corrections can produce flavor correlations [43] such as those observed in leading charm production.

The charm hadron x_F distribution, where $x_F = (2m_T/\sqrt{s})\sinh y$, has the factorized form [38]

$$\frac{d\sigma}{dx_F} = \frac{\sqrt{s}}{2} x_a x_b \int H_{AB}(x_a, x_b) \frac{1}{E_1} \frac{D_{H/c}(z_3)}{z_3} \, dz_3 \, dy_2 \, dp_T^2 \ , \tag{2.1}$$

where a and b are the initial partons, 1 and 2 are the produced charm quarks with $m_c = 1.5$ GeV, and 3 and 4 are the final-state charm hadrons. The convolution of the subprocess cross sections for $q\overline{q}$ annihilation and gluon fusion with the parton

densities is included in $H_{AB}(x_a, x_b)$,

$$H_{AB}(x_a, x_b) = \sum_q [f_q^A(x_a) f_{\overline{q}}^B(x_b) + f_{\overline{q}}^A(x_a) f_q^B(x_b)] \frac{d\hat{\sigma}_{q\overline{q}}}{d\hat{t}} + f_g^A(x_a) f_g^B(x_b) \frac{d\hat{\sigma}_{gg}}{d\hat{t}} \ , \quad (2.2)$$

where A and B are the interacting hadrons and the scale dependence of the parton densities has been suppressed. The subprocess cross sections can be found in Ref. [5]. Since we study $c\overline{c}$ production with several different projectiles, we specify the general $q\overline{q}$ convolution for three light flavors:

$$\begin{aligned} \sum_q [f_q^A(x_a) f_{\overline{q}}^B(x_b) + f_{\overline{q}}^A(x_a) f_q^B(x_b)] &= u^A(x_a)\overline{u}^B(x_b) + \overline{u}^A(x_a)u^B(x_b) \\ &+ d^A(x_a)\overline{d}^B(x_b) + \overline{d}^A(x_a)d^B(x_b) + s^A(x_a)\overline{s}^B(x_b) + \overline{s}^A(x_a)s^B(x_b) \end{aligned} \quad (2.3)$$

Parton distributions of the hyperon are not available. However, using baryon number and momentum sum rules, a set of parton distributions for the Σ^- can be inferred from the proton distributions:

$$\int_0^1 u_v^p(x)\, dx = \int_0^1 d_v^{\Sigma^-}(x)\, dx = 2 \quad (2.4)$$

$$\int_0^1 d_v^p(x)\, dx = \int_0^1 s_v^{\Sigma^-}(x)\, dx = 1 \ . \quad (2.5)$$

We also identify $s^p(x) = u^{\Sigma^-}(x)$. Similar relations can be made for the sea quarks. The gluon distributions are thus assumed to be the same in the Σ^- and the proton. Both the GRV LO 94 [44] and MRS D$^{-'}$ [45] parton distribution functions with $\bar{u} \neq \bar{d} \neq \bar{s}$ were used. Other, older distributions with a symmetric sea, $\bar{u} = \bar{d} = \bar{s}$, produce identical results for $\Sigma^- p$ and pp interactions.

The fragmentation functions, $D_{H/c}(z)$, describe the hadronization of the charm quark where $z = p_H/p_c$ is the fraction of the charm quark momentum carried by the charm hadron, assumed to be collinear to the charm quark. According to the

factorization theorem, fragmentation is independent of the initial state and thus cannot produce flavor correlations, precluding a leading charm effect. This uncorrelated fragmentation will be modeled by two extremes: a delta function, $\delta(z-1)$, and the Peterson function [46], extracted from e^+e^- data. The Peterson function, derived from a non-hadronic initial state, predicts a softer x_F distribution than observed in hadroproduction, even at moderate x_F [38] since the fragmentation decelerates the charm quark. The parameters of the Peterson function we use here are taken from e^+e^- studies of D production [47]. Typically fits to charm baryon fragmentation functions suggest increased deceleration of the charm quark in final-state baryons relative to mesons. On the other hand, the delta-function assumes that the charm quark coalesces with a low-x spectator sea quark or a low momentum secondary quark with little or no momentum loss [38]. This assumption is more consistent with low p_T charm hadroproduction data [32, 48, 49] than Peterson fragmentation.

In Fig. 2.1(a) we show the inclusive x_F distributions calculated for both types of fragmentation in $\Sigma^- p$ interactions at 330 GeV. Both sets of parton distributions are also shown. Very little difference in either total cross section or shape of the x_F distributions can be discerned between the two sets of parton distributions. The delta function results in harder distributions than those predicted by Peterson fragmentation for $x_F > 0.2$. However, as shown in [13], even with this hard fragmentation the fusion model cannot account for the shape of leading charm baryon distributions. Figure 2.1(b) shows the relative contributions from gg fusion and $q\overline{q}$ annihilation to the total cross section at 650 GeV, the energy of the SELEX beam, using the GRV LO 94 parton densities. Gluon fusion clearly dominates the production until $x_F \approx 0.6$.

We have checked that this is also true at the lower energy of the WA89 experiment, 330 GeV.

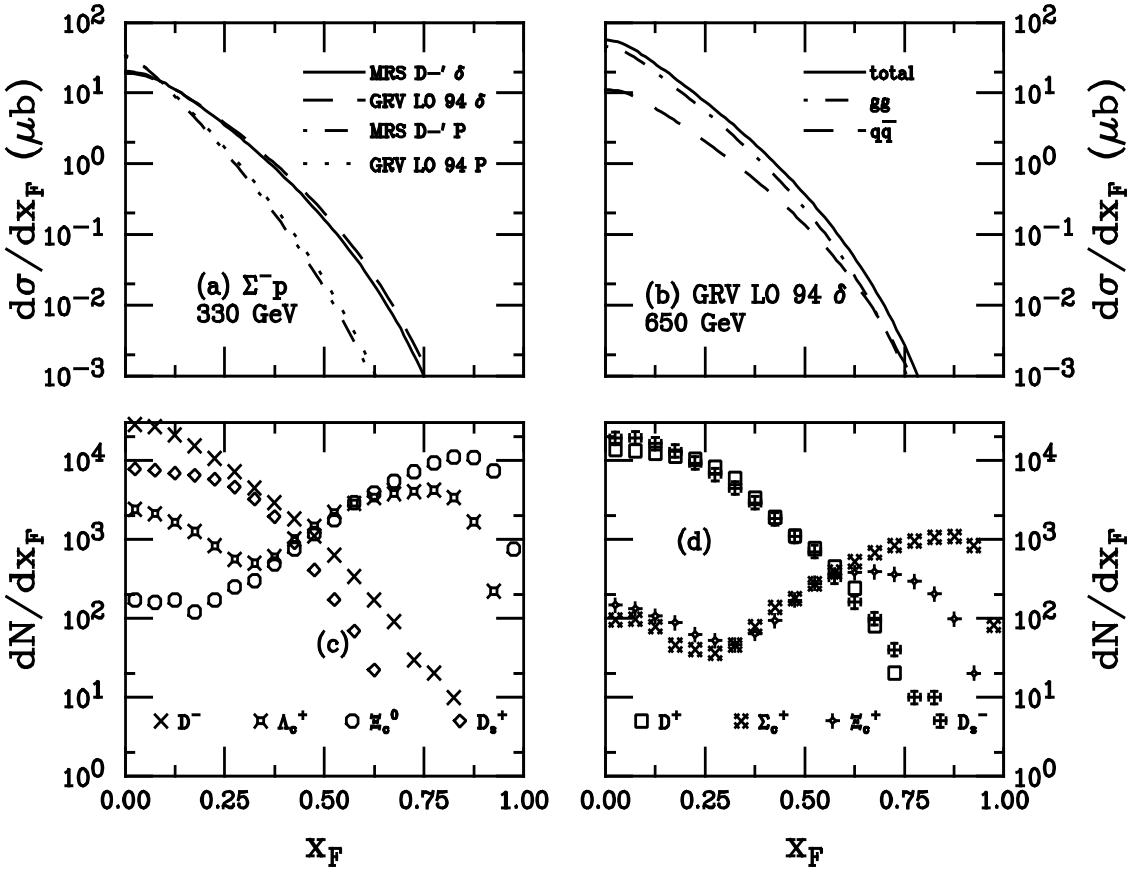

Figure 2.1: Charm production by leading-twist fusion in $\Sigma^- p$ interactions. (a) Two parton distribution functions with two different fragmentation functions are shown at 330 GeV. The curves show calculations with the MRS D$-'$ parton distributions with delta function fragmentation (solid) and the Peterson function (dot-dashed) and with the GRV LO 94 parton distributions with delta function fragmentation (dashed) and the Peterson function (dotted). In (b) calculations with the GRV LO 94 parton distributions with delta function fragmentation are given at 650 GeV for the $q\overline{q}$ component (dashed), gg component (dot-dashed) and the total production cross section (solid). Charm hadron production in PYTHIA 6.115 at 330 GeV is shown in (c) and (d) with the distributions labeled as indicated.

We compare the $\Sigma^- p$ distributions with those from pp and $\pi^- p$ interactions at the same energies with our two choices of parton distributions in Figs. 2.2 and 2.3 respectively. Since the differences between the $\Sigma^- p$ and pp x_F distributions are rather

small due to the dominance of gluon fusion, in Fig. 2.2(a) we show the ratio $\Sigma^- p/pp$ at 330 GeV. The differences between $\Sigma^- p$ and pp production are somewhat larger for the GRV LO 94 distributions than the MRS D$-'$, due to the relative assumptions of $\overline{u}/\overline{d}$. The GRV LO 94 set is based on more recent data than the MRS D$-'$ and should thus more accurately reflect the sea quark abundancies in the proton. In contrast, assumptions concerning charm quark fragmentation do not strongly affect the relative rates. In Fig. 2.2(b) we see that the relative $q\overline{q}$ contribution to pp production is somewhat larger at $x_F \approx 0$ than in $\Sigma^- p$ production at the same energy but this does not affect the point where gg fusion ceases to dominate $c\overline{c}$ production. The pion valence distributions are harder, allowing charm production at larger x_F than with a baryon beam, as shown in Fig. 2.3. For the pion, we use the GRV LO pion set [50] with the GRV LO 94 proton set and with the MRS D$-'$ distributions we use the SMRS P2 pion distributions [51]. However, the valence $\overline{u}$ quark in the π^- does not change the relative importance of $q\overline{q}$ annihilation at 650 GeV, as seen in Fig. 2.3(b). Much lower energies are needed for the π^- antiquark to lead to dominance of $q\overline{q}$ annihilation in $c\overline{c}$ production.

The charm hadron distributions from PYTHIA 6.115 [39] for the three projectiles at 330 GeV beam energy are also shown in Figs. 2.1-2.3 (c) and (d). The PYTHIA calculations, based on 10^7 events, use all default program settings along with the GRV LO 94 parton distributions. We note that in PYTHIA the hyperon valence quark distributions are an average of the proton valence distributions, $d_v^\Sigma = s_v^\Sigma = (u_v^p + d_v^p)/3$. In (c) the D^-, D_s^+, Λ_c and Ξ_c^0 x_F distributions are shown while the D^+, D_s^-, Σ_c^0 and Ξ_c^+ distributions are given in (d). The magnitude of the curves reflect the relative

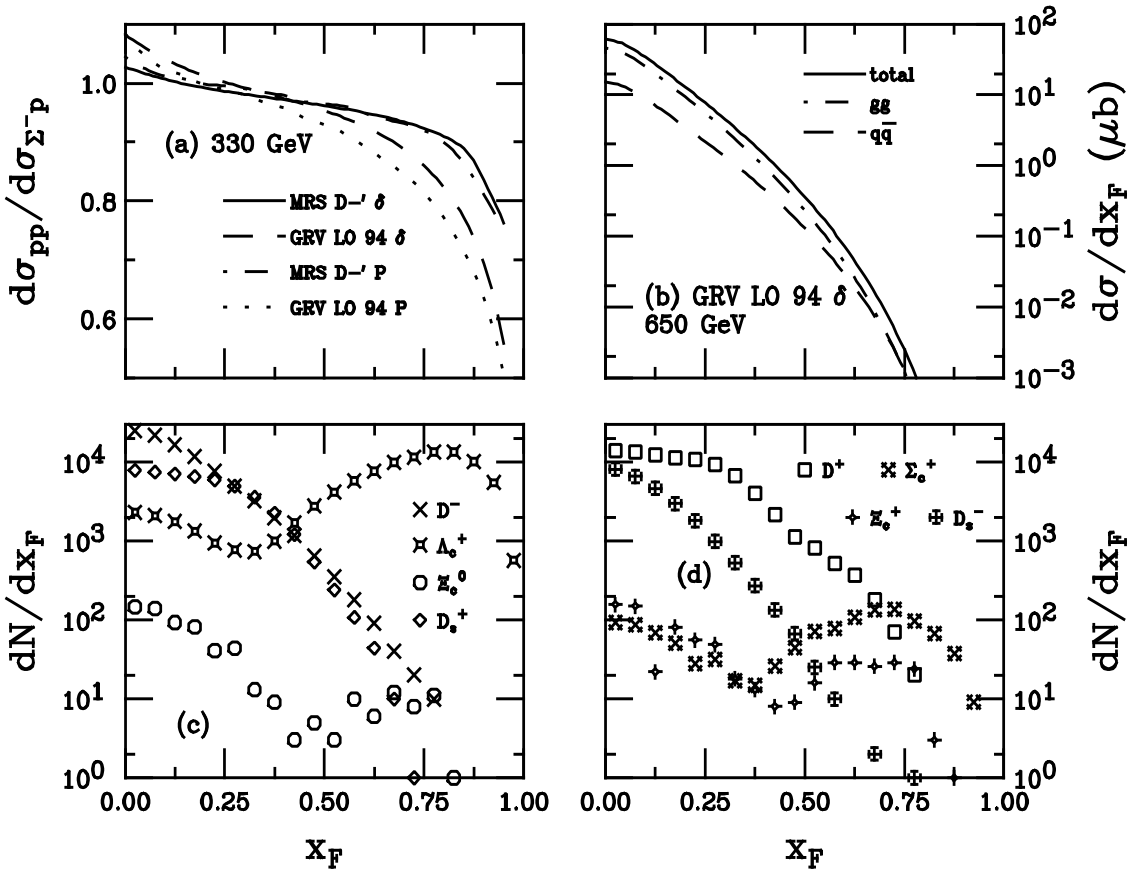

Figure 2.2: Charm production by leading-twist fusion in pp interactions. (a) The cross section ratios $\sigma_{pp}/\sigma_{\Sigma^- p}$ are given for two parton distribution functions with two different fragmentation functions at 330 GeV. The curves show calculations with the MRS D$-'$ parton distributions with delta function fragmentation (solid) and the Peterson function (dot-dashed) and with the GRV LO 94 parton distributions with delta function fragmentation (dashed) and the Peterson function (dotted). In (b) calculations with the GRV LO 94 parton distributions with delta function fragmentation are given at 650 GeV for the $q\overline{q}$ component (dashed), gg component (dot-dashed) and the total production cross section (solid). Charm hadron production in PYTHIA 6.115 at 330 GeV is shown in (c) and (d) with the distributions labeled as indicated.

abundancies of charm hadrons produced by PYTHIA.

The Lund string fragmentation model [39] produces charm quarks at string endpoints. The strings pull the charm quarks toward the opposite endpoints, typically the beam remnants. When the two string endpoints are moving in the same general direction, the charm hadron can be produced with larger longitudinal momentum

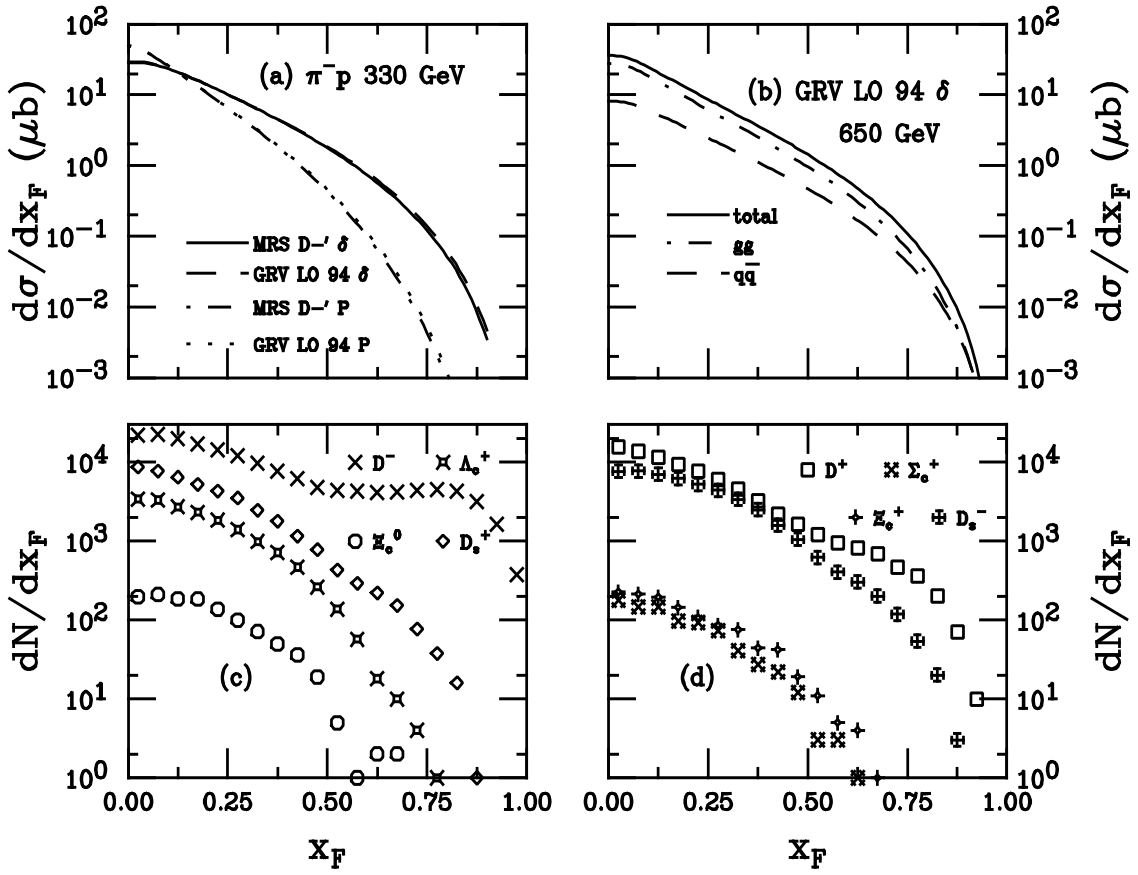

Figure 2.3: Charm production by leading-twist fusion in $\pi^- p$ interactions. (a) Two parton distribution functions with two different fragmentation functions are shown at 330 GeV. The curves show calculations with the MRS D$-'$ parton distributions with delta function fragmentation (solid) and the Peterson function (dot-dashed) and with the GRV LO 94 parton distributions with delta function fragmentation (dashed) and the Peterson function (dotted). In (b) calculations with the GRV LO 94 parton distributions using delta function fragmentation are given at 650 GeV for the $q\overline{q}$ component (dashed), gg component (dot-dashed) and the total production cross section (solid). Charm hadron production in PYTHIA 6.115 at 330 GeV is shown in (c) and (d) with the distributions labeled as indicated.

than the charm quark. In the case where the string invariant mass is too small for multiple particle production, a single hadron is produced [52], as in the $\Sigma_c^0(ddc)$ and $\Xi_c^0(dsc)$ which share two valence quarks with the Σ^-. These distributions have a minimum at $x_F \sim 0.3$ and 0.1 respectively and a peak at $x_F \sim 0.8$, illustrating the acceleration undergone by charm quarks by strings with small invariant mass. The

Λ_c and Ξ_c^+ are also accelerated by string fragmentation but the effect is not as strong because only one valence quark is in common with the projectile.

In contrast, with a proton beam, as shown in Fig. 2.2, only the Λ_c shows strong forward acceleration due to the common u and d quarks with the maximum in the x_F distribution occurring at $x_F \approx 0.8$. A second peak is notable for the Σ_c^0 but the acceleration effect is weaker for charm-strange baryon production, presumably due to the additional mass of the strange quark. While meson production does not show any significant leading behavior with a baryon projectile, the situation is reversed with the π^- beam where D and D_s production is clearly forward of all charm baryon production, produced centrally in the forward x_F region. We will make further comparisons with PYTHIA when our full model is discussed.

2.3 Intrinsic Particle Production

The wavefunction of a hadron in QCD can be represented as a superposition of Fock state fluctuations, *e.g.* $|n_V\rangle$, $|n_V g\rangle$, $|n_V Q\overline{Q}\rangle$, ... components where $n_V \equiv dds$ for a Σ^-, uud for a proton and $\overline{u}d$ for a π^-. When the projectile scatters in the target, the coherence of the Fock components is broken and the fluctuations can hadronize either by uncorrelated fragmentation as for leading twist production or coalescence with spectator quarks in the wavefunction [17, 18]. The intrinsic heavy quark Fock components are generated by virtual interactions such as $gg \to Q\overline{Q}$ where the gluons couple to two or more projectile valence quarks. The probability to produce $Q\overline{Q}$ fluctuations scales as $\alpha_s^2(M_{Q\overline{Q}})/m_Q^2$ relative to leading-twist production [53]. Intrinsic

$Q\overline{Q}$ Fock states are dominated by configurations with equal rapidity constituents so that, unlike sea quarks generated from a single parton, the intrinsic heavy quarks carry a large fraction of the parent momentum [17].

The frame-independent probability distribution of an n–particle $c\overline{c}$ Fock state is

$$\frac{dP_{\rm ic}^n}{dx_i \cdots dx_n} = N_n \alpha_s^4(M_{c\overline{c}}) \frac{\delta(1-\sum_{i=1}^n x_i)}{(m_h^2 - \sum_{i=1}^n (\widehat{m}_i^2/x_i))^2} \ , \tag{2.6}$$

where N_n normalizes the $|nc\overline{c}\rangle$ probability, $P_{\rm ic}^n$, and $n = 4$, 5 for meson and baryon production from the $|n_V c\overline{c}\rangle$ configuration. The delta function conserves longitudinal momentum. The dominant Fock configurations are closest to the light-cone energy shell and therefore the invariant mass, $M^2 = \sum_i \widehat{m}_i^2/x_i$, is minimized where $\widehat{m}_i^2 = k_{T,i}^2 + m_i^2$ is the effective transverse mass of the $i^{\rm th}$ particle and x_i is the light-cone momentum fraction. Assuming $\langle \vec{k}_{T,i}^2 \rangle$ is proportional to the square of the constituent quark mass, we choose $\widehat{m}_q = 0.45$ GeV, $\widehat{m}_s = 0.71$ GeV, and $\widehat{m}_c = 1.8$ GeV [37, 38].

The intrinsic charm production cross section for a single charm hadron from the n-particle state can be related to $P_{\rm ic}^n$ and the inelastic hN cross section by

$$\sigma_{\rm ic}^n(hN) = P_{\rm ic}^n \sigma_{hN}^{\rm in} \frac{\mu^2}{4\widehat{m}_c^2} \ . \tag{2.7}$$

The factor of $\mu^2/4\widehat{m}_c^2$ arises from the soft interaction which breaks the coherence of the Fock state. To set the scale of the coherence factor μ we asssume that the NA3 diffractive J/ψ cross section [6] can be attributed to intrinsic charm. In this experiment the nuclear dependence of J/ψ production in $\pi^- A$ interactions separates into a "hard" contribution with a nearly linear A dependence at low x_F and a high x_F "diffractive" contribution scaling as A^β where $\beta = 0.77$ for pion and 0.71 for proton beams, characteristic of soft interactions. Then we assume that the diffractive

fraction of the production cross section [6] is the same for charmonium and charm hadrons. In Ref. [22], $\mu^2 \sim 0.2$ GeV^2 was found, however, calculations with more recent parton densities suggest that $\mu^2 \sim 0.1$ GeV^2. We thus obtain $\sigma^4_{\rm ic}(\pi N) \approx 0.5$ μb and $\sigma^5_{\rm ic}(pN) \approx 0.7$ μb at 200 GeV. We take $P^5_{\rm ic} = 0.31\%$, as determined from an analysis of the EMC charm structure function data [9, 54]. A recent reanalysis of the EMC data with next-to-leading order calculations of leading twist and intrinsic charm electroproduction is consistent with the presence of an intrinsic charm component in the proton at large $x_{\rm Bj}$ of $\approx 1\%$ or less [55]. For simplicity, we will always assume that the total probability for a charm quark in an $|n_V c\overline{c}\rangle$ state is 0.31% [9, 54, 55], regardless of the projectile identity.

The inelastic $\Sigma^- p$ cross section has not been measured. However the total and elastic Λp cross sections have been parameterized for beam momenta less than 200 GeV albeit with large statistical uncertainties. Extrapolating these cross sections to 330 GeV, we found that $\sigma^{\rm in}_{\Lambda p} > \sigma^{\rm in}_{pp}$ at this energy which seems unlikely. To be conservative, we therefore scaled $\sigma^{\rm in}_{pp}$ down to $\sigma^{\rm in}_{\Lambda p}$ at the highest measured Λp momentum, 21.0 GeV. We then used the energy dependence of $\sigma^{\rm in}_{pp}$ thereafter as the energy dependence for $\Sigma^- p$ interactions at larger values of $\sqrt{s}$.

There are two ways of producing charm hadrons from intrinsic $c\overline{c}$ states. The first is by uncorrelated fragmentation, previously discussed in Section 2. Additionally, if the projectile has the corresponding valence quarks, the charm quark can also hadronize by coalescence with the valence spectators. The coalescence mechanism thus introduces flavor correlations between the projectile and the final-state hadrons, producing *e.g.* Ξ^0_c's with a large fraction of the Σ^- momentum.

First we briefly discuss charm production by uncorrelated fragmentation. If we assume that the c quark fragments into a D meson, the D distribution is

$$\frac{dP_{\rm ic}^{nF}}{dx_D} = \int dz \prod_{i=1}^{n} dx_i \frac{dP_{\rm ic}^{n}}{dx_1 \ldots dx_n} D_{D/c}(z) \delta(x_D - z x_c) \ , \tag{2.8}$$

These distributions are assumed for all intrinsic charm production by uncorrelated fragmentation with $D_{H/c}(z) = \delta(z-1)$. We will not use Peterson function fragmentation further in this work.

The coalescence distributions, on the other hand, are specific for the individual charm hadrons. It is reasonable to assume that the intrinsic charm Fock states are fragile and can easily materialize into charm hadrons in high-energy, low momentum transfer reactions through coalesence. These contributions, taken from Ref. [17], do not include any binding energy of the produced hadrons or any mass effects. The coalescence contribution to charm hadron production is

$$\frac{dP_{\rm ic}^{nC}}{dx_H} = \int \prod_{i=1}^{n} dx_i \frac{dP_{\rm ic}^{n}}{dx_1 \ldots dx_n} \delta(x_H - x_{H_1} - \cdots - x_{H_{n_V}}) \ . \tag{2.9}$$

The coalescence function is simply a delta function combining the momentum fractions of the quarks in the Fock state configuration that make up the valence quarks of the final-state hadron.

We now compare and contrast D^-, D^+, D_s^- and D_s^+ meson and Λ_c, Σ_c^0, Ξ_c^0 and Ξ_c^+ baryon production by coalescence from Σ^-, p and π^- projectiles. We note that not all of these hadrons can be produced from the minimal intrinsic charm Fock state configuration, $|n_V c\bar{c}\rangle$. However, coalescence can also occur within higher fluctuations of the intrinsic charm Fock state. For example, in the proton, the D^+ and Ξ_c^0 can be produced by coalescence from $|n_V c\bar{c}d\bar{d}\rangle$ and $|n_V c\bar{c}s\bar{s}\rangle$ configurations. These higher

Fock state probabilities can be obtained using earlier results [36, 56]. In a previous study of $\psi\psi$ production from $|n_V c\overline{c}c\overline{c}\rangle$ states [56] the double intrinsic charm production probability, $P_{\rm icc}$, was determined assuming that all the measured $\psi\psi$ pairs [7, 8] arise from these configurations. The resulting upper bound on the model, $\sigma_{\psi\psi} = \sigma_{\rm ic}^{\psi\psi}(\pi^- N) \approx 20$ pb set by experiment [7], requires $P_{\rm icc} \approx 4.4\%\ P_{\rm ic}$ [56, 57]. This value can then be used to estimate the probability of light quark pairs in an intrinsic charm state. We expect that the probability of additional light quark pairs in the Fock states to be larger than $P_{\rm icc}$,

$$P_{\rm icq} \approx \left(\frac{\widehat{m}_c}{\widehat{m}_q}\right)^2 P_{\rm icc}\ , \tag{2.10}$$

leading to $P_{\rm icu} = P_{\rm icd} \approx 70.4\%\ P_{\rm ic}$ and $P_{\rm ics} \approx 28.5\%\ P_{\rm ic}$. To go to still higher configurations, *e.g.* for Ξ_c^+ production from a π^-, one can make the similar assumption that $P_{\rm icsu} = 70.4\% P_{\rm ics}$.

In Table 2.1 we show the minimum number of partons needed in each configuration to produce a given charm hadron. When more than the minimal $|n_V c\overline{c}\rangle$ state is necessary for coalescence to occur, the additional light quark pairs required in the state are indicated. While we include the eight particle configuration necessary to produce a Ξ_c^+ by coalescence from a π^- projectile, we will confine our discussion to charm hadron production from the minimal state and states with one additional $q\overline{q}$ pair only.

The total intrinsic charm contribution to charm hadron production is a combination of uncorrelated fragmentation and coalescence. In previous works [22, 36, 37, 38] only production by uncorrelated fragmentation from the minimal $|n_V c\overline{c}\rangle$ states and

Particle	$\Sigma^-(dds)$	$p(uud)$	$\pi^-(\overline{u}d)$
$D^-(d\overline{c})$	5	5	4
$D^+(\overline{d}c)$	$7(d\overline{d})$	$7(d\overline{d})$	$6(d\overline{d})$
$\Lambda_c(udc)$	$7(u\overline{u})$	5	$6(u\overline{u})$
$\Sigma_c^0(ddc)$	5	$7(d\overline{d})$	$6(d\overline{d})$
$D_s^-(s\overline{c})$	5	$7(s\overline{s})$	$6(s\overline{s})$
$D_s^+(\overline{s}c)$	$7(s\overline{s})$	$7(s\overline{s})$	$6(s\overline{s})$
$\Xi_c^0(dsc)$	5	$7(s\overline{s})$	$6(s\overline{s})$
$\Xi_c^+(usc)$	$7(u\overline{u})$	$7(s\overline{s})$	$8(s\overline{s}u\overline{u})$

Table 2.1: The lowest number of partons needed in an intrinsic charm Fock state configuration for the charm particle to be produced by coalescence. Note that 4 and 5 correspond to the minimal $|n_V c\overline{c}\rangle$ configuration while the higher states refer to $|n_V c\overline{c}d\overline{d}\rangle$ *etc.*

coalescence from the minimum Fock state configuration was considered. This was because a significant leading effect is present only in the minimal configuration, *i.e.* there is no difference between D^+ and D^- mesons produced from $|n_V c\bar{c}d\bar{d}\rangle$ states. Also, as more partons are included in the Fock state, the coalescence distributions soften and approach the fragmentation distributions, eventually producing charm hadrons with less momentum than uncorrelated fragmentation from the minimal $c\bar{c}$ state if a sufficient number of $q\bar{q}$ pairs are included. There is then no longer any advantage to introducing more light quark pairs into the configuration—the relative probability will decrease while the potential gain in momentum is not significant. However, if some fraction of the final-state hadrons are assumed to be produced from higher Fock configurations, then all possible final-states from those configurations should also be included. Therefore in this paper, we consider production by fragmentation and coalescence from the minimal state and the next higher states with $u\bar{u}$, $d\bar{d}$ and $s\bar{s}$ pairs.

The probability distributions, $(1/P_{\rm ic}^n)(dP_{\rm ic}^n/dx_H)$, are given in Figs. 2.4-2.6 for Σ^-, p and π^- projectiles respectively. It is clear from Fig. 2.4 that the Σ^- projectile allows the greatest coalescence production of charm hadrons from the minimal Fock configuration, Fig. 2.4(a). The charm baryons are quite fast, taking more than 50% of the projectile momentum. The difference between charm and charm-strange hadron production is very small due to the strange and light quark mass difference. Because the strange quark is more massive, it carries a somewhat larger fraction of the Σ^- momentum than the light quarks, resulting in a slightly larger average momentum for the Ξ_c^0 and the D_s^- relative to the Σ_c^0 and D^-, on the order of 3–4% as can be seen

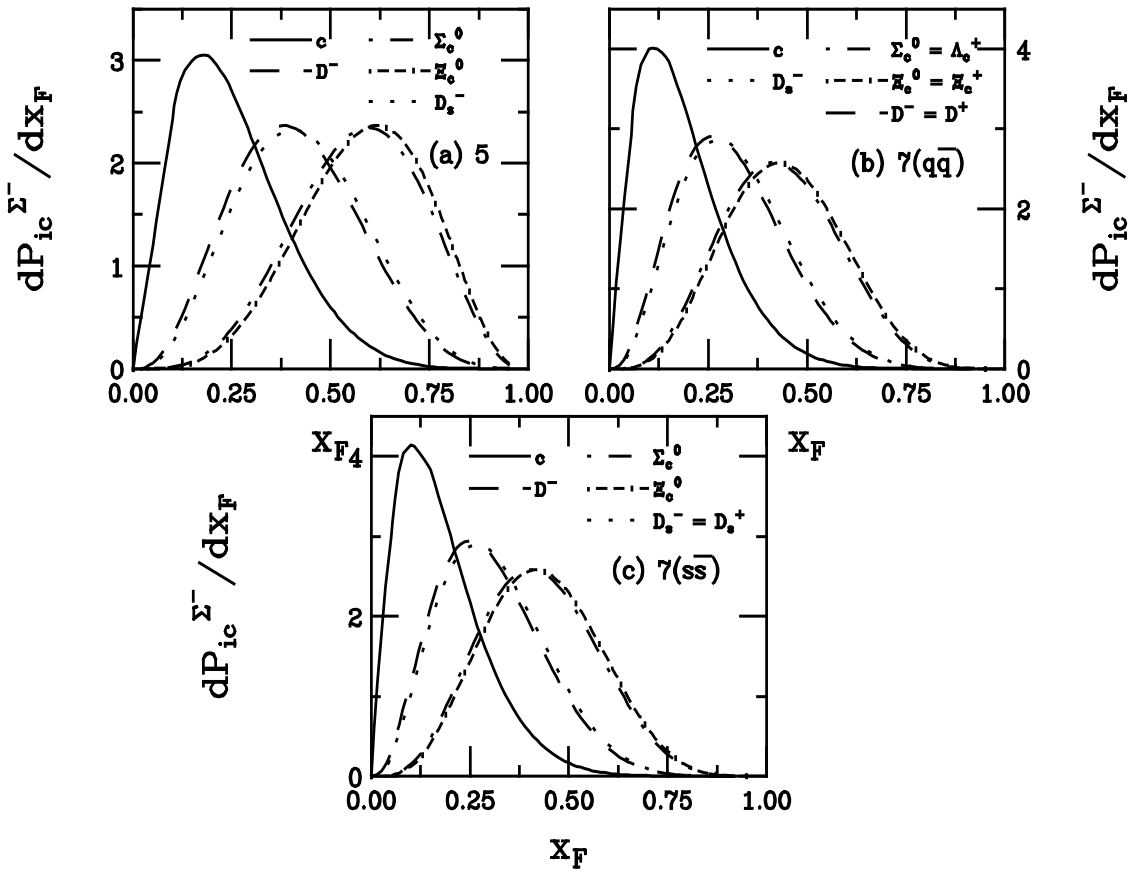

Figure 2.4: Charm hadron production in the intrinsic charm model with a Σ^- projectile. The probability distributions, $(1/P_{\rm ic}^n)(dP_{\rm ic}^n/dx_H)$, for uncorrelated fragmentation and coalescence are given for the minimal 5-particle Fock state (a) and for the 7-particle Fock states with light quarks $q = u$, d (b) and with strange quarks (c). The solid curve in each case is the charm quark distribution which also serves as the hadron distribution for independent fragmentation. The other curves are the probability distributions for hadron production by coalescence, including: D^- (dashed), Σ_c^0 (dot-dashed), Ξ_c^0 (dot-dash-dashed) and D_s^- (dotted). If the shape of the probability distribution is the same for any two hadrons (such as the Σ_c^0 and the Λ_c^+ in (b)) in a configuration, it is indicated.

in Tables 2.2 2.3 and 2.4. The c quark distribution itself, leading to uncorrelated fragmentation, carries $\approx 25\%$ of the projectile momentum in the minimal state. This is reduced by $\approx 35\%$ in the seven-particle Fock configurations. In this model, the c and $\overline{c}$ probability distributions are identical. We note that these higher configurations can produce, for example, Σ_c^0 and Λ_c baryons from $|n_V c\overline{c}d\overline{d}\rangle$ and $|n_V c\overline{c}u\overline{u}\rangle$

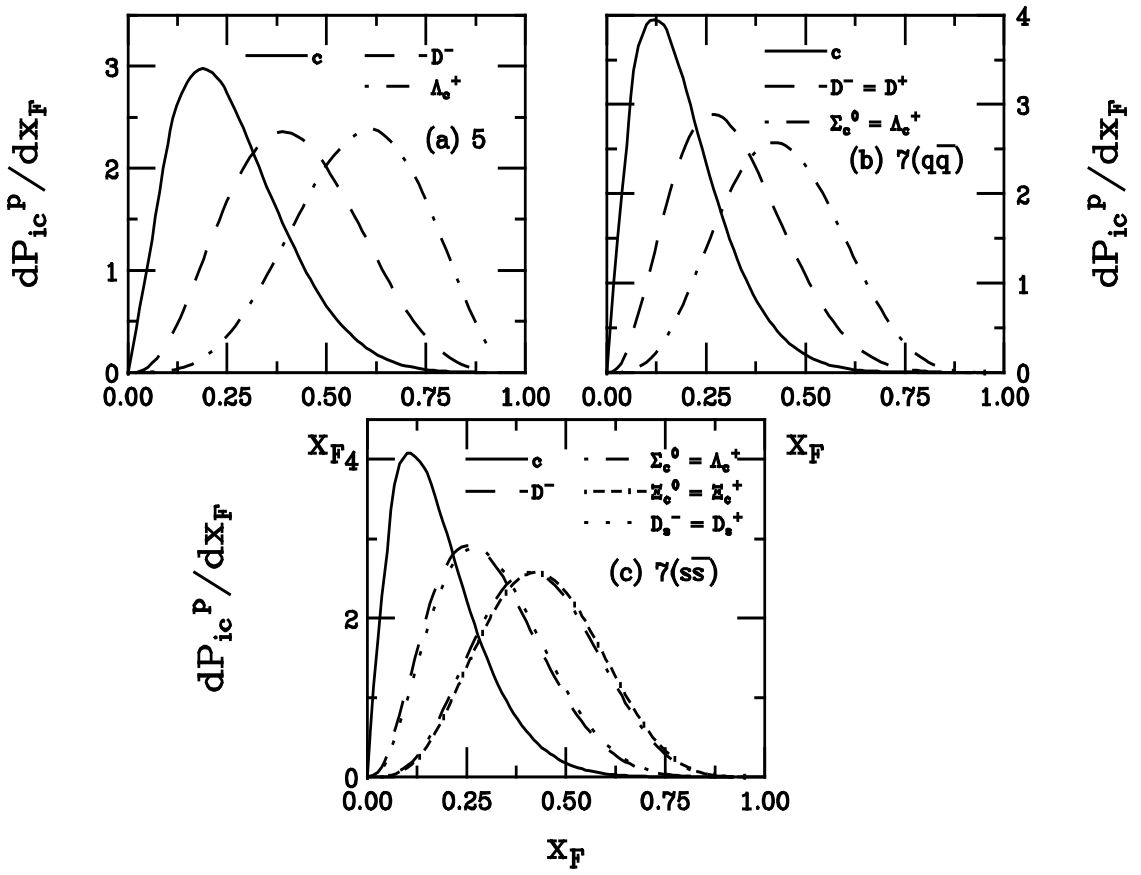

Figure 2.5: Charm hadron production in the intrinsic charm model with a proton projectile. The probability distributions, $(1/P_{\rm ic}^n)(dP_{\rm ic}^n/dx_H)$, for uncorrelated fragmentation and coalescence are given for the minimal 5-particle Fock state (a) and for the 7-particle Fock states with light quarks $q = u$, d (b) and with strange quarks (c). The solid curve in each case is the charm quark distribution which also serves as the hadron distribution for independent fragmentation. The other curves are the probability distributions for hadron production by coalescence, including: D^- (dashed), Λ_c^+ (dot-dashed), Ξ_c^0 (dot-dash-dashed) and D_s^- (dotted). If the shape of the probability distribution is the same for any two hadrons (such as the Σ_c^0 and the Λ_c^+ in (b)) in a configuration, it is indicated.

states respectively with the same probability distribution, shown in Fig. 2.4(b), but not necessarily with the same relative probability, as we will show shortly. Introducing an $s\overline{s}$ pair to the 7-particle configuration reduces the average momentum of the final state hadron by $\approx 2\%$ over the average in the 7-particle configurations with lighter $q\overline{q}$ pairs. In addition to the reduction of the average momentum of the c quark

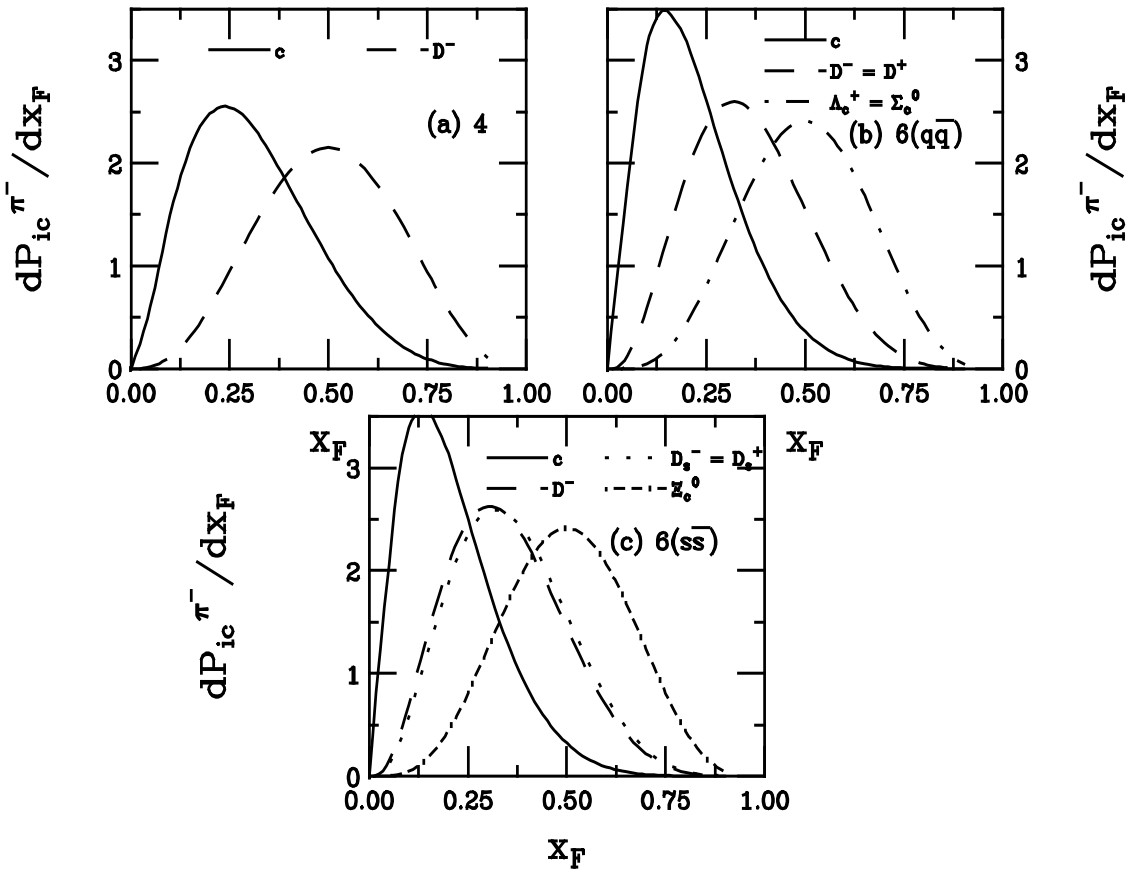

Figure 2.6: Charm hadron production in the intrinsic charm model with a π^- projectile. The probability distributions, $(1/P_{\rm ic}^n)(dP_{\rm ic}^n/dx_H)$, for uncorrelated fragmentation and coalescence are given for the minimal 5-particle Fock state (a) and for the 7-particle Fock states with light quarks $q = u$, d (b) and with strange quarks (c). The solid curve in each case is the charm quark distribution which also serves as the hadron distribution for independent fragmentation. The other curves are the probability distributions for hadron production by coalescence, including: D^- (dashed), Λ_c^+ (dot-dashed), Ξ_c^0 (dot-dash-dashed) and D_s^- (dotted). If the shape of the probability distribution is the same for any two hadrons (such as the Σ_c^0 and the Λ_c^+ in (b)) in a configuration, it is indicated.

in the higher configurations, the final-state charm hadron momentum from this configuration is reduced as well, suggesting that no more significant contribution to the overall momentum of the final hadron will be obtained by including yet higher Fock configurations.

While fewer charm hadrons can be directly produced from the minimal config-

State	Particle	$\Sigma^-(n_V = dds)$	$p(n_V = uud)$	$\pi^-(n_V = \overline{u}d)$
$\|n_V c\overline{c}\rangle$	c	0.251	0.256	0.308
"	$D^-(d\overline{c})$	0.41	0.419	0.499
"	$\Lambda_c(udc)$	-	0.58	-
"	$\Sigma_c^0(ddc)$	0.573	-	-
"	$D_s^-(s\overline{c})$	0.427	-	-
"	$\Xi_c^0(dsc)$	0.59	-	-

Table 2.2: The average value of x_F for charm particles produced by coalescence from Σ^-, p and π^- projectiles in $|n_V c\overline{c}\rangle$ states. In this case, $q\overline{q} = u\overline{u}$, $d\overline{d}$.

uration of a proton projectile, as evident from Fig. 2.5, their average momentum is somewhat higher than the Σ^- due to the abscence of the strange valence quark. However, this only affects the final-state average momentum by 1-2%. Final-state charm hadrons from a pion projectile, shown in Fig. 2.6 have, on average, 20% more momentum than from a baryon projectile because the total velocity is shared between fewer initial partons. Note also that mesons from a four-particle Fock configuration and baryons from a six-particle Fock state each receive half of the projectile momentum.

2.4 Model Predictions

We now turn to specific predictions of our model. We begin with the x_F distribution of the final-state charm hadrons. The x_F distribution for final-state hadron H is

$\|n_V c\bar{c}q\bar{q}\rangle$	c	0.185	0.188	0.219
"	$D^-(d\bar{c}) = D^+(\bar{d}c)$	0.31	0.314	0.359
"	$\Lambda_c(udc)$	0.433	0.438	0.5
"	$\Sigma_c^0(ddc)$	0.433	0.438	0.5
"	$D_s^-(s\bar{c})$	0.32	-	-
"	$\Xi_c^0(dsc) = \Xi_c^+(usc)$	0.444	-	-

Table 2.3: The average value of x_F for charm particles produced by coalescence from Σ^-, p and π^- projectiles in $|n_V c\bar{c}q\bar{q}\rangle$ states. In this case, $q\bar{q} = u\bar{u}$, $d\bar{d}$.

$\|n_V c\bar{c}s\bar{s}\rangle$	c	0.179	0.181	0.211
"	$D^-(d\bar{c})$	0.302	0.306	0.349
"	$\Lambda_c(udc)$	-	0.429	-
"	$\Sigma_c^0(ddc)$	0.424	-	-
"	$D_s^-(s\bar{c}) = D_s^+(\bar{s}c)$	0.312	0.316	0.361
"	$\Xi_c^0(dsc)$	0.434	0.439	0.5
"	$\Xi_c^+(usc)$	0.434	-	-

Table 2.4: The average value of x_F for charm particles produced by coalescence from Σ^-, p and π^- projectiles in $|n_V c\bar{c}s\bar{s}\rangle$ states. In this case, $q\bar{q} = u\bar{u}$, $d\bar{d}$.

the sum of the leading-twist fusion and intrinsic charm components,

$$\frac{d\sigma_{hN}^{H}}{dx_F} = \frac{d\sigma_{\rm lt}^{H}}{dx_F} + \frac{d\sigma_{\rm ic}^{H}}{dx_F} \ , \tag{2.11}$$

where $d\sigma_{\rm ic}^{H}/dx_F$ is related to dP^{H}/dx_F by

$$\frac{d\sigma_{\rm ic}^{H}}{dx_F} = \sigma_{hN}^{\rm in}\frac{\mu^2}{4\widehat{m}_c^2}\frac{dP_H}{dx_F} \ . \tag{2.12}$$

The probability distribution is the sum of all contributions from the $|n_V c\overline{c}\rangle$ and the $|n_V c\overline{c}q\overline{q}\rangle$ configurations with $q = u$, d, and s and includes uncorrelated fragmentation and coalescence when appropriate, as described below. We use the same fragmentation function, either the delta or Peterson function, to calculate uncorrelated fragmentation in both leading twist fusion and intrinsic charm. In this section, we use only the delta function.

Since experimental information on the relative rates of charm hadron production is incomplete, we assume that all the lowest lying charm hadrons produced by uncorrelated fragmentation have equal probability in both leading-twist fusion and intrinsic charm. There are 10 charm hadrons—and the same number of anticharm hadrons—if excited charm hadrons such as D^* and $\Lambda_c^+(2593)$ are excluded. Therefore the probability distribution for uncorrelated fragmentation into each of these hadrons is 10% of the total probability. As can be seen in Table 1, only a fraction of the possible final-state hadrons can be produced by coalescence. We use a simple counting scheme to arrive at the coalescence probability which enhances the production of leading charm at large x_F. We note that the combined probability of fragmentation and coalescence of all charm hadrons cannot exceed the total production probability of the Fock state configuration. Thus when a particular final-state hadron can be

produced both by uncorrelated fragmentation and coalescence, we multiply the sum of the fragmentation and coalescence probabilities by 0.5 to keep the total probability fixed.

As a concrete example of how the total probability distributions of charm hadron production from the intrinsic charm model is calculated, we will describe D^+ and D^- production from the Σ^- beam in our model in detail. The full complement of equations for all the final-state charm hadrons from Σ^-, p and π^- projectiles considered in this work can be found in the appendix. In the $|ddsc\overline{c}\rangle$ configuration, there are four final-state hadrons with a valence c quark ($2\Xi_c^0$, Σ_c^0 and J/ψ) and also four final-state hadrons with a valence $\overline{c}$ quark ($2D^-$, D_s^- and J/ψ). Note that the J/ψ has been counted in each category. The D^- is then produced by coalescence with 50% of the total coalescence probability for hadrons with a valence $\overline{c}$ as well as by uncorrelated fragmentation of the $\overline{c}$ while the D^+ is only produced by uncorrelated fragmentation from this state. The probability distributions from this minimal Fock configuration are then

$$\frac{dP^5_{D^-}}{dx_F} = \frac{1}{2}\left(\frac{1}{10}\frac{dP^{5F}_{\rm ic}}{dx_F} + \frac{1}{2}\frac{dP^{5C}_{\rm ic}}{dx_F}\right) \tag{2.13}$$

$$\frac{dP^5_{D^+}}{dx_F} = \frac{1}{10}\frac{dP^{5F}_{\rm ic}}{dx_F} \tag{2.14}$$

where F refers to uncorrelated fragmentation and C to coalescence into the specific final-state with the associated probability distribution, shown in Fig. 2.4(a). The $|ddsc\overline{c}q\overline{q}\rangle$ configurations where $q\overline{q} = u\overline{u}$, $d\overline{d}$ and $s\overline{s}$ allow coalescence production of eight final-state hadrons with a valence c and five final-state hadrons with a valence $\overline{c}$ in each case. We will discuss D^+ and D^- from each of these configurations in turn.

When $q\overline{q} = u\overline{u}$, the possible hadrons produced by coalescence are: $2\Xi_c^+$, Ξ_c^0, $2\Lambda_c^+$, Σ_c^0, D^0 and J/ψ with a valence c and $2D^-$, D_s^-, $\overline{D}^0$ and J/ψ with a valence $\overline{c}$. A final-state D^+ can be produced by coalescence from the $d\overline{d}$ configuration in one of the eight possible final-state hadrons with a valence c quark ($3\Sigma_c^0$, $3\Xi_c^0$, D^+ and J/ψ) while the D^- is produced by coalescence in three out of five combinations ($3D^-$, D_s^- and J/ψ) with a valence $\overline{c}$. The $s\overline{s}$ configuration yields no D^+ by coalescence—$4\Xi_c^0$, Σ_c^0, $\Omega_c^0(ssc)$, D_s^+ and J/ψ are allowed—while $2D^-$ are allowed out of 5 possible hadrons with valence $\overline{c}$ quarks—$2D^-$, $2D_s^-$ and J/ψ. Finally, the total intrinsic charm probability distribution for these mesons is:

$$\begin{aligned}\frac{dP_{D^-}}{dx_F} &= \frac{1}{2}\left(\frac{1}{10}\frac{dP_{\rm ic}^{5F}}{dx_F}+\frac{1}{2}\frac{dP_{\rm ic}^{5C}}{dx_F}\right)+\frac{1}{2}\left(\frac{1}{10}\frac{dP_{\rm icu}^{7F}}{dx_F}+\frac{2}{5}\frac{dP_{\rm icu}^{7C}}{dx_F}\right)\\ &\quad+\frac{1}{2}\left(\frac{1}{10}\frac{dP_{\rm icd}^{7F}}{dx_F}+\frac{3}{5}\frac{dP_{\rm icd}^{7C}}{dx_F}\right)+\frac{1}{2}\left(\frac{1}{10}\frac{dP_{\rm ics}^{7F}}{dx_F}+\frac{2}{5}\frac{dP_{\rm ics}^{7C}}{dx_F}\right) \qquad (2.15)\\ \frac{dP_{D^+}}{dx_F} &= \frac{1}{10}\frac{dP_{\rm ic}^{5F}}{dx_F}+\frac{1}{10}\frac{dP_{\rm icu}^{7F}}{dx_F}+\frac{1}{2}\left(\frac{1}{10}\frac{dP_{\rm icd}^{7F}}{dx_F}+\frac{1}{8}\frac{dP_{\rm icd}^{7C}}{dx_F}\right)+\frac{1}{10}\frac{dP_{\rm ics}^{7F}}{dx_F}\ . \qquad (2.16)\end{aligned}$$

Lastly we note that only fragmentation from the minimal Fock state was included along with coalescence from the lowest possible configuration in earlier work [22, 36, 38]. This corresponds to the first term of the D^- probability distribution while the D^+ distribution would be proportional to $0.5((1/10)dP_{\rm ic}^{5F}/dx_F + (1/8)dP_{\rm icd}^{7C}/dx_F)$.

We must also account for the fact that most of the data are taken on nuclear targets. In this case, the model assumes a linear A dependence for leading-twist fusion and an A^α dependence for the intrinsic charm component [6] where $\alpha = 0.77$ for pions and 0.71 for protons (and Σ^-)

$$\frac{d\sigma_{hA}^H}{dx_F} = A\frac{d\sigma_{\rm lt}^H}{dx_F} + A^\alpha\frac{d\sigma_{\rm ic}^H}{dx_F}\ , \qquad (2.17)$$

This A dependence is included in the calculations. The intrinsic charm contribution to the longitudinal momentum distributions per nucleon is thus reduced for nuclear targets.

We now compare the model calculations, both the full model of eqs. (2.15) and (2.16) and the simpler model used previously, to the WA89 data [13] on carbon and copper targets in Fig. 2.7. Since the data are unnormalized, we have normalized all curves to the first data point. The dot-dashed and dotted curves are results with the previous simplified model [22, 36, 38] on carbon and copper targets respectively. The full model is illustrated in the solid and dashed curves for the same targets. The agreement with the data is quite reasonable given both the low statistics of the data and our normalization to the first data point rather than fitting the normalization to the data. The differences in the model distributions are most obvious for the Σ_c^0, shown in Fig. 2.7(c). The simpler model emphasizes the coalescence production from the $|n_V c\overline{c}\rangle$ state only. As can be seen from Fig. 2.4 and Tables 2.2 2.3 and 2.4, the average x_F of the coalescence distribution is more than a factor of two larger than that of a Σ_c^0 production by independent fragmentation of a c quark, producing a shoulder in the x_F distribution, particularly for the carbon target (dot-dashed curve). Because the Σ_c^0 is produced by coalescence with $\approx 30\%$ less average momentum from the 7-particle Fock states, the intermediate x_F region is partially filled in, resulting in a smoother x_F distribution even though the probability is reduced for the higher Fock states. Similar results can be seen for the other charm hadrons in Fig. 2.7.

Note that the model results are in much better agreement with the data than the PYTHIA simulations at the same energy with the default settings, shown in

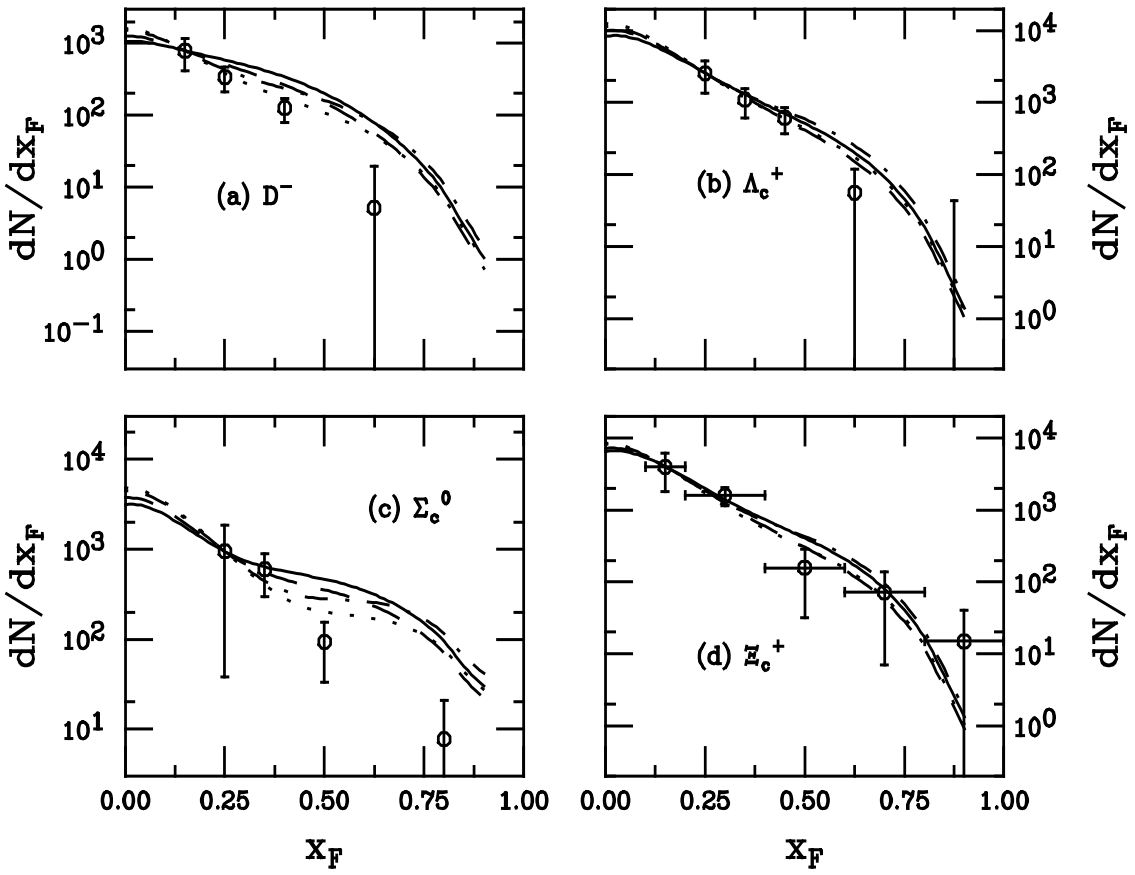

Figure 2.7: Model predictions are compared to the $\Sigma^- A$ data of Ref. [13] for (a) D^-, (b) Λ_c^+, (c) Σ_c^0 and (d) Ξ_c^+. The solid and dashed curves represent our full model, with the intrinsic charm probability distributions given in eqs. (A-1)-(A-8) for carbon and copper targets respectively. The dot-dashed and dotted curves contrast the results for carbon and copper targets respectively with the simplified model which considers only fragmentation from the minimal Fock state and coalescence only from the state with the minimum number of partons necessary to produce it.

Fig. 2.1(c) and (d). If the PYTHIA predictions are superimposed on Fig. 2.7 with the same normalization as our model, the PYTHIA results would considerably exceed the data at large x_F for the charm baryons. In particular, since the c quark is pulled forward by a valence dd diquark, the Σ_c^0 rate from PYTHIA at $x_F \approx 0.8$ would exceed the data by nearly four orders of magnitude. The differences in the results are also obvious in Table 2.5 and 2.6 where the average x_F of all the model distributions on a copper target are compared to PYTHIA calculations with a proton target at the

This Model				
Particle	Σ^-Cu (330)	Σ^-Cu (650)	π^-Cu (650)	pCu (800)
$D^-(d\overline{c})$	0.192	0.147	0.169	0.120
$D^+(\overline{d}c)$	0.133	0.112	0.152	0.107
$\Lambda_c(udc)$	0.145	0.118	0.154	0.146
$\Sigma_c^0(ddc)$	0.187	0.140	0.154	0.107
$D_s^-(s\overline{c})$	0.165	0.129	0.151	0.106
$D_s^+(\overline{s}c)$	0.132	0.111	0.151	0.105
$\Xi_c^0(dsc)$	0.221	0.160	0.151	0.106
$\Xi_c^+(usc)$	0.160	0.126	0.150	0.106

Table 2.5: The average value of x_F for charm particles produced in the full model for Σ^-, p and π^- projectiles on a copper target. The model results are given at 330 GeV and 650 GeV for Σ^-Cu interactions, 650 GeV for π^-Cu interactions and 800 GeV for pCu interactions.

same energy.

Another way to quantify leading charm production is through the asymmetry between leading and nonleading charm. The asymmetry is defined as

$$A(x_F) = \frac{d\sigma_L/dx_F - d\sigma_{NL}/dx_F}{d\sigma_L/dx_F + d\sigma_{NL}/dx_F} \tag{2.18}$$

where L represents the leading and NL the nonleading charm hadron. High statistics data has previously been available only from π^- beams where a significant enhancement of D^- over D^+ production was seen at $x_F > 0.3$ [11, 12, 31], in qualitative agreement with the intrinsic charm calculation of Ref. [22]. The model [36] also correctly predicted the symmetric production of D_s^- and D_s^+ mesons and Λ_c^+ and $\overline{\Lambda}_c^+$

PYTHIA				
Particle	$\Sigma^- p$ (330)	$\Sigma^- p$ (650)	$\pi^- p$ (650)	pp (800)
$D^-(d\overline{c})$	0.14	0.126	0.254	0.113
$D^+(\overline{d}c)$	0.18	0.159	0.173	0.160
$\Lambda_c(udc)$	0.54	0.468	0.153	0.604
$\Sigma_c^0(ddc)$	0.72	0.707	0.146	0.35
$D_s^-(s\overline{c})$	0.155	0.139	0.172	0.097
$D_s^+(\overline{s}c)$	0.171	0.154	0.16	0.153
$\Xi_c^0(dsc)$	0.76	0.767	0.157	0.123
$\Xi_c^+(usc)$	0.55	0.477	0.156	0.155

Table 2.6: The average value of x_F for charm particles produced in PHYTHIA for Σ^-, p and π^- projectiles on a copper target. The results are given at 330 GeV and 650 GeV for Σ^-Cu interactions, 650 GeV for π^-Cu interactions and 800 GeV for pCu interactions.

baryons by π^- beams [35, 49, 58].

Statistics are unfortunately limited on charm production by baryon beams. Recently the WA89 collaboration has presented the D^-/D^+, D_s^-/D_s^+ and $\Lambda_c^+/\overline{\Lambda}_c^+$ asymmetries from their Σ^- data [14]. In Fig. 2.8 we compare our calculations with both models to this data as well as show a prediction for the asymmetry between the D^- and Ξ_c^0, both of which are produced from the partons of the minimal Fock configuration. The full model gives a larger asymmetry betwen D^- and D^+ at low x_F than the simpler assumptions of previous work [22, 36] because D^- production at intermediate x_F is enhanced by coalescence production from the 7-particle configurations, see also Fig. 2.7(a). Our results with the full model are in qualitative agreement with the data, shown in Fig. 2.8(a). The measured D_s^-/D_s^+ and $\Lambda_c^+/\overline{\Lambda}_c^+$ asymmetries are larger than our predictions at intermediate x_F. The probability distribution for $\overline{\Lambda}_c^+$ in our model is

$$\frac{dP_{\overline{\Lambda}_c^+}}{dx_F} = \frac{1}{10}\frac{dP_{\rm ic}^{4F}}{dx_F} + \frac{1}{10}\frac{dP_{\rm icu}^{6F}}{dx_F} + \frac{1}{10}\frac{dP_{\rm icd}^{6F}}{dx_F} + \frac{1}{10}\frac{dP_{\rm ics}^{6F}}{dx_F} \ . \tag{2.19}$$

Some of the discrepancies between the model and the data may arise from the relatively low statistics of the D_s and Λ_c measurements. Our model is also quite crude in overall normalization for the different final states since we assume that all final-state hadrons are produced by independent fragmentation with the same probability. Not enough high statistics data exist yet for us to use experimental absolute production rates as a guide. The asymmetry between D^- and Ξ_c^0 is interesting because the $|ddsc\overline{c}\rangle$ state of the Σ^- can be thought of as a virtual $D^-\Xi_c^0$ fluctuation, as has been suggested for proton fluctuations into $K^+\Lambda$ [59, 60] and $D^-\Lambda_c^+$ [60]. The D^-/Ξ_c^0 is

positive at first since the D^- x_F distribution is larger at intermediate x_F, especially when the 7-particle configurations are included. At larger x_F, the baryon distributions always lead over charm mesons produced in the same configuration, causing the D^-/Ξ_c^0 asymmetry to approach -1 as $x_F \to 1$. Similar results should be expected from the models of Refs. [59, 60].

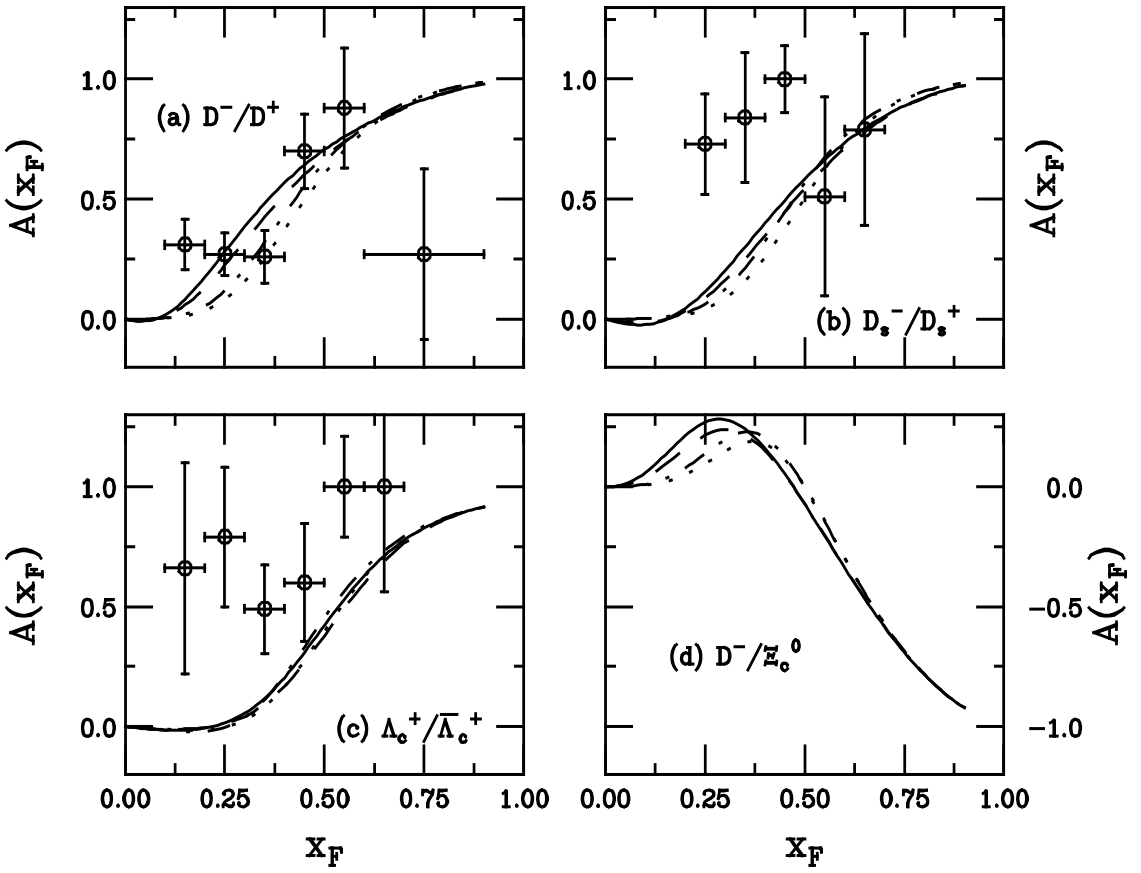

Figure 2.8: Model predictions are compared to the $\Sigma^- A$ data of Ref. [14] for the following asymmetries: (a) D^-/D^+, (b) D_s^-/D_s^+ and (c) $\Lambda_c^+/\overline{\Lambda}_c^+$, as well as our prediction for the (d) D^-/Ξ_c^0 asymmetry. The solid and dashed curves represent our full model, with the intrinsic charm probability distributions given in eqs. (A-1)-(A-8) for carbon and copper targets respectively. The dot-dashed and dotted curves for carbon and copper targets respectively contrast the results with the simplified model which considers only fragmentation from the minimal Fock state and coalescence only from the state with the minimum number of partons necessary to produce it.

We now turn to predictions of charm hadron production at SELEX with 650 GeV

beams of Σ^- and π^- [15]. First we give the charm hadron x_F distributions for Σ^-Cu interactions and the relevant asymmetries in Fig. 2.9. Since the leading-twist fusion cross section grows faster than $\sigma_{\rm ic}^H$, the average x_F of the particles studied decreases $\approx 30\%$ from 330 GeV to 650 GeV. A smaller decrease is found from the PYTHIA model, showing the relative strength of the string fragmentation mechanism, as can be seen in Table 2.6. The Ξ_c^0 is clearly the hardest distribution, followed by the Σ_c^0. The Ξ_c^0 leads the Σ_c^0 because the more massive valence s quark carries more of the Σ^- velocity than the d valence quarks. The Ξ_c^+ leads the Λ_c^+ in the 7-particle $u\overline{u}$ state for the same reason. The D^- and D_s^-, also produced from the 5-particle state have the hardest meson distributions but lag the baryons. The D^+ and D_s^+ have the softest distributions with the D^+ slightly harder because the quarks in the $d\overline{d}$ configuration get slightly more velocity than the $s\overline{s}$ configuration with the more massive strange quarks. The asymmetries, which should be compared to the dashed curves in Fig. 2.8, are somewhat reduced at higher energies, again due to the larger leading-twist cross section.

Since SELEX will also measure charm hadroproduction with a π^- beam at the same energy, these predictions are shown in Fig. 2.10. Because only the D^- is produced from the minimal Fock state configuration, it shows the hardest x_F distribution in Fig. 2.10(a). Note that since $c\overline{c}$ production by leading-twist fusion alone is already significantly harder than the equivalent production by baryon projectiles, the distributions produced by coalescence from 6-particle configurations are not substantially enhanced over the fusion cross section, even at large x_F. The intrinsic charm cross section is proportional to $\sigma_{\pi N}^{\rm in}$ which increases with energy more slowly than the

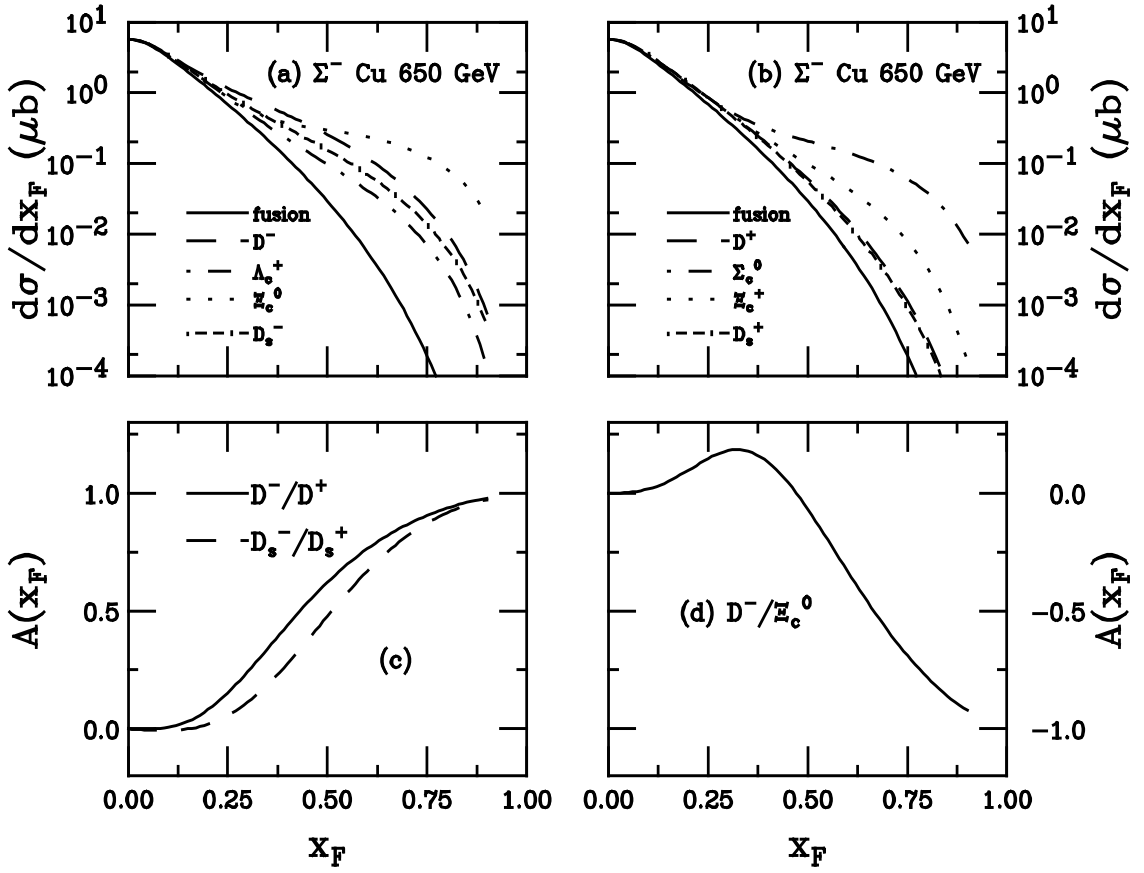

Figure 2.9: Predictions for charm hadron production are given in our full model for Σ^-Cu interactions at 650 GeV. The individual x_F distributions are given in (a) and (b). All cross sections are compared to the leading twist fusion calculation in the solid curve. In (a) the hadron distributions are D^- (dashed), Λ_c^+ (dot-dashed), Ξ_c^0 (dotted) and D_s^- (dot dashed dashed). In (b) the hadron distributions are D^+ (dashed), Σ_c^0 (dot-dashed), Ξ_c^+ (dotted) and D_s^+ (dot dashed dashed). Predictions of the asymmetries are given in (c) for D^-/D^+ (solid) and D_s^-/D_s^+ (dashed) while the prediction for the D^-/Ξ_c^0 asymmetry is given in (d).

leading-twist cross section, further decreasing the predicted leading charm enhancement. Additionally, we note that charm baryons lead mesons produced by coalescence only in the 6-particle configurations since the baryons take $\approx 50\%$ of the pion momentum while the mesons take less, as seen in Fig. 2.6 and Tables 2.2 2.3 and 2.4. The PYTHIA distributions in Fig. 2.3, aside from the leading D^-, are more central, also evident from Table 2.6. In Fig. 2.10(c), only the D^-/D^+ asymmetry is shown

because the model predicts identical D_s^- and D_s^+ meson and Λ_c and $\overline{\Lambda}_c^+$ baryon distributions, see the appendix, hence no asymmetry. We note that the asymmetry is reduced compared to calculations at lower energy [22].

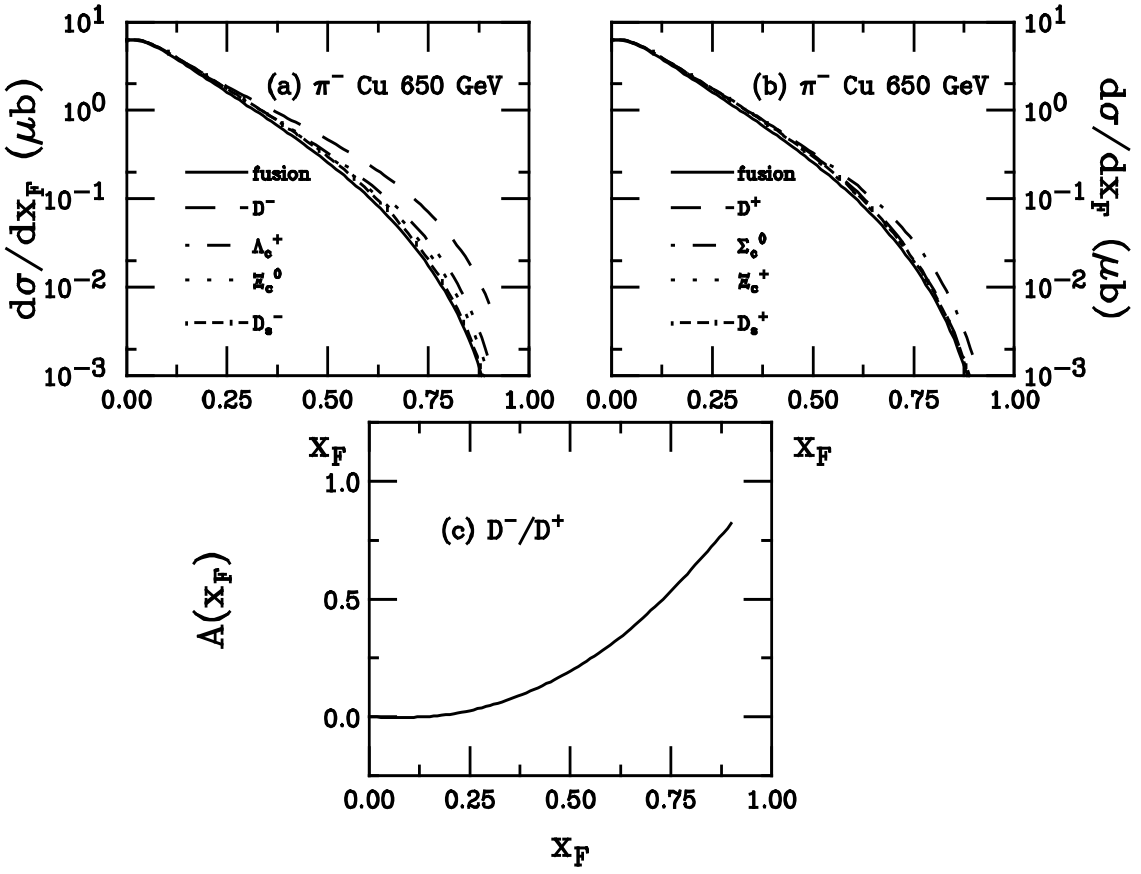

Figure 2.10: Predictions for charm hadron production are given in our full model for 650 GeV π^-Cu interactions. The individual x_F distributions are given in (a) and (b). All cross sections are compared to the leading twist fusion calculation in the solid curve. In (a) the hadron distributions are D^- (dashed), Λ_c^+ (dot-dashed), Ξ_c^0 (dotted) and D_s^- (dot dashed dashed). In (b) the hadron distributions are D^+ (dashed), Σ_c^0 (dot-dashed), Ξ_c^+ (dotted) and D_s^+ (dot dashed dashed). A prediction of the D^-/D^+ asymmetry is given in (c).

The primary proton beam for fixed-target experiments at Fermilab is 800 GeV so for completeness, we also give predictions for a possible pA measurement at this energy in Fig. 2.11. In this case, the Λ_c^+ has the hardest x_F distribution followed by the D^-, both of which are produced by coalescence from the 5-particle Fock state. Again,

the Σ_c^0 and D^+ are somewhat harder than the Ξ_c^+ and D_s^+ distributions respectively due to the relative partitioning of the parton velocity in the 7-particle $u\overline{u}$ and $d\overline{d}$ configurations compared to the 7-particle $s\overline{s}$ state. The model predicts a strong D^-/D^+ asymmetry as well as a D^-/Λ_c^+ asymmetry, comparable to the D^-/Ξ_c^0 asymmetry predicted for the $\Sigma^- A$ interactions. On the other hand, the D_s^-/D_s^+ asymmetry is quite weak. Such measurements with a proton beam would provide a useful complement to a high statistics Σ^- measurement. A comprehensive understanding of data with proton projectiles has suffered in the past from a lack of statistics and high precision proton data, compared to that from Σ^- and π^- projectiles, could eliminate certain models.

2.5 Summary and Conclusions

We have refined the intrinsic charm model of Refs. [22, 36, 38], including both the minimal Fock state and all the configurations with an additional $q\overline{q}$ pair. We have applied a simple counting scheme to determine the relative contribution of each state to the final charm hadron distribution. The model compares rather favorably to the x_F distributions measured by WA89 [13] and produces reasonable agreement with their measured D^-/D^+ asymmetry while falling short of the D_s^-/D_s^+ and $\Lambda_c/\overline{\Lambda}_c$ data [14] at intermediate x_F.

Further, we have made predictions for charm hadron production at the energy of SELEX for both Σ^- and π^- projectiles. Predictions for production by an 800 GeV proton beam are also given. High statistics data on charm production from a

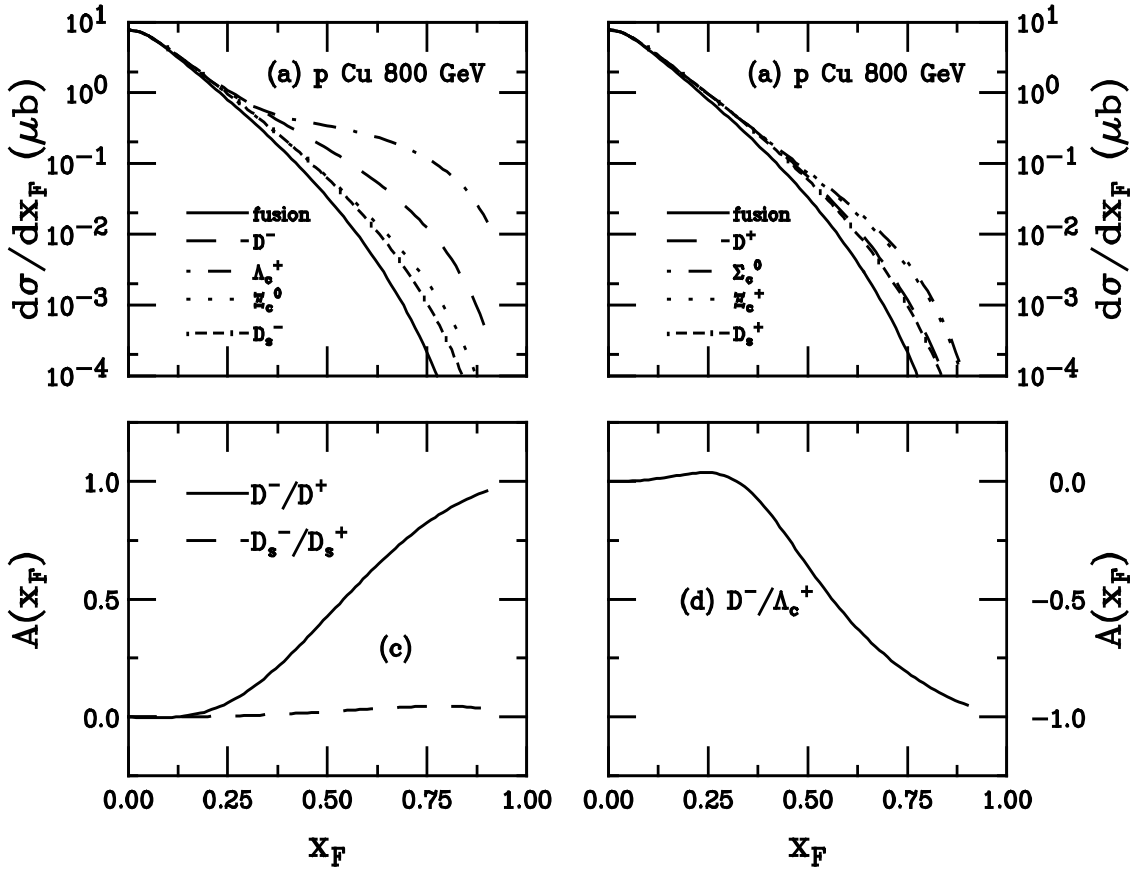

Figure 2.11: Predictions for charm hadron production are given in our full model for pCu interactions at 800 GeV. The individual x_F distributions are given in (a) and (b). All cross sections are compared to the leading twist fusion calculation in the solid curve. In (a) the hadron distributions are D^- (dashed), Λ_c^+ (dot-dashed), Ξ_c^0 (dotted) and D_s^- (dot dashed dashed). In (b) the hadron distributions are D^+ (dashed), Σ_c^0 (dot-dashed), Ξ_c^+ (dotted) and D_s^+ (dot dashed dashed). Predictions of the asymmetries are given in (c) for D^-/D^+ (solid) and D_s^-/D_s^+ (dashed) while the prediction for the D^-/Λ_c^+ asymmetry is given in (d).

combination of these projectiles could eliminate certain classes of models and perhaps distinguish between coalescence in the initial state, as in the intrinsic charm model, and in the final state, as in models such as PYTHIA [39]. The simple counting scheme employed here could be replaced with relative rates from data. However, the shapes of the distributions would not change significantly in our model. Therefore a collection of charm production data could define the role of intrinsic charm in future

experiments.

Chapter 3

Higher Twist Contributions To R-Hadron Phenomenology In The Light Gluino Scenario

Higher Twist Contributions To R-Hadron Phenomenology In The Light Gluino Scenario

T. Gutierrez[a], R. Vogt[a,b1], and J.F. Gunion[a2]

[a]Physics Department
University of California at Davis
Davis, California 95616
and
[b]Nuclear Science Division
Lawrence Berkeley National Laboratory
Berkeley, California 94720

ABSTRACT

The open light gluino window allows non-trivial higher twist gluino contributions to the proton wave function. Using a two-component model originally developed for charm hadroproduction, higher twist intrinsic gluino contributions to final state R-hadron formation are shown to enhance leading twist production in the forward x_F region. We calculate R-hadron production at $p_{\rm lab} = 800$ GeV in pp, pBe, and pCu interactions with light gluino masses of 1.2, 1.5, 3.5, and 5.0 GeV.

PACS numbers:

[1]This work was supported in part by the Director, Office of Energy Research, Division of Nuclear Physics of the Office of High Energy and Nuclear Physics of the U. S. Department of Energy under Contract Number DE-AC03-76SF00098.

[2]Work supported in part by the U.S. Department of Energy and the U.C. Davis Institute for High Energy Physics.

3.1 Introduction

The gluino is the supersymmetric partner of the gluon. It is an electromagnetically neutral, adjoint fermion with the same color structure as its boson counterpart. As yet, no clear experimental evidence of supersymmetric particles has been found. The most likely reason for this is the large expected mass of the supersymmetric particles ($\Lambda_{\rm SUSY} \sim 1$ TeV). However, an intriguing scenario exists whereby the gluino is not only the lightest supersymmetric particle but also very light compared to the SUSY scale, $m_{\tilde{g}} \ll 100$ GeV. This possibility arises naturally in a number of quite attractive models characterized by special boundary conditions at the grand unification scale [23, 61] and in certain models of gauge-mediated supersymmetry breaking [62].

Light gluinos are predicted to form relatively light bound states of quarks or gluons and gluinos called R-hadrons [24]. The lightest predicted R-hadrons include mesinos ($q\bar{q}\tilde{g}$), two barinos, $R^+(uud\tilde{g})$ and $S^0(uds\tilde{g})$, gluinoballs ($\tilde{g}\tilde{g}$), and the glueballino or R^0 ($\tilde{g}g$). The properties of R-hadrons including their mass, decay modes, and lifetimes depend strongly on the mass of the gluino.

There have been many theoretical and experimental attempts to find evidence for and/or exclude the light gluino scenario. Searches for R-hadrons produced in fixed target experiments have been performed for a number of the predicted R-hadron decay channels [25, 26, 27, 63]. Effects of a light gluino on QCD observables have been analyzed [64]. Stable particle searches, Υ decays, beam dump experiments *etc.* all have potential sensitivity to the presence of a light gluino or the R-hadrons. A brief summary of the various possible resulting constraints on a light gluino is given in

Ref. [28]. In addition, Ref. [65] claims that $m_{\tilde{g}} > 2.5 - 3$ GeV is excluded on the basis of their analysis of OPAL data. Although these various analyses are, in combination, potentially sensitive to most regions of light gluino mass, all rely on model-dependent inputs. As a result, we believe that at present it is impossible to *definitively* exclude any gluino mass below $4 - 5$ GeV. Thus, it is of great interest to find additional approaches for discovering and/or constraining light gluinos and the R-hadrons.

In this paper, we will explore the possibility of detecting R-hadrons at large x_F in pp and pA fixed-target interactions. Our calculations will be restricted to the $m_{\tilde{g}} \sim 1.2 - 5$ GeV region where we can be confident that the semi-perturbative techniques that we employ are reliable. This region is of particular phenomenological interest because of the analogy that can be drawn between heavy quark and light gluino production. Indeed, if the gluino and heavy quark masses are comparable, one might anticipate observation of hard gluino production analogous to that already observed in high-x_F charm hadroproduction [11, 12, 14, 31, 32, 33]. The leading-twist pQCD predictions for charm production in pp and pA collisions fail to account for many features of the high-x_F data. These include unexpectedly large production rates and anomalies such as flavor correlations between the produced hadrons and the valence spectators, manifested as leading charm and a strong D^+/D^- asymmetry in $\pi^- A$ interactions [11, 12, 14, 31, 32, 33], double J/Ψ production at large x_F [7, 8], and Feynman scaling of J/Ψ production in pA interactions [6, 66], all of which suggest a breakdown of factorization [34] at large x_F. The anomalies and cross section enhancement may be partly explained by higher twist terms in the operator product expansion (OPE) on the light cone associated with the dynamics of the QCD bound

state. Analgous terms should be present for light gluinos.

The intrinsic charm model (IC) [16, 17] approximates non-perturbative higher twist Fock-state contributions of heavy quarks in hadronic wave functions. The phenomenological predictions of IC directly address the above puzzles in charm hadroproduction [22, 29, 36, 37, 38, 56]. For example, IC provides a coalescence mechanism whereby final state hadrons can share valence quarks with the projectile, naturally producing leading particles.

In analogy with leading charm, we study R-hadron distributions using "intrinsic gluinos" ($\mathrm{I\tilde{G}}$) in regions of phase space where the gluino mass and momentum fractions conspire so that higher twist effects cannot be ignored. In this paper, we calculate enhancements over the leading twist R-hadrons x_F distributions with gluino masses $m_{\tilde{g}} = 1.2$, 1.5, 3.5, and 5.0 GeV. Both pp and pA interactions at $p_{\rm lab} = 800$ GeV are considered.

3.2 pQCD Light Gluino Hadroproduction

In pQCD, gluinos are produced in pairs by gg fusion and $q\bar{q}$ annihilation, $gg, q\bar{q} \to \tilde{g}\tilde{g}$, as well as quark-gluon scattering to squark and gluino, $qg \to \tilde{q}\tilde{g}$. Precision Z-pole data has constrained the squark mass to be greater than 100 GeV, quite large compared to the light gluino masses considered here. Therefore, we expect that the qg contribution with the virtual squark in the t-channel will be small compared to the other contributions, particularly at fixed-target energies.

The leading twist inclusive R-hadron x_F distribution at leading order is obtained

from the gluino x_F distribution ($x_F = (2m_T/\sqrt{s})\sinh y$) which has the factorized form in pQCD

$$\frac{d\sigma}{dx_F} = \sum_{i,j} \frac{\sqrt{s}}{2} \int dz_3 dy_2 d^2p_T \frac{1}{E_1} \frac{D_{H/\tilde{g}}(z_3)}{z_3} f_i^A(x_a) f_j^B(x_b) \frac{1}{\pi} \frac{d\hat{\sigma}_{ij}}{d\hat{t}} \ . \tag{3.1}$$

Here a and b are the initial partons from projectile and target hadrons A and B, 1 and 2 are the produced gluinos, and 3 is the final-state R-hadron. The sum over i and j extends over all partonic gluino production subprocesses. A K factor of 2.5 is included to account for NLO corrections. Since the K factor is approximately constant with x_F for charm production except as $x_F \to 1$, we assume that the K factor for gluino production is also independent of x_F.

The fragmentation functions, $D_{H/\tilde{g}}(z)$ with $z = x_H/x_{\tilde{g}}$, describe the collinear fragmentation of final state R-hadrons from the produced gluinos. For simplicity, a delta function was used for hadronization, $D_{H/\tilde{g}}(z) = \delta(z-1)$. This assumption results in the hardest x_F distribution at leading twist since the R-hadron carries all of the gluino's momentum. Other fragmentation functions would soften these distributions. Note that for any fragmentation function to factorize, it must be independent of the initial state (*i.e.* it only depends on z_3 and not x_a). Thus, regardless of the fragmentation function used, all R-hadrons will be decoupled from the initial state to leading twist.

The partonic cross sections for gluino production in Eq. (3.1) are [67]

$$\begin{aligned}\frac{d\hat{\sigma}_{gg\to\tilde{g}\tilde{g}}}{d\hat{t}} = \frac{9\pi\alpha_s^2}{4\hat{s}^2} \Bigg[&\frac{2(m_{\tilde{g}}^2 - \hat{t})(\hat{u} - m_{\tilde{g}}^2)}{\hat{s}^2} + \frac{m_{\tilde{g}}^2(\hat{s} - 4m_{\tilde{g}}^2)}{(m_{\tilde{g}}^2 - \hat{t})(\hat{u} - m_{\tilde{g}}^2)} \\ &+ \frac{(m_{\tilde{g}}^2 - \hat{t})(\hat{u} - m_{\tilde{g}}^2) - 2m_{\tilde{g}}^2(m_{\tilde{g}}^2 + \hat{t})}{(m_{\tilde{g}}^2 - \hat{t})^2} + \frac{(m_{\tilde{g}}^2 - \hat{t})(\hat{u} - m_{\tilde{g}}^2) + m_{\tilde{g}}^2(\hat{u} - \hat{t})}{\hat{s}(m_{\tilde{g}}^2 - \hat{t})}\end{aligned} \tag{3.2}$$

$$+\frac{(m_{\tilde{g}}^2-\hat{u})(\hat{t}-m_{\tilde{g}}^2)-2m_{\tilde{g}}^2(m_{\tilde{g}}^2+\hat{u})}{(m_{\tilde{g}}^2-\hat{u})^2}+\frac{(m_{\tilde{g}}^2-\hat{u})(\hat{t}-m_{\tilde{g}}^2)+m_{\tilde{g}}^2(\hat{t}-\hat{u})}{\hat{s}(m_{\tilde{g}}^2-\hat{u})}\Bigg]$$

$$\frac{d\hat{\sigma}_{q\bar{q}\to\tilde{g}\tilde{g}}}{d\hat{t}}=\frac{\pi\alpha_s^2}{\hat{s}^2}\Bigg[\frac{32}{27}\frac{(m_{\tilde{g}}^2-\hat{t})^2}{(m_{\tilde{q}}^2-\hat{t})^2}+\frac{32}{27}\frac{(\hat{u}-m_{\tilde{g}}^2)^2}{(\hat{u}-m_{\tilde{q}}^2)^2}+\frac{8}{27}\frac{m_{\tilde{g}}^2\hat{s}}{(m_{\tilde{q}}^2-\hat{t})(\hat{u}-m_{\tilde{q}}^2)} \tag{3.3}$$

$$+\frac{8}{3}\frac{(m_{\tilde{g}}^2-\hat{t})^2+(\hat{u}-m_{\tilde{g}}^2)^2+2m_{\tilde{g}}^2\hat{s}}{\hat{s}^2}$$

$$+\frac{8}{3}\frac{(m_{\tilde{g}}^2-\hat{t})^2+m_{\tilde{g}}^2\hat{s}}{\hat{s}(\hat{t}-m_{\tilde{q}}^2)}+\frac{8}{3}\frac{(\hat{u}-m_{\tilde{g}}^2)^2+m_{\tilde{g}}^2\hat{s}}{\hat{s}(\hat{u}-m_{\tilde{q}}^2)}\Bigg]$$

$$\frac{d\hat{\sigma}_{gq\to\tilde{q}\tilde{g}}}{d\hat{t}}=\frac{\pi\alpha_s^2}{\hat{s}^2}\Bigg[\frac{4}{9}\frac{m_{\tilde{g}}^2-\hat{t}}{\hat{s}}+\frac{(m_{\tilde{g}}^2-\hat{t})\hat{s}+2m_{\tilde{g}}^2(m_{\tilde{q}}^2-\hat{t})}{(m_{\tilde{g}}^2-\hat{t})^2} \tag{3.4}$$

$$-\frac{(\hat{s}-m_{\tilde{q}}^2+m_{\tilde{g}}^2)(m_{\tilde{q}}^2-\hat{t})-m_{\tilde{g}}^2\hat{s}}{\hat{s}(m_{\tilde{g}}^2-\hat{t})}+\frac{4}{9}\frac{(\hat{u}-m_{\tilde{g}}^2)(\hat{u}+m_{\tilde{q}}^2)}{(\hat{u}-m_{\tilde{q}}^2)^2}$$

$$+\frac{1}{2}\frac{(m_{\tilde{q}}^2-\hat{t})(2\hat{u}+m_{\tilde{g}}^2+\hat{t})}{2(\hat{t}-m_{\tilde{g}}^2)(\hat{u}-m_{\tilde{q}}^2)}+\frac{1}{2}\frac{(m_{\tilde{g}}^2-\hat{t})(\hat{s}+2\hat{t}-2m_{\tilde{q}}^2)}{2(\hat{t}-m_{\tilde{g}}^2)(\hat{u}-m_{\tilde{q}}^2)}$$

$$+\frac{1}{2}\frac{(\hat{u}-m_{\tilde{g}}^2)(\hat{t}+m_{\tilde{g}}^2+2m_{\tilde{q}}^2)}{2(\hat{t}-m_{\tilde{g}}^2)(\hat{u}-m_{\tilde{q}}^2)}+\frac{1}{18}\frac{\hat{s}(\hat{u}+m_{\tilde{g}}^2)+2(m_{\tilde{q}}^2-m_{\tilde{g}}^2)(m_{\tilde{g}}^2-\hat{u})}{\hat{s}(\hat{u}-m_{\tilde{q}}^2)}\Bigg] .$$

We calculate leading twist pQCD gluino distributions for 800 GeV pp interactions. Figure 3.1 shows the gluino distributions using the MRS D-' parton distributions in the proton [45] with $m_{\tilde{g}} = 1.2, 1.5, 3.5$, and 5.0 GeV and $m_{\tilde{q}} = 100$ GeV. The characteristic falloff at large x_F is similar to heavy quark production. Choosing a larger squark mass would only marginally decrease the total cross section because the gq channel is suppressed by the large squark mass. The gluino production cross section is a strong function of mass. The cross section is largest for $m_{\tilde{g}} = 1.2$ GeV and decreases by a factor of 3 for $m_{\tilde{g}} = 1.5$ GeV. There is then a drop of 250 to the $m_{\tilde{g}} = 3.5$ GeV gluino cross section and another factor of 20 between the 3.5 and 5 GeV cross sections. Additionally, the falloff of the cross section with x_F becomes steeper as $m_{\tilde{g}}$ is increased.

Charm hadroproduction phenomenology has taught us that higher twist contri-

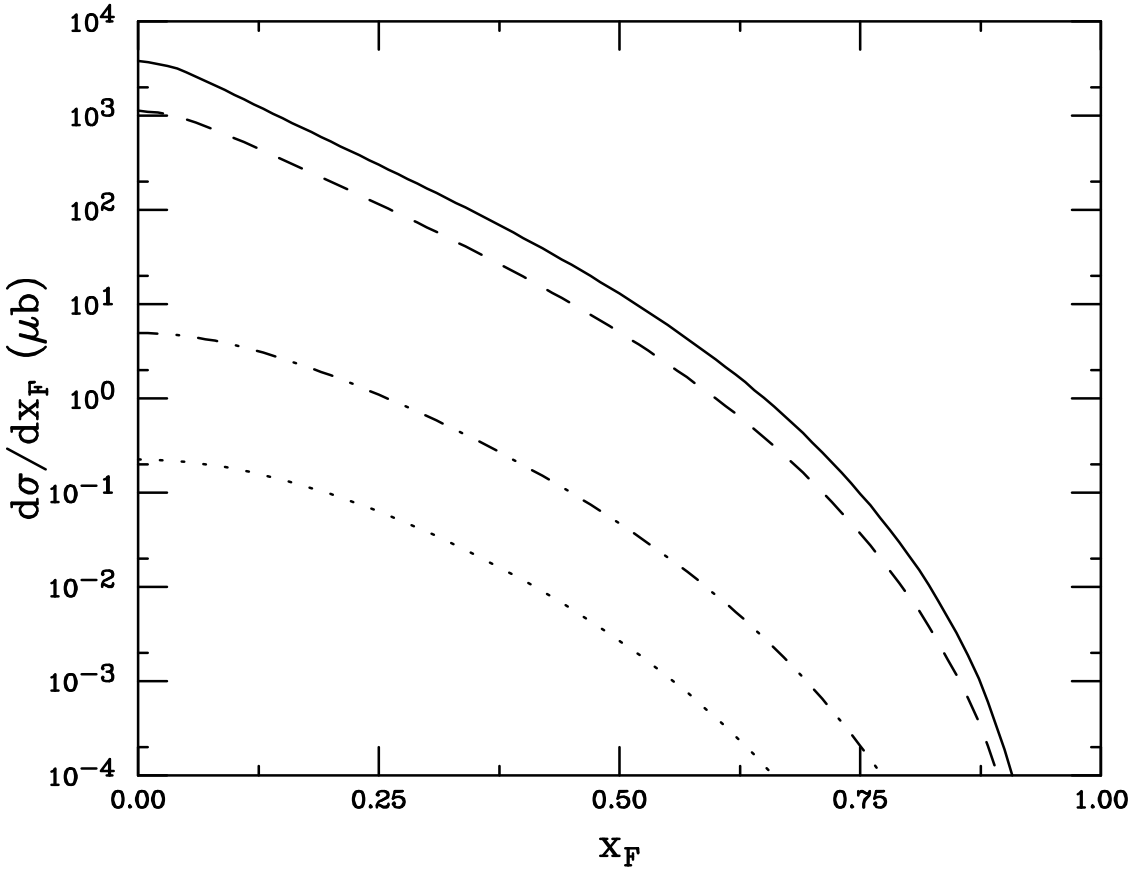

Figure 3.1: 800 GeV QCD pp gluino production for several gluino masses. The curves are $m_{\tilde{g}} = 1.2$ GeV (solid), 1.5 GeV (dashed), 3.5 GeV (dot-dashed), and 5.0 GeV (dotted).

butions can become comparable to leading twist in certain parts of phase space, introducing correlations between the initial and final states. These effects will be addressed in the next section.

3.3 Intrinsic Contribution to Higher Twist

In deep inelastic scattering, higher twist terms in the OPE are suppressed by a factor of $1/Q^{2n}$. These terms are essentially irrelevant when Q^2 is large. Analogously, in hadroproduction, a similar suppression of $1/M^2$ typically renders higher-twist effects

unimportant except in regions where pQCD is seemingly inapplicable (*i.e.* where M^2 is small). However, it has been shown that in the simultaneous $M^2 \to \infty$ and $x \to 1$ limit with $M^2(1-x)$ fixed, a new hard scale emerges where higher twist contributions to the cross section become comparable to leading twist [18, 19, 20]. In the case of heavy quark production, this new scale can be associated with either the resolution of the transverse size of the intrinsic heavy quark pair or with the transverse resolution of any "pre-coalesced" hadrons inside the parent hadron. The heavy quark fluctuations can carry a large fraction of the projectile's forward momentum since the constituents of the bound state move with the same velocity. The Fock state may be broken up by an interaction with soft gluons in the target, producing a leading hadron containing a heavy parton.

The bound state wave function for a state containing higher-twist contributions can be obtained from the Bethe-Salpeter formalism evaluated at equal "time" on the light cone [17, 21]:

$$(M^2 - \Sigma_{i=1}^{n} \frac{\hat{m}_i^2}{x_i})\Psi(x_i, k_{T_i}) = \int_0^1 [dy] \int \frac{[d^2 l_T]}{16\pi^2} \tilde{K}(x_i, k_{T_i}; y_i, l_{T_i}; M^2)\Psi(y_i, l_{T_i}) \qquad (3.5)$$

where M is the mass of the projectile hadron. The transverse mass of an individual parton is defined by $\hat{m_i}^2 = k_{T_i}^2 + m_i^2$, where k_{T_i} is the transverse momentum of the i^{th} parton in the n-particle Fock state, $|q_1, ..., q_i, ..., q_n\rangle$. The momentum fraction of the i^{th} parton in the Fock state is x_i, $[dy] = \Pi_{i=1}^{n} dy_i \delta(1 - \Sigma_{i=1}^{n} y_i)$ is a longitudinal momentum conserving metric and $[d^2 l_T] = \Pi_{i=1}^{n} d^2 l_{T_i} \delta^2(\Sigma_{i=1}^{n} \vec{l}_{T_i})$. The interaction kernel is $\tilde{K}$.

The simplest way to create final state hadron distributions from a specific Fock state wave function is now described. The vertex function on the right hand side

of Eq. (3.5) is assumed to be slowly varying with momentum. The operator on the left hand side of the equation is then evaluated at the average transverse momentum of each parton, $\langle k_{T_i}^2 \rangle$, with the constraint $\Sigma_i^n \vec{k}_{T_i} = 0$. With these assumptions, the transverse mass of each parton is fixed and the vertex function becomes constant. The probability distribution is then proportional to the square of the wave function which is now inversely proportional to the off-shell parameter $\Delta = M^2 - \Sigma_{i=1}^n \langle \hat{m}_i^2 \rangle / x_i$ where $\langle \hat{m}_i^2 \rangle$ is the average transverse mass squared of the i^{th} parton. After longitudinal momentum conservation is specified by $\delta(1 - \Sigma_{i=1}^n x_i)$, the probability distribution becomes

$$\frac{d^n P_n(x_1, ..., x_n)}{\Pi_{i=1}^n dx_n} = N_n \delta(1 - \Sigma_{i=1}^n x_i) \Delta^{-2} \tag{3.6}$$

where N_n is the normalization constant for an n-particle distribution. The probability distributions as a function of x for any final state hadron can be generated by integrating Eq. (3.6) including final state coalescence constraints.

The characteristic shape of the longitudinal momentum distribution of the final state hadron can now be obtained up to an overall normalization constant. The important feature of this model is that final state particles are not "produced" in a collision, as such, but are rather "intrinsic" to the projectile's Fock state and are liberated after a soft interaction with the target. This intrinsic source of final state particles acts as a perturbation to the dominant parton fusion mechanism. However, unlike parton fusion, it incorporates flavor correlations between the initial and final states. This mechanism will dominate the total cross section in the limit $x_F \to 1$ since $x_F \sim x$ when the final-state hadron evolves directly from the projectile wave

function.

In this paper, we assume that the model developed for heavy quark hadroproduction at higher twist can be applied to gluino production in the proton wave function. Final-state R-hadron production from I$\tilde{\text{G}}$ states is described in the remainder of this section along with its relationship to IC production. The characteristic shapes of the intrinsic distributions in the proton were generated for the gluino alone and for the $R^+(uud\tilde{g})$ and $S^0(uds\tilde{g})$, and the $R^0(g\tilde{g})$. In all cases, the "minimal Fock state" was used to generate the final state coalescence. This emphasizes the most leading final states.

The gluino can fragment into a R-hadron, just as in pQCD production. In this uncorrelated case [68], the hadron x_F distribution is

$$\frac{dP_{i\tilde{g}}^{kF}}{dx_H} = N_k \int \Pi_{j=1}^{k} dx_j dz \delta(1 - \sum_{i=1}^{k} x_i) \frac{D_{H/\tilde{g}}(z)}{z} \delta(x_H - z x_{\tilde{g}}) \Delta^{-2} \ , \tag{3.7}$$

where k indicates the order of the Fock state containing the intrinsic gluinos (*i.e.* the $x_{\tilde{g}}$'s are included among the x_i). Gluinos are produced in pairs because other supersymmetric vertices involving squarks and photinos are highly suppressed due to their much greater masses. The minimal proton Fock state with a gluino pair then has five particles, $|uud\tilde{g}\tilde{g}\rangle$. Fragmentation of other, higher, Fock states will have a smaller production probability and produce gluinos with lower average momentum. For consistency with the coalescence production described below, we include fragmentation of six and seven particle Fock states with R^0 and S^0 production respectively.

R-hadron production by coalescence is specific to each hadron. The intrinsic gluino Fock states are fragile and can easily collapse into a new hadronic state through a

soft interaction with the target, as is the case for IC states. The coalescence function is assumed to be a delta function. The momentum fraction of the of the final state hadron is the sum of the momentum fractions of the of the R-hadron valence constituents from the proton wave function. The three R-hadrons we consider are all calculated from only the minimal Fock state required for their production by coalescence. Thus, only the most leading configuration is used. As in the fragmentation case in Eq. (3.7), including higher Fock components does not significantly increase the total rate because the other Fock state probabilities are smaller and also does not enhance the yield at large x_F because the average x_F of coalescence is reduced relative to that from the minimal Fock state.

The five-particle Fock state $|uud\tilde{g}\tilde{g}\rangle$ produces the most leading R-hadron, the R^+, because the R^+ is generated from four of the five constituents of the Fock state.

$$\frac{dP^{5C}_{i\tilde{g}}}{dx_{R^+}} = N_5 P_C^5 \int \Pi_{j=1}^5 dx_j \delta(1 - \sum_{i=1}^5 x_i) \delta(x_{R^+} - x_u - x_u - x_d - x_{\tilde{g}}) \Delta^{-2}. \tag{3.8}$$

Here, P_C^5 is a factor incorporating the coalescence probability given the five-constituent Fock state. Note that in this case, the R^+ x_F distribution is proportional to the gluino distribution in Eq. (3.7), obtained by setting $D_{H/\tilde{g}}(z) = \delta(1-z)$, with $k = 5$ evaluated at $1 - x_F$.

The R^0 is generated from a six-particle Fock state, $|uud g\tilde{g}\tilde{g}\rangle$. Unlike the gluinos, single gluons can be included in the higher-twist Fock state since one gluon can couple to two quarks in the Fock state. The six-particle state is the most leading state for R^0 production. The coalescence of R^0 hadrons is described by

$$\frac{dP^{6C}_{i\tilde{g}}}{dx_{R^0}} = N_6 P_C^6 \int \Pi_{j=1}^6 dx_j \delta(1 - \sum_{i=1}^6 x_i) \delta(x_{R_0} - x_g - x_{\tilde{g}}) \Delta^{-2}. \tag{3.9}$$

The last R-hadron we consider is the S^0 which, since it contains an s quark, must be produced from a seven-particle Fock state, $|uuds\bar{s}\tilde{g}\tilde{g}\rangle$. The S^0 will have a harder x_F distribution than the R^0 even though the average momentum fraction of each constituent in the seven-particle state is smaller than those of the six-particle state. This harder x_F distribution is due to the greater number of S^0 constituents, four, rather than the two R^0 constituents. In this case,

$$\frac{dP_{i\tilde{g}}^{7C}}{dx_{S^0}} = N_7 P_C^7 \int \Pi_{j=1}^7 dx_j \delta(1 - \sum_{i=1}^7 x_i)\delta(x_{S_0} - x_u - x_d - x_s - x_{\tilde{g}})\Delta^{-2}. \qquad (3.10)$$

In what follows, the coalescence probabilities $P_C^{5,6,7}$ appearing in Eqs. (3.8), (3.9),(3.10) are taken to be unity. That is, it is assumed that the gluinos will always coalesce.

Figure 3.2 shows (using arbitrary normalization) the characteristic x dependence of the probability distributions in Eqs. (3.7)-(3.10) with $m_{\tilde{g}} = 1.2$ GeV. The single gluino distribution is calculated using $k = 5$ and $D_{H/\tilde{g}}(z) = \delta(1 - z)$ in Eq. (3.7). R-hadrons produced by uncorrelated fragmentation have the softest x_F distributions, $\langle x_{\tilde{g}} \rangle = 0.24$ when $k = 5$. Contributions from progressively higher single gluino Fock states have smaller relative probabilities, as we discuss below, and a decreased $\langle x_{\tilde{g}} \rangle$, which would eventually build up a gluino sea in the proton. The distributions from coalescence are all forward of the single gluino distribution. As expected, since the R^+ takes all three of the proton valence quarks, it is the most leading R-hadron with $\langle x_{R^+} \rangle = 0.76$. The distributions for the other final state particles, the S_0 and the R_0, are softer with $\langle x_{S^0} \rangle = 0.56$ and $\langle x_{R^0} \rangle = 0.35$ respectively.

We have shown the results with the lowest gluino mass we consider. Increasing the mass increases the average x_F of the gluino distribution of uncorrelated fragmentation,

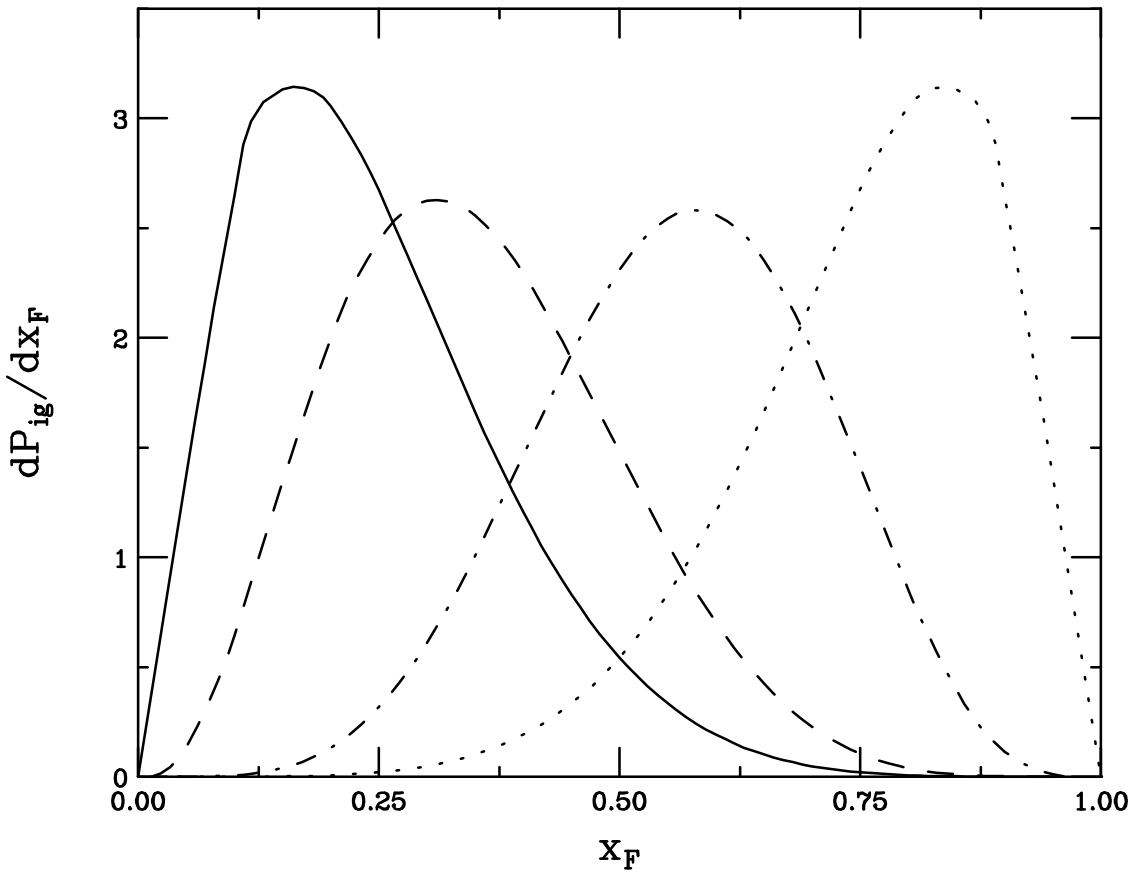

Figure 3.2: The x distribution of intrinsic R-hadrons in the proton with $m_{\tilde{g}} = 1.2$ GeV. The curves are $\tilde{g}$ (solid), R^0 (dashed), S^0 (dot-dashed), and R^+ (dotted).

Eq. (3.7), but leaves the average x_F of the R hadrons unchanged in the mass range we consider.

The intrinsic gluino production cross section for R-hadrons, from an n-particle Fock state is written by analogy with the IC cross section

$$\sigma^n_{i\tilde{g}}(pp) = G_C P^n_{i\tilde{g}} \alpha_s^4(m_{\tilde{g}\tilde{g}}) \sigma^{\rm in}_{pp} \frac{\mu^2}{4\hat{m}^2_{\tilde{g}}} \ , \tag{3.11}$$

where G_C is a color factor. The inelastic pp cross section is $\sim$ 35 mb at 800 GeV. The ratio $\mu^2/4\hat{m}^2_{\tilde{g}}$ sets the scale at which the higher and leading twist contributions are comparable. We use $\mu^2 \sim 0.2$ GeV^2, consistent with attributing the diffractive fraction of the total J/ψ production cross section to IC [22, 29, 36]. There is a

factor of α_s^4 because the intrinsic state couples to two of the projectile valence quarks. The higher-twist contribution then contains two more powers of α_s than the leading-twist contribution. This factor is included in the cross section rather than in the probability distributions as done previously [22, 29] to more explicitly show the effect of this dependence on the cross section when the mass of the intrinsic state is changed.

Since the intrinsic charm cross section is [22]

$$\sigma_{ic}^n(pp) = P_{ic}^n \alpha_s^4(m_{c\bar{c}}) \sigma_{pp}^{\text{in}} \frac{\mu^2}{4\hat{m}_c^2} \ , \tag{3.12}$$

the two cross sections are related by

$$\frac{\sigma_{i\tilde{g}}^n(pp)}{\sigma_{ic}^n(pp)} = \frac{G_C P_{i\tilde{g}}^n}{P_{ic}^n} \frac{\hat{m}_c^2}{\hat{m}_{\tilde{g}}^2} \frac{\alpha_s^4(m_{\tilde{g}\tilde{g}})}{\alpha_s^4(m_{c\bar{c}})} \tag{3.13}$$

The relative color factor between intrinsic gluinos and intrinsic charm, represented by G_C, may enhance the I$\tilde{\text{G}}$ contribution over that of IC because of the color octet nature of the gluino. However, in this work, to isolate mass effects, we assume the color factors for I$\tilde{\text{G}}$ are the same as IC, setting $G_C = 1$. Changing G_C would effectively scale the cross section ratio in Eq. (3.13) by a constant factor. The overall effect of changing G_C is small relative to the leading-twist cross section unless G_C is very large. The intrinsic charm mass is used as the scale from which to approximately evolve the intrinsic gluino cross section as previously done for intrinsic beauty [22]. Note that when $G_C = 1$, if $\hat{m}_{\tilde{g}} = \hat{m}_c$, the I$\tilde{\text{G}}$ and IC cross sections are the same. The I$\tilde{\text{G}}$ cross sections are normalized by scaling $P_{i\tilde{g}}$ in proportion to P_{ic}, as described below.

A limit of $P_{ic}^5 = 0.31\%$ was placed on the intrinsic charm probability in the five-particle state $|uudc\overline{c}\rangle$ by charm structure function data [9, 54, 55]. The higher Fock state probabilities were obtained from an estimate of double J/Ψ production [7, 8],

resulting in $P^7_{icc} \sim 4.4\% P^5_{ic}$ [56]. Mass scaling was used to obtain the mixed intrinsic charm probabilities, $P^7_{iqc} \sim (\hat{m}_c/\hat{m}_q)^2 P^7_{icc}$ [36]. To obtain the n-particle gluino Fock state probabilities, $P^n_{i\tilde{g}}$, we assume that the same relationships hold for the gluino states. The five-particle gluino state then scales as

$$P^5_{i\tilde{g}} = \frac{\hat{m}_c^2}{\hat{m}_{\tilde{g}}^2} P^5_{ic} \ . \tag{3.14}$$

Assuming $P^7_{i\tilde{g}\tilde{g}} = 4.4\% P^7_{i\tilde{g}}$, the seven-particle Fock state probabilities are

$$P^7_{iq\tilde{g}} = \frac{\hat{m}_c^2}{\hat{m}_q^2} P^7_{i\tilde{g}\tilde{g}} \ . \tag{3.15}$$

Thus, if $\hat{m}_{\tilde{g}} = \hat{m}_c$, $P^5_{ic} = P^5_{i\tilde{g}}$ and $P^7_{icc} = P^7_{i\tilde{g}\tilde{g}}$. For simplicity, the probability for the mixed gluon-gluino proton six-particle Fock state was set equal to the seven-particle mixed probability with $\hat{m}_g = \hat{m}_q$. The effective transverse masses used were $\hat{m}_q = \hat{m}_g = 0.45$ GeV, $\hat{m}_s = 0.71$ GeV, and $\hat{m}_c = 1.8$ GeV. The transverse mass of the gluino, $\hat{m}_{\tilde{g}}$, is fixed to the values of $m_{\tilde{g}}$ used in the leading twist calculation.

3.4 Composite Model Predictions

In this section, we calculate the total x_F distribution of final-state R-hadrons including both leading- and higher-twist contributions. The model predictions for R^+, R^0 and S^0 production on proton and nuclear targets are then given at 800 GeV.

The final state $d\sigma/dx_F$ distribution is the sum of the leading twist pQCD distribution and the higher twist intrinsic contributions. Since many experiments use a nuclear target, the characteristic A dependence of each contribution is included,

$$\frac{d\sigma}{dx_F} = A \frac{d\sigma_{lt}}{dx_F} + A^\beta \frac{d\sigma_{i\tilde{g}}}{dx_F} \ . \tag{3.16}$$

The first term is the leading twist term whereas the second term is the higher twist I$\tilde{\text{G}}$ contribution. Leading twist necessarily involves single parton interactions between the target and the projectile and thus cannot account for collective nuclear effects. Thus, the leading twist cross section scales linearly with the number of nucleons in the target modulo nuclear shadowing effects. The nuclear dependence of J/ψ production in pA interactions shows that if the nuclear dependence is parameterized by A^α, $\alpha \to 2/3$ as $x_F \to 1$ [6, 66]. The emergence of this surface effect at large x_F is consistent with spectators in the projectile coupling to soft gluons from the front face of the target rather than the volume. The NA3 collaboration extracted the A dependence of J/ψ production at large x_F and obtained $\beta = 0.71$ in Eq. (3.16) [6]. We use the same value of β for charm production since the available data on the charm A dependence [69] leads us to expect a similar A dependence for charm and J/ψ production at large x_F.

The intrinsic gluino contribution to R-hadron production includes contributions from both hadronization of single gluinos by uncorrelated fragmentation, Eq. (3.7), and coalescence into final-state R-hadrons, described in Eqs. (3.8)-(3.10). That is,

$$\frac{dP^n_{i\tilde{g}}}{dx_F} = \xi_1 \frac{dP^{nF}_{i\tilde{g}}}{dx_F} + \xi_2 \frac{dP^{nC}_{i\tilde{g}}}{dx_F} \tag{3.17}$$

where $P^{nF}_{i\tilde{g}}$ and $P^{nC}_{i\tilde{g}}$ are the I$\tilde{\text{G}}$ contributions from fragmentation and coalescence respectively. The parameters ξ_1 and ξ_2 allow adjustment of the relative gluino fragmentation and coalescence contributions. We used single gluino fragmentation from the same Fock state as the coalesced hadron. That is, for R^+, $k = 5$ in Eq. (3.7), while $k = 6$ for R^0 and $k = 7$ for S^0. We fix $\xi_1 = \xi_2 = 0.5$ for simplicity. For a

more realistic accounting of all possible contributions to Eq. (3.17) for charm production, see Ref. [29] for relative charm hadron production probabilities in the proton. The respective fragmentation and coalescence probability distributions in Eq. (3.17) are converted to cross sections using Eq. (3.11) and added to the leading twist cross section as in Eq. (3.16).

We calculate R-hadron production at 800 GeV in pp, pBe, and pCu interactions with $m_{\tilde{g}} = \hat{m}_{\tilde{g}} = 1.2$, 1.5, 3.5, and 5.0 GeV. Delta function fragmentation was used for single intrinsic gluino production by uncorrelated fragmentation and for leading twist hadronization. That is, we take $D_{H/\tilde{g}}(z) = \delta(1-z)$ in Eqs. (3.1) and (3.7).

Figure 3.3 shows the normalized R-hadron x_F distributions calculated according to Eq. (3.11) in pp interactions with $m_{\tilde{g}} = 1.2$ GeV. The difference in the yields as $x_F \to 0$ is due to the difference in probability for the five, six, and seven particle Fock states. The R^0 and S^0 cross sections are similar at low x_F because we have assumed $P^6_{ig\tilde{g}} = P^7_{iq\tilde{g}}$, as described in the previous section. However, the shapes are different at low x_F because the probability distribution for uncorrelated fragmentation has a smaller average $\langle x_F \rangle$ when $k = 7$ in Eq. (3.7). The R^+ has the largest cross section of the three hadrons. Its distribution is symmetric around $x_F = 0.5$ because the fragmentation yield and the R^+ yield from coalescence are symmetric in the five particle Fock state. The S^0 yield increases near $x_F \sim 0.25$ due to the forward peak of the S^0 coalescence distribution seen in Fig. 3.2. The yield at low x_F is relatively reduced because the fragmentation calculation with $k = 7$ is narrower so that the two peaks are effectively separated in Fig. 3.2. Since the fragmentation peak for $k = 6$ and the R^0 coalescence distribution lie close together, they blend into a broad peak

for the R^0 x_F distribution.

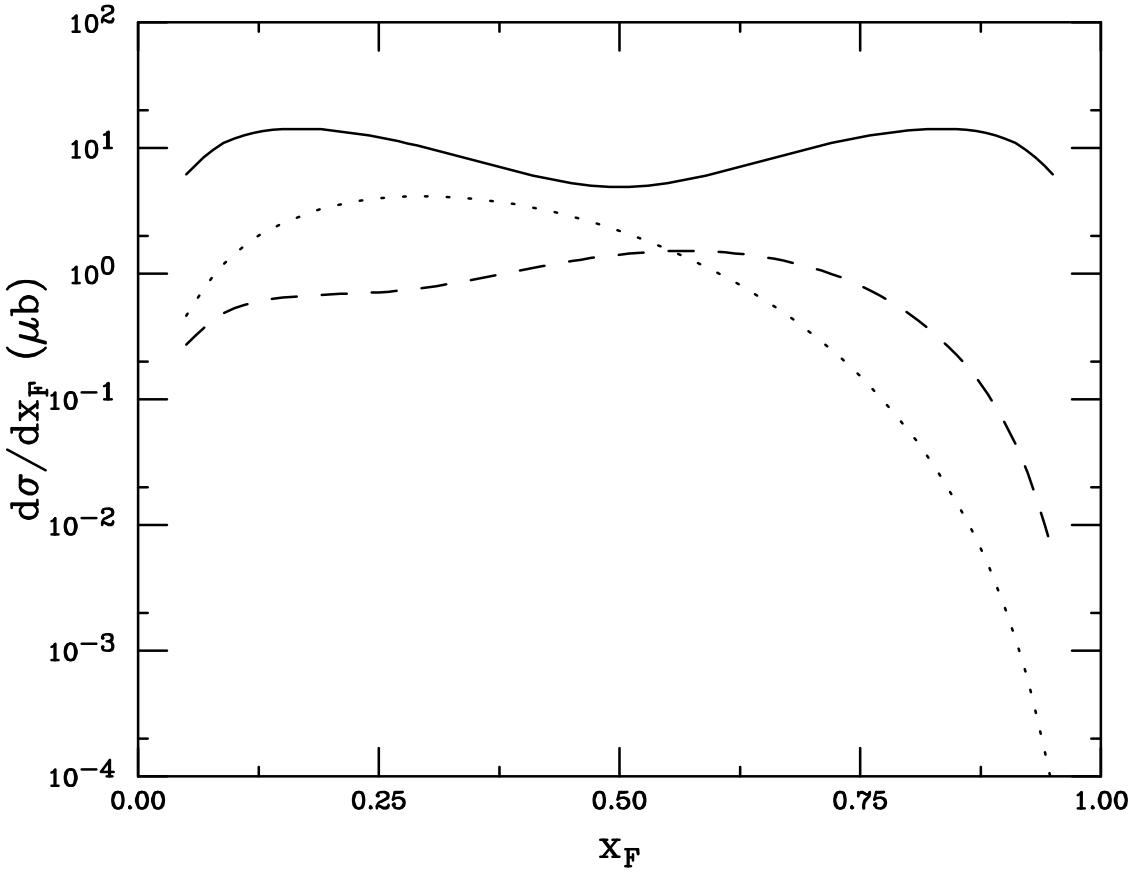

Figure 3.3: Intrinsic gluino higher twist contributions to intrinsic gluino $d\sigma_{i\tilde{g}}/dx_F$ in R-hadron production with $m_{\tilde{g}} = 1.2$ GeV. The solid curve is R^+, the dotted curve is R^0, and the dashed curve is S^0. Each distribution includes the contribution from independent uncorrelated fragmentation of a gluino.

Figures 3.4, 3.5, and 3.6 show the predicted R^+, S^0, and R^0 x_F distributions per nucleon in pp, pBe, and pCu interactions at 800 GeV calculated according to Eq. (3.16). Each figure includes all four gluino masses. As $x_F \to 0$ the x_F distributions of all targets are equal for a given $m_{\tilde{g}}$. This indicates the dominance of leading twist production at low x_F, independent of the final state. As $x_F \to 1$ the higher twist terms begin to contribute. These higher twist effects are suppressed in nuclear targets because of their slower relative growth as a function of A compared to the

leading twist A dependence. Although larger mass gluinos are more difficult to create, the relative contribution to the total cross section from higher-twist production in Eq. (3.16) increases with gluino mass because of the slower decrease of the intrinsic gluino contribution relative to the mass suppression of the leading twist cross section. The greater mass suppression of the leading twist cross section also influences the value of x_F where the higher twist contribution begins to appear. Increasing the gluino mass leads to intrinsic gluino effects appearing at lower x_F. This effect is seen in Figs. 3.4-3.6. When $m_{\tilde{g}} = 1.2$, I$\tilde{\text{G}}$ effects become obvious near $x_F \sim 0.5$ while I$\tilde{\text{G}}$ contributions begin to appear for $x_F \sim 0.2$ in R^0 production when $m_{\tilde{g}} = 5.0$ GeV.

Dramatic leading effects are predicted for the R^+ which, as pointed out above, shares three valence quarks with the proton in a minimal five-particle Fock state configuration. This characteristic "hardening" of the x_F distribution for $x_F > 0.6$ should be clear in a successful R^+ search. However, the leading effects are also present for the other particles. The S^0 is the next hardest distribution, sharing two valence quarks with the proton while the R^0 tends to be the softest, since no projectile valence quarks are shared.

For a clearer comparison of the leading effects predicted for each final state R-hadron, Figs. 3.7-3.10 show the R^+, S^0, and R^0 distributions together in pp interactions with $m_{\tilde{g}} = 1.2, 1.5, 3.5$, and 5.0 GeV respectively. The leading twist gluino distribution is also shown for comparison. In each case, the intrinsic contribution begins to emerge from the leading twist calculation between $x_F \sim 0.2$ and $x_F \sim 0.4$. In Fig. 3.8, with $m_{\tilde{g}} = 1.5$ GeV, the predicted R^+ enhancement at $x_F \sim 0.8$ is about 700 times larger than the leading twist prediction. At the same value of $m_{\tilde{g}}$ and

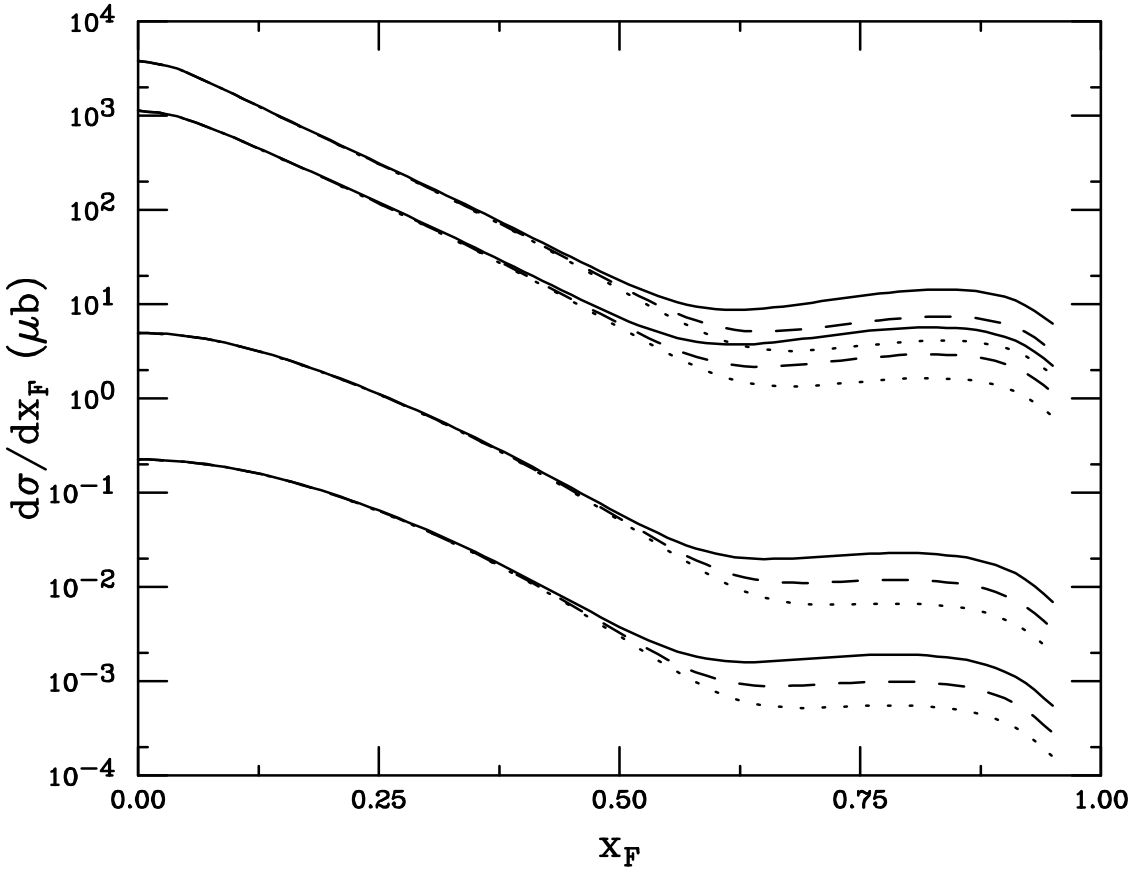

Figure 3.4: R^+ x_F distribution from 800 GeV protons on various targets. Four gluino masses are chosen, $m_{\tilde{g}} = 1.2$ GeV (top), 1.5 GeV, 3.5 GeV, and 5.0 GeV (bottom). For each mass, there is a triplet of curves representing different targets: proton (solid), Be (dashed), and Cu (dotted).

x_F, the S^0 contribution is about 40 times greater while the R^0 is just under 6 times greater. When the gluino mass is increased to $m_{\tilde{g}} = 5.0$ GeV, shown in Fig. 3.10, the R^0 dominates R-hadron yields for $x_F < 0.6$. This is a consequence of the increased $\langle x_F \rangle$ for single gluino fragmentation at the larger mass. Although the cross sections are small at $m_{\tilde{g}} = 5.0$ GeV since the gluino mass is comparable to the bottom mass, the predicted enhancements over the leading-twist baseline are quite large: 2.5×10^3 for the R^+, 1.6×10^3 for the S^0, and 281 for the R^0. The enhancements are in fact larger than those with smaller gluino masses due to the greater mass suppression of

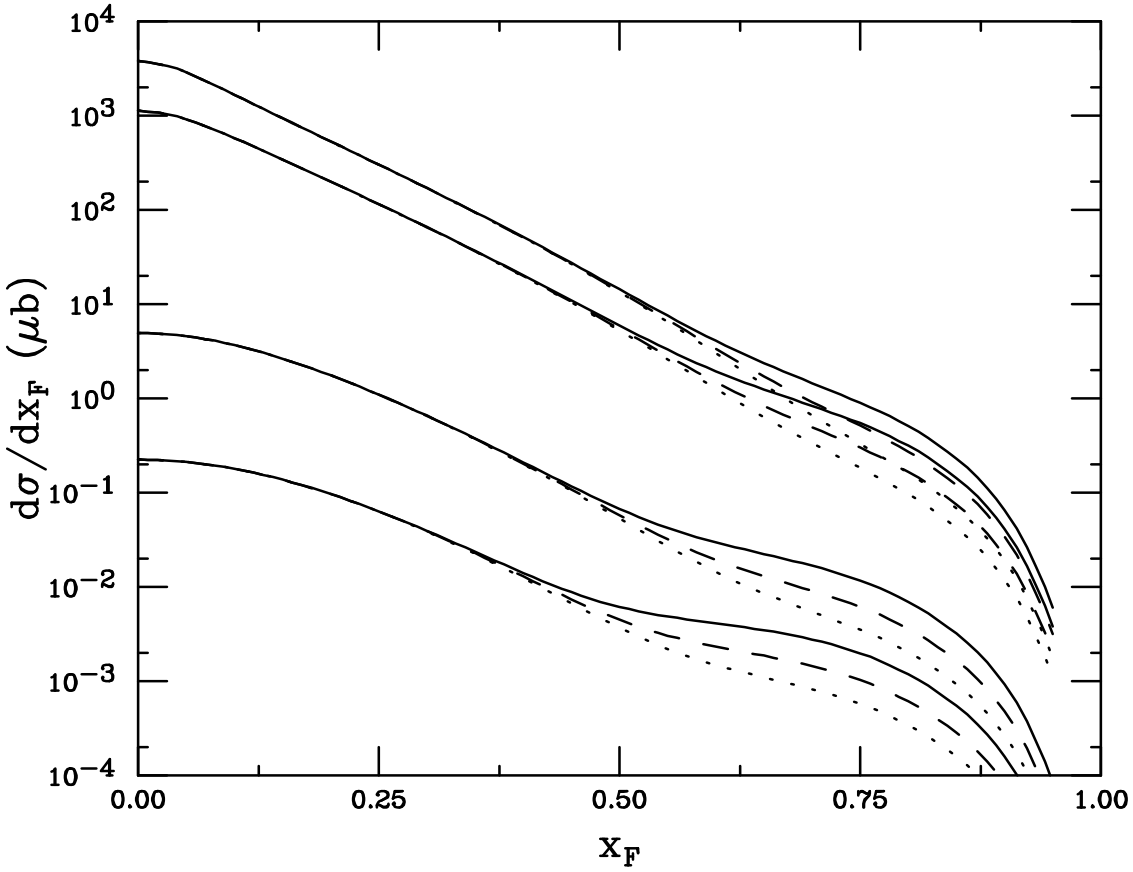

Figure 3.5: S^0 x_F distribution from 800 GeV protons on various targets. Four gluino masses are chosen, $m_{\tilde{g}} = 1.2$ GeV (top), 1.5 GeV, 3.5 GeV, and 5.0 GeV (bottom). For each mass, there is a triplet of curves representing different targets: proton (solid), Be (dashed), and Cu (dotted).

the leading twist cross section.

3.5 Conclusions

The light gluino window opens the possibility of non-trivial higher twist gluino contributions to the proton wave function. In analogy to charm hadroproduction, intrinsic gluino Fock components contribute to final state R-hadron formation, enhancing gluino production over leading twist parton fusion in the forward x_F region.

In this work, we have studied a "maximally leading" scenario for final state R-

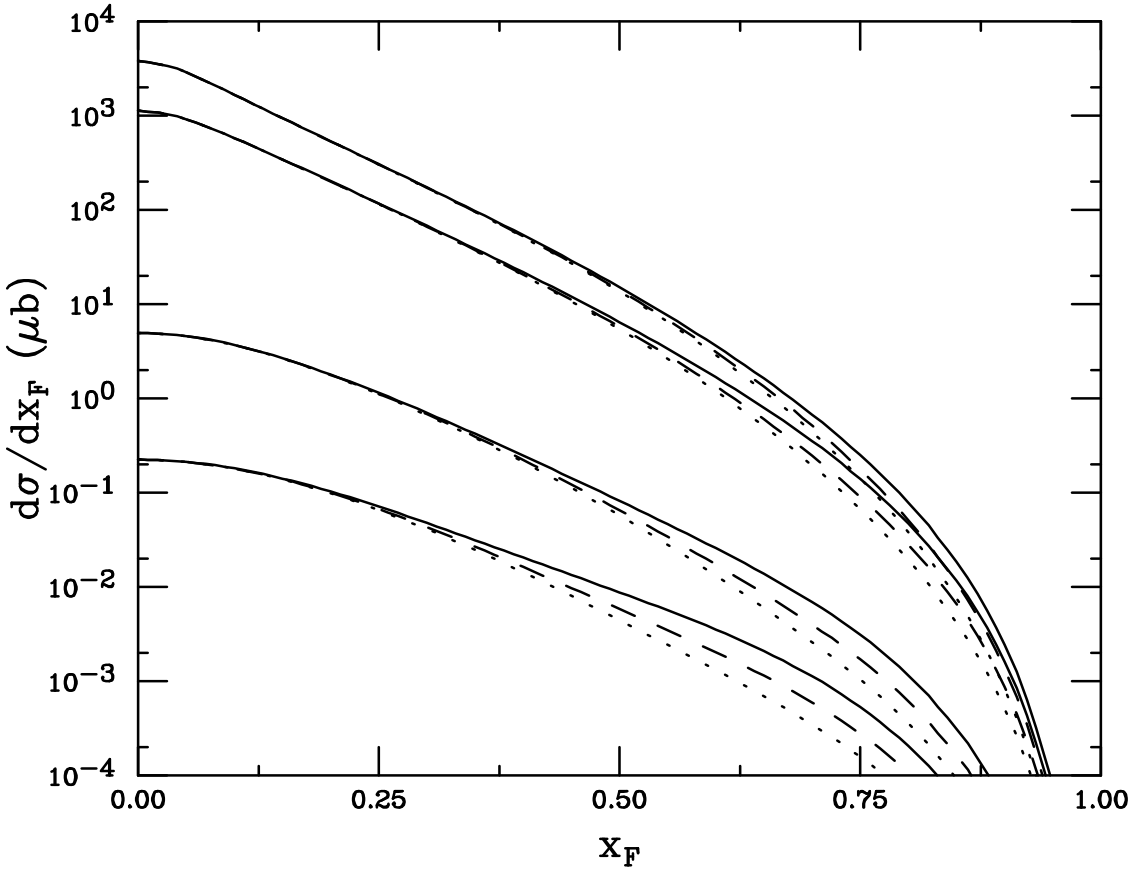

Figure 3.6: R^0 x_F distribution from 800 GeV protons on various targets. Four gluino masses are chosen, $m_{\tilde{g}} = 1.2$ GeV (top), 1.5 GeV, 3.5 GeV, and 5.0 GeV (bottom). For each mass, there is a triplet of curves representing different targets: proton (solid), Be (dashed), and Cu (dotted).

hadrons in pp and pA interactions at 800 GeV. Our model predicts that the contributions of higher-twist intrinsic states lead to strong flavor correlations between initial and final states for $x_F > 0.6$. The large intrinsic gluino enhancements at high x_F over the leading-twist predictions imply that this region of phase space could be especially appropriate for R-hadron searches in the light gluino scenario. For $m_{\tilde{g}}$ in the $1-5$ GeV range, a mass region where substantial evidence for the analogous intrinsic heavy quark states exists and for which our computational techniques should be most reliable, the enhancements are very significant (factors of several hundred to several

thousand being common). The magnitudes we predict for these enhancements may even be conservative since the increased color factor associated with intrinsic gluinos compared to intrinsic charm has been neglected.

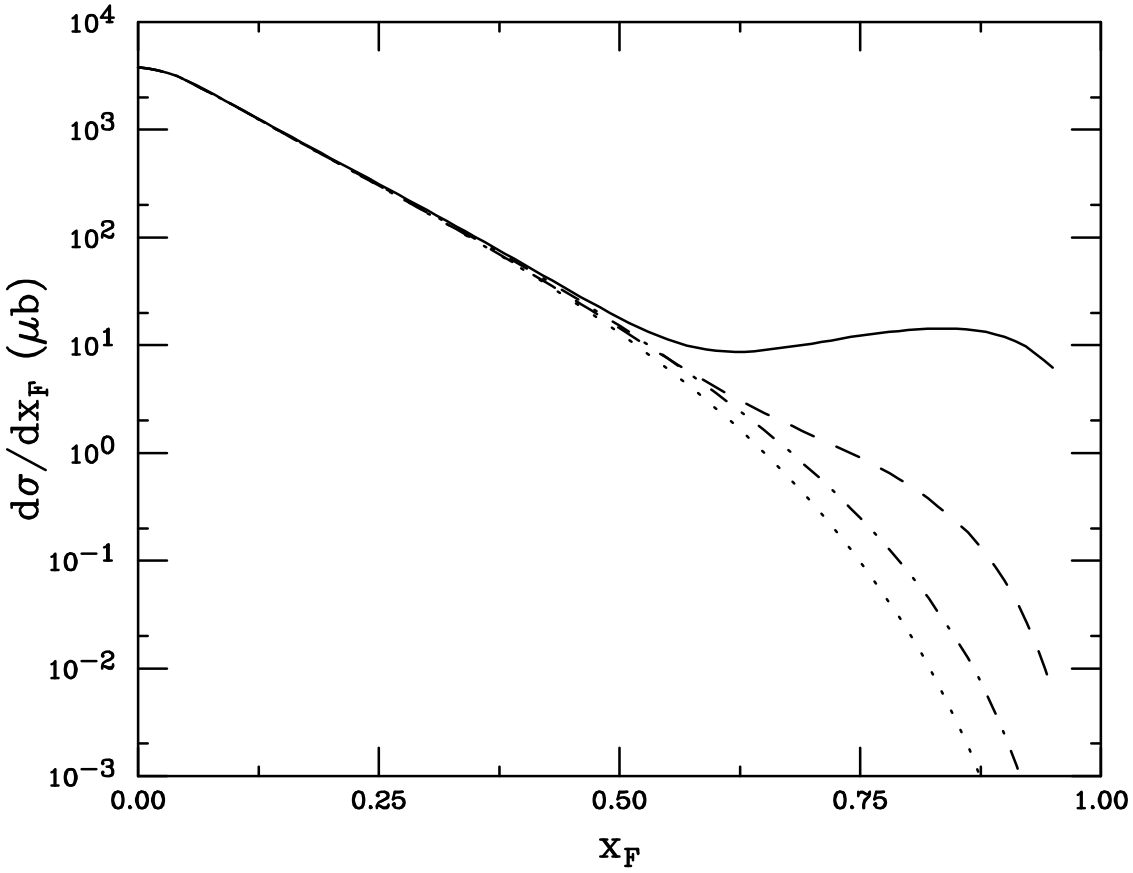

Figure 3.7: Intrinsic gluino enhancement to x_F distribution for various R-hadrons with $m_{\tilde{g}} = 1.2$ GeV. The lower curve is the fusion baseline for gluino production with a delta function fragmentation. The curves are R^+ (solid), S^0 (dashed), R^0 (dot-dashed), and the leading twist gluino production (dotted).

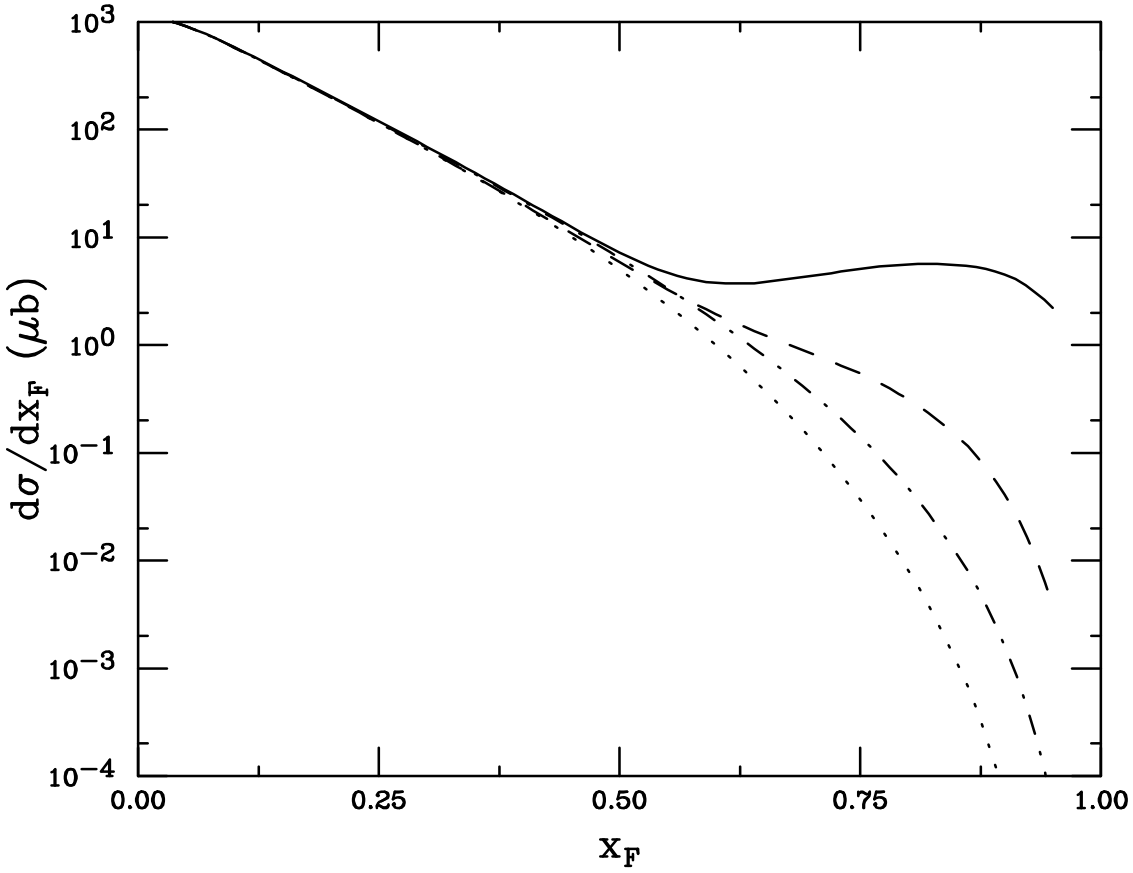

Figure 3.8: Intrinsic gluino enhancement to x_F distribution for various R-hadrons with $m_{\tilde{g}} = 1.5$ GeV. The lower curve is the fusion baseline for gluino production with a delta function fragmentation. The curves are R^+ (solid), S^0 (dashed), R^0 (dot-dashed), and the leading twist gluino production (dotted).

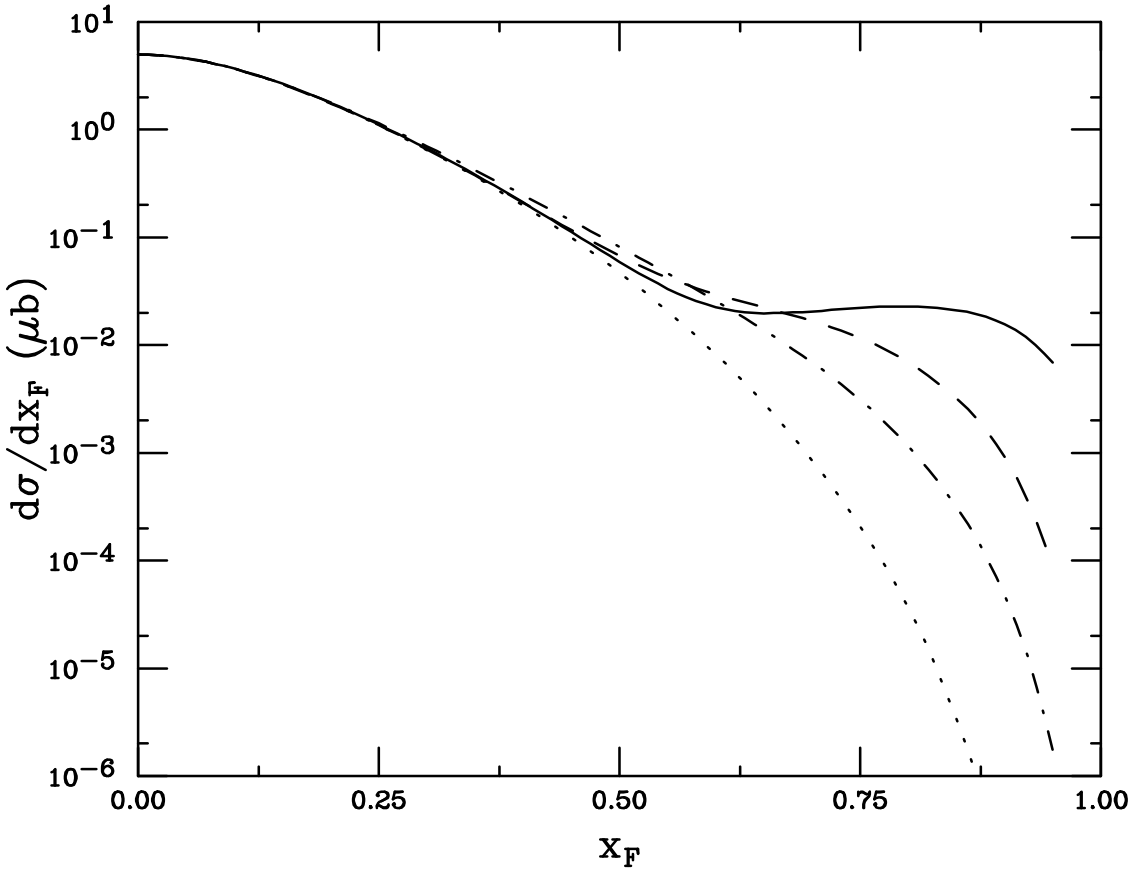

Figure 3.9: Intrinsic gluino enhancement to x_F distribution for various R-hadrons with $m_{\tilde{g}} = 3.5$ GeV. The lower curve is the fusion baseline for gluino production with a delta function fragmentation. The curves are R^+ (solid), S^0 (dashed), R^0 (dot-dashed), and the leading twist gluino production (dotted).

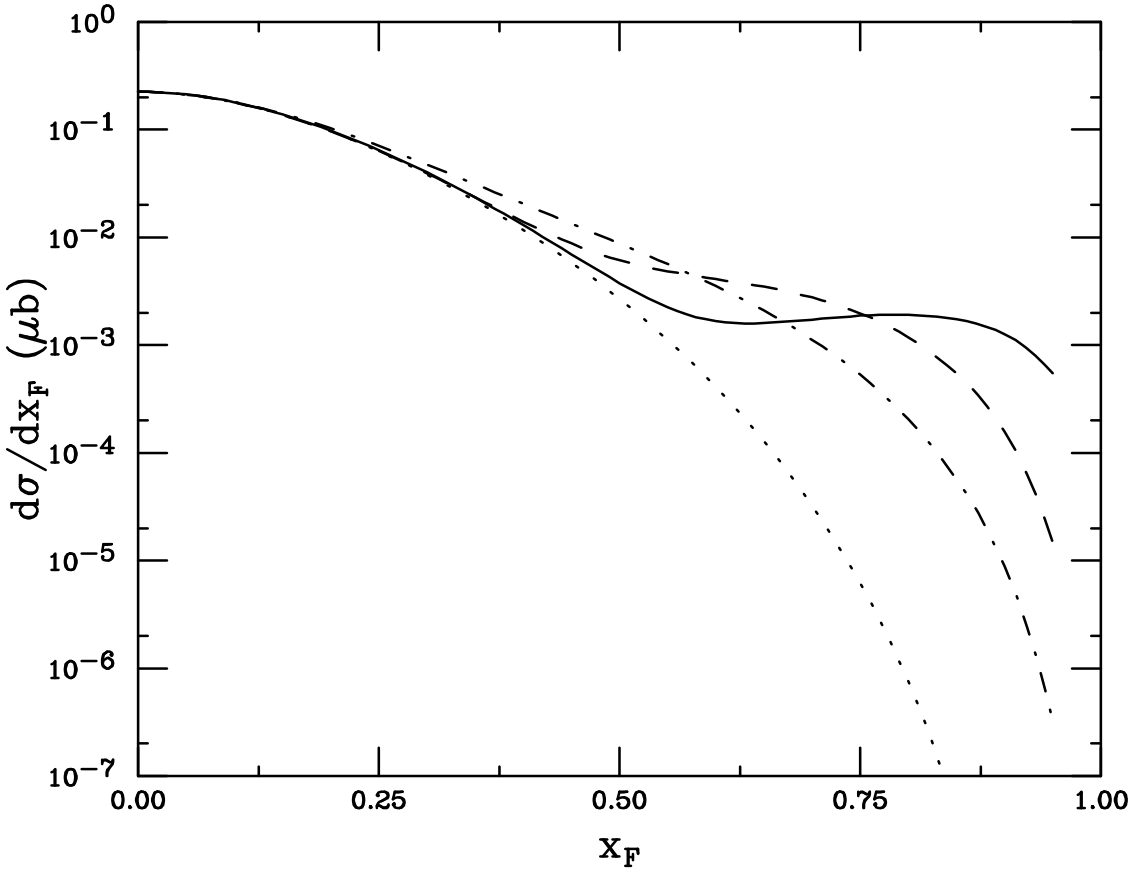

Figure 3.10: Intrinsic gluino enhancement to x_F distribution for various R-hadrons with $m_{\tilde{g}} = 5.0$ GeV. The lower curve is the fusion baseline for gluino production with a delta function fragmentation. The curves are R^+ (solid), S^0 (dashed), R^0 (dot-dashed), and the leading twist gluino production (dotted).

Chapter 4

Closing Remarks

Intrinsic models, such as those considered in this work, are interesting because they help illuminate the boundary between perturbative and nonperturbative QCD. Where data are available, intrinsic calculations are in overall agreement with experiment. This gives strong support for intrinsic heavy quark states and the subsequent initial state coalescence mechanisms presented herein. However, measurements in the large x_F region of phase space, where these effects are accentuated, are difficult and better statistics are still required. The best data concern D meson production with π and Σ^- beams. There is still plenty of room for exploration. Data concerning leading charm produced in pp and pA interactions are sparse while charm baryon production for all beams is still not well measured.

Since publication of the paper presented in Chapter 2, SELEX has completed data acquisition and has started their analysis. These data will provide the highest statistics for leading charm and leading charm-strange hadrons yet available. As analysis continues, comparisons with the predictions made in Chapter 2 will soon be possible.

There are also realistic, but somewhat more exotic, systems where the intrinsic charm model can be applied. There are those who want to look for doubly and triply charm baryons. The two-component model can be applied to these systems assuming one could handle the perturbative production of multiple heavy quark pairs. Moreover, the intrinsic charm model could realistically be applied to kaon beams where one would have leading D_s mesons and the associated leading-nonleading asymmetries.

Furthermore, large x measurements of the charm structure function in DIS may provide further support for intrinsic heavy quark states. With better statistics, if

anomalously high charm production is found at large x, this would confirm the EMC data which originally motivated the development of the intrinsic charm model.

Although somewhat speculative, intrinsic gluino states, as explored in Chapter 3, may be an inevitability of the light gluino scenario. A modified intrinsic charm model makes quantitative predictions about nontrivial intrinsic gluino enhancements to the x_F spectra of R-hadrons. These predictions may motivate experimentalists to consider investigating the large x_F region of phase space in their search for the light gluino.

One possible future project involves the calculation of the contribution of intrinsic strangeness to the hadroproduction of leading strange particles. Here the primary challenge will be to characterize the the leading twist contribution since pQCD will be unreliable. Furthermore, higher twist intrinsic strangeness contributions can be directly compared to strange quark parton distribution functions obtained from global analysis. This will give some insight into the mass scaling normalization methodology currently used for intrinsic states.

In closing, prospects for further exploring the presence of intrinsic states in hadrons look promising.

Appendix

Here we give the probability distributions for D^-, D^+, D_s^- and D_s^+ mesons and Λ_c^+, Σ_c^0, Ξ_c^0 and Ξ_c^+ baryons for production by the minimal and first three higher Fock state configurations from Σ^-, proton and π^- projectiles. The probability distributions for each final state are given in Figs. 3.12-2.6. We note that the predictions for Λ_c^+ and Σ_c^+ are identical in all cases because their quark content is the same. Recall that $P_{\rm ic}^5 = 0.31\%$, $P_{\rm icu}^7 = P_{\rm icd}^7 = 70.4\%\ P_{\rm ic}^5$ and $P_{\rm ics}^7 = 28.5\%\ P_{\rm ic}^5$.

We begin with the Σ^-. In the $|ddsc\overline{c}\rangle$ configuration, there are four final-state hadrons with a valence c quark ($2\Xi_c^0$, Σ_c^0 and J/ψ) and also four final-state hadrons with a valence $\overline{c}$ quark ($2D^-$, D_s^- and J/ψ). The $|ddsc\overline{c}q\overline{q}\rangle$ configurations where $q\overline{q} = u\overline{u}$, $d\overline{d}$ and $s\overline{s}$ allow coalescence production of eight possible final-state hadrons with a valence c and five possible final-state hadrons with a valence $\overline{c}$. When $q\overline{q} = u\overline{u}$, the possible hadrons produced by coalescence are $2\Xi_c^+$, Ξ_c^0, $2\Lambda_c^+$, Σ_c^0, D^0 and J/ψ with a valence c and $2D^-$, D_s^-, $\overline{D}^0$ and J/ψ with a valence $\overline{c}$. The $d\overline{d}$ configuration allows coalescence production of the following hadrons with a valence c quark, $3\Sigma_c^0$, $3\Xi_c^0$, D^+ and J/ψ, and, with a valence $\overline{c}$, $3D^-$, D_s^- and J/ψ. The $s\overline{s}$ configuration yields $4\Xi_c^0$, Σ_c^0, $\Omega_c^0(ssc)$, D_s^+ and J/ψ while the final-state valence $\overline{c}$ quarks hadrons are $2D^-$, $2D_s^-$ and J/ψ. We have:

$$\begin{aligned}
\frac{dP_{D^-}}{dx_F} &= \frac{1}{2}\left(\frac{1}{10}\frac{dP_{\rm ic}^{5F}}{dx_F} + \frac{1}{2}\frac{dP_{\rm ic}^{5C}}{dx_F}\right) + \frac{1}{2}\left(\frac{1}{10}\frac{dP_{\rm icu}^{7F}}{dx_F} + \frac{2}{5}\frac{dP_{\rm icu}^{7C}}{dx_F}\right) \\
&\quad + \frac{1}{2}\left(\frac{1}{10}\frac{dP_{\rm icd}^{7F}}{dx_F} + \frac{3}{5}\frac{dP_{\rm icd}^{7C}}{dx_F}\right) + \frac{1}{2}\left(\frac{1}{10}\frac{dP_{\rm ics}^{7F}}{dx_F} + \frac{2}{5}\frac{dP_{\rm ics}^{7C}}{dx_F}\right) \qquad \text{(A-1)} \\
\frac{dP_{D^+}}{dx_F} &= \frac{1}{10}\frac{dP_{\rm ic}^{5F}}{dx_F} + \frac{1}{10}\frac{dP_{\rm icu}^{7F}}{dx_F} + \frac{1}{2}\left(\frac{1}{10}\frac{dP_{\rm icd}^{7F}}{dx_F} + \frac{1}{8}\frac{dP_{\rm icd}^{7C}}{dx_F}\right) + \frac{1}{10}\frac{dP_{\rm ics}^{7F}}{dx_F} \qquad \text{(A-2)} \\
\frac{dP_{\Lambda_c^+}}{dx_F} &= \frac{1}{10}\frac{dP_{\rm ic}^{5F}}{dx_F} + \frac{1}{2}\left(\frac{1}{10}\frac{dP_{\rm icu}^{7F}}{dx_F} + \frac{1}{4}\frac{dP_{\rm icu}^{7C}}{dx_F}\right) + \frac{1}{10}\frac{dP_{\rm icd}^{7F}}{dx_F} + \frac{1}{10}\frac{dP_{\rm ics}^{7F}}{dx_F} \qquad \text{(A-3)}
\end{aligned}$$

$$\frac{dP_{\Sigma_c^0}}{dx_F} = \frac{1}{2}\left(\frac{1}{10}\frac{dP_{\rm ic}^{5F}}{dx_F}+\frac{1}{4}\frac{dP_{\rm ic}^{5C}}{dx_F}\right)+\frac{1}{2}\left(\frac{1}{10}\frac{dP_{\rm icu}^{7F}}{dx_F}+\frac{1}{8}\frac{dP_{\rm icu}^{7C}}{dx_F}\right)$$
$$+\frac{1}{2}\left(\frac{1}{10}\frac{dP_{\rm icd}^{7F}}{dx_F}+\frac{3}{8}\frac{dP_{\rm icd}^{7C}}{dx_F}\right)+\frac{1}{2}\left(\frac{1}{10}\frac{dP_{\rm ics}^{7F}}{dx_F}+\frac{1}{8}\frac{dP_{\rm ics}^{7C}}{dx_F}\right) \quad \text{(A-4)}$$

$$\frac{dP_{D_s^-}}{dx_F} = \frac{1}{2}\left(\frac{1}{10}\frac{dP_{\rm ic}^{5F}}{dx_F}+\frac{1}{4}\frac{dP_{\rm ic}^{5C}}{dx_F}\right)+\frac{1}{2}\left(\frac{1}{10}\frac{dP_{\rm icu}^{7F}}{dx_F}+\frac{1}{5}\frac{dP_{\rm icu}^{7C}}{dx_F}\right)$$
$$+\frac{1}{2}\left(\frac{1}{10}\frac{dP_{\rm icd}^{7F}}{dx_F}+\frac{1}{5}\frac{dP_{\rm icd}^{7C}}{dx_F}\right)+\frac{1}{2}\left(\frac{1}{10}\frac{dP_{\rm ics}^{7F}}{dx_F}+\frac{2}{5}\frac{dP_{\rm ics}^{7C}}{dx_F}\right) \quad \text{(A-5)}$$

$$\frac{dP_{D_s^+}}{dx_F} = \frac{1}{10}\frac{dP_{\rm ic}^{5F}}{dx_F}+\frac{1}{10}\frac{dP_{\rm icu}^{7F}}{dx_F}+\frac{1}{10}\frac{dP_{\rm icd}^{7F}}{dx_F}+\frac{1}{2}\left(\frac{1}{10}\frac{dP_{\rm ics}^{7F}}{dx_F}+\frac{1}{8}\frac{dP_{\rm ics}^{7C}}{dx_F}\right) \quad \text{(A-6)}$$

$$\frac{dP_{\Xi_c^0}}{dx_F} = \frac{1}{2}\left(\frac{1}{10}\frac{dP_{\rm ic}^{5F}}{dx_F}+\frac{1}{2}\frac{dP_{\rm ic}^{5C}}{dx_F}\right)+\frac{1}{2}\left(\frac{1}{10}\frac{dP_{\rm icu}^{7F}}{dx_F}+\frac{1}{8}\frac{dP_{\rm icu}^{7C}}{dx_F}\right)$$
$$+\frac{1}{2}\left(\frac{1}{10}\frac{dP_{\rm icd}^{7F}}{dx_F}+\frac{3}{8}\frac{dP_{\rm icd}^{7C}}{dx_F}\right)+\frac{1}{2}\left(\frac{1}{10}\frac{dP_{\rm ics}^{7F}}{dx_F}+\frac{1}{2}\frac{dP_{\rm ics}^{7C}}{dx_F}\right) \quad \text{(A-7)}$$

$$\frac{dP_{\Xi_c^+}}{dx_F} = \frac{1}{10}\frac{dP_{\rm ic}^{5F}}{dx_F}+\frac{1}{2}\left(\frac{1}{10}\frac{dP_{\rm icu}^{7F}}{dx_F}+\frac{1}{4}\frac{dP_{\rm icu}^{7C}}{dx_F}\right)+\frac{1}{10}\frac{dP_{\rm icd}^{7F}}{dx_F}+\frac{1}{10}\frac{dP_{\rm ics}^{7F}}{dx_F}\ . \quad \text{(A-8)}$$

Fewer charm hadrons are produced by coalescence from the five-quark configuration of the proton since it has no valence strange quark. In the $|uudc\overline{c}\rangle$ configuration, there are four final-state hadrons with a valence c quark ($2\Lambda_c^+$, $\Sigma_c^{++}(uuc)$ and J/ψ) and also four final-state hadrons with a valence $\overline{c}$ quark ($2\overline{D}^0$, D^- and J/ψ). The $|uudc\overline{c}q\overline{q}\rangle$ configurations allow coalescence production of eight possible final-state hadrons with a valence c and five possible final-state hadrons with a valence $\overline{c}$. When $q\overline{q}=u\overline{u}$, the possible hadrons produced by coalescence are: $3\Lambda_c^+$, $3\Sigma_c^{++}$, D^0 and J/ψ with a valence c and D^-, $3\overline{D}^0$ and J/ψ with a valence $\overline{c}$. The $d\overline{d}$ configuration allows coalescence production of the following hadrons with a valence c quark, $4\Lambda_c^+$, Σ_c^0, Σ_c^{++}, D^+ and J/ψ, and, with a valence $\overline{c}$, $2D^-$, $2\overline{D}^0$ and J/ψ. The $s\overline{s}$ configuration yields $2\Xi_c^+$, Ξ_c^0, $2\Lambda_c^+$, Σ_c^{++}, D_s^+ and J/ψ while the final-state valence $\overline{c}$ quarks hadrons are $2D^-$, $\overline{D}^0$, D_s^- and J/ψ. Then:

$$\frac{dP_{D^-}}{dx_F} = \frac{1}{2}\left(\frac{1}{10}\frac{dP_{\rm ic}^{5F}}{dx_F}+\frac{1}{4}\frac{dP_{\rm ic}^{5C}}{dx_F}\right)+\frac{1}{2}\left(\frac{1}{10}\frac{dP_{\rm icu}^{7F}}{dx_F}+\frac{1}{5}\frac{dP_{\rm icu}^{7C}}{dx_F}\right)$$

$$+\frac{1}{2}\left(\frac{1}{10}\frac{dP^{7F}_{\rm icd}}{dx_F}+\frac{2}{5}\frac{dP^{7C}_{\rm icd}}{dx_F}\right)+\frac{1}{2}\left(\frac{1}{10}\frac{dP^{7F}_{\rm ics}}{dx_F}+\frac{1}{5}\frac{dP^{7C}_{\rm ics}}{dx_F}\right) \quad \text{(A-9)}$$

$$\frac{dP_{D^+}}{dx_F} = \frac{1}{10}\frac{dP^{5F}_{\rm ic}}{dx_F}+\frac{1}{10}\frac{dP^{7F}_{\rm icu}}{dx_F}+\frac{1}{2}\left(\frac{1}{10}\frac{dP^{7F}_{\rm icd}}{dx_F}+\frac{1}{8}\frac{dP^{7C}_{\rm icd}}{dx_F}\right)+\frac{1}{10}\frac{dP^{7F}_{\rm ics}}{dx_F} \quad \text{(A-10)}$$

$$\frac{dP_{\Lambda_c^+}}{dx_F} = \frac{1}{2}\left(\frac{1}{10}\frac{dP^{5F}_{\rm ic}}{dx_F}+\frac{1}{2}\frac{dP^{5C}_{\rm ic}}{dx_F}\right)+\frac{1}{2}\left(\frac{1}{10}\frac{dP^{7F}_{\rm icu}}{dx_F}+\frac{3}{8}\frac{dP^{7C}_{\rm icu}}{dx_F}\right)$$
$$+\frac{1}{2}\left(\frac{1}{10}\frac{dP^{7F}_{\rm icd}}{dx_F}+\frac{1}{2}\frac{dP^{7C}_{\rm icd}}{dx_F}\right)+\frac{1}{2}\left(\frac{1}{10}\frac{dP^{7F}_{\rm ics}}{dx_F}+\frac{1}{4}\frac{dP^{7C}_{\rm ics}}{dx_F}\right) \quad \text{(A-11)}$$

$$\frac{dP_{\Sigma_c^0}}{dx_F} = \frac{1}{10}\frac{dP^{5F}_{\rm ic}}{dx_F}+\frac{1}{10}\frac{dP^{7F}_{\rm icu}}{dx_F}+\frac{1}{2}\left(\frac{1}{10}\frac{dP^{7F}_{\rm icd}}{dx_F}+\frac{1}{8}\frac{dP^{7C}_{\rm icd}}{dx_F}\right)+\frac{1}{10}\frac{dP^{7F}_{\rm ics}}{dx_F} \quad \text{(A-12)}$$

$$\frac{dP_{D_s^-}}{dx_F} = \frac{1}{10}\frac{dP^{5F}_{\rm ic}}{dx_F}+\frac{1}{10}\frac{dP^{7F}_{\rm icu}}{dx_F}+\frac{1}{10}\frac{dP^{7F}_{\rm icd}}{dx_F}+\frac{1}{2}\left(\frac{1}{10}\frac{dP^{7F}_{\rm ics}}{dx_F}+\frac{1}{5}\frac{dP^{7C}_{\rm ics}}{dx_F}\right) \quad \text{(A-13)}$$

$$\frac{dP_{D_s^+}}{dx_F} = \frac{1}{10}\frac{dP^{5F}_{\rm ic}}{dx_F}+\frac{1}{10}\frac{dP^{7F}_{\rm icu}}{dx_F}+\frac{1}{10}\frac{dP^{7F}_{\rm icd}}{dx_F}+\frac{1}{2}\left(\frac{1}{10}\frac{dP^{7F}_{\rm ics}}{dx_F}+\frac{1}{8}\frac{dP^{7C}_{\rm ics}}{dx_F}\right) \quad \text{(A-14)}$$

$$\frac{dP_{\Xi_c^0}}{dx_F} = \frac{1}{10}\frac{dP^{5F}_{\rm ic}}{dx_F}+\frac{1}{10}\frac{dP^{7F}_{\rm icu}}{dx_F}+\frac{1}{10}\frac{dP^{7F}_{\rm icd}}{dx_F}+\frac{1}{2}\left(\frac{1}{10}\frac{dP^{7F}_{\rm ics}}{dx_F}+\frac{1}{8}\frac{dP^{7C}_{\rm ics}}{dx_F}\right) \quad \text{(A-15)}$$

$$\frac{dP_{\Xi_c^+}}{dx_F} = \frac{1}{10}\frac{dP^{5F}_{\rm ic}}{dx_F}+\frac{1}{10}\frac{dP^{7F}_{\rm icu}}{dx_F}+\frac{1}{10}\frac{dP^{7F}_{\rm icd}}{dx_F}+\frac{1}{2}\left(\frac{1}{10}\frac{dP^{7F}_{\rm ics}}{dx_F}+\frac{1}{4}\frac{dP^{7C}_{\rm ics}}{dx_F}\right) . \quad \text{(A-16)}$$

Charm and anticharm hadron production is more symmetric from the π^- because the projectile contains a valence antiquark of its own. In the minimal $|\overline{u}dc\overline{c}\rangle$ configuration, there are two possible final-state hadrons with a valence c quark (D^0 and J/ψ) and also two possible final-state hadrons with a valence $\overline{c}$ quark (D^- and J/ψ). The $|\overline{u}dc\overline{c}q\overline{q}\rangle$ configurations allow coalescence production of four possible final-state hadrons with a valence c and likewise four possible final-state hadrons with a valence $\overline{c}$. When $q\overline{q} = u\overline{u}$, the possible hadrons produced by coalescence are: Λ_c^+, $2D^0$ and J/ψ with a valence c and D^-, $\overline{D}^0$, $\overline{\Sigma}_c^{++}$ and J/ψ with a valence $\overline{c}$. The $d\overline{d}$ configuration allows coalescence production of the following hadrons with a valence c quark, Σ_c^0, D^0, D^+ and J/ψ, and, with a valence $\overline{c}$, D^-, $\overline{D}^0$, $\overline{\Lambda}_c^+$ and J/ψ. The $s\overline{s}$ configuration yields Ξ_c^0, D_s^+, D^0 and J/ψ with a valence c while the possible final-state valence

$\overline{c}$ quarks hadrons are D^-, D_s^-, $\overline{\Xi}_c^+$ and J/ψ. In this case:

$$\begin{aligned}
\frac{dP_{D^-}}{dx_F} &= \frac{1}{2}\left(\frac{1}{10}\frac{dP_{\rm ic}^{4F}}{dx_F}+\frac{1}{2}\frac{dP_{\rm ic}^{4C}}{dx_F}\right)+\frac{1}{2}\left(\frac{1}{10}\frac{dP_{\rm icu}^{6F}}{dx_F}+\frac{1}{4}\frac{dP_{\rm icu}^{6C}}{dx_F}\right) \\
&\quad +\frac{1}{2}\left(\frac{1}{10}\frac{dP_{\rm icd}^{6F}}{dx_F}+\frac{1}{2}\frac{dP_{\rm icd}^{6C}}{dx_F}\right)+\frac{1}{2}\left(\frac{1}{10}\frac{dP_{\rm ics}^{6F}}{dx_F}+\frac{1}{4}\frac{dP_{\rm ics}^{6C}}{dx_F}\right) \qquad \text{(A-17)} \\
\frac{dP_{D^+}}{dx_F} &= \frac{1}{10}\frac{dP_{\rm ic}^{4F}}{dx_F}+\frac{1}{10}\frac{dP_{\rm icu}^{6F}}{dx_F}+\frac{1}{2}\left(\frac{1}{10}\frac{dP_{\rm icd}^{6F}}{dx_F}+\frac{1}{4}\frac{dP_{\rm icd}^{6C}}{dx_F}\right)+\frac{1}{10}\frac{dP_{\rm ics}^{6F}}{dx_F} \qquad \text{(A-18)} \\
\frac{dP_{\Lambda_c^+}}{dx_F} &= \frac{1}{10}\frac{dP_{\rm ic}^{4F}}{dx_F}+\frac{1}{2}\left(\frac{1}{10}\frac{dP_{\rm icu}^{6F}}{dx_F}+\frac{1}{4}\frac{dP_{\rm icu}^{6C}}{dx_F}\right)+\frac{1}{10}\frac{dP_{\rm icd}^{6F}}{dx_F}+\frac{1}{10}\frac{dP_{\rm ics}^{6F}}{dx_F} \qquad \text{(A-19)} \\
\frac{dP_{\Sigma_c^0}}{dx_F} &= \frac{1}{10}\frac{dP_{\rm ic}^{4F}}{dx_F}+\frac{1}{10}\frac{dP_{\rm icu}^{6F}}{dx_F}+\frac{1}{2}\left(\frac{1}{10}\frac{dP_{\rm icd}^{6F}}{dx_F}+\frac{1}{4}\frac{dP_{\rm icd}^{6C}}{dx_F}\right)+\frac{1}{10}\frac{dP_{\rm ics}^{6F}}{dx_F} \qquad \text{(A-20)} \\
\frac{dP_{D_s^-}}{dx_F} &= \frac{1}{10}\frac{dP_{\rm ic}^{4F}}{dx_F}+\frac{1}{10}\frac{dP_{\rm icu}^{6F}}{dx_F}+\frac{1}{10}\frac{dP_{\rm icd}^{6F}}{dx_F}+\frac{1}{2}\left(\frac{1}{10}\frac{dP_{\rm ics}^{6F}}{dx_F}+\frac{1}{4}\frac{dP_{\rm ics}^{6C}}{dx_F}\right) \qquad \text{(A-21)} \\
\frac{dP_{D_s^+}}{dx_F} &= \frac{1}{10}\frac{dP_{\rm ic}^{4F}}{dx_F}+\frac{1}{10}\frac{dP_{\rm icu}^{6F}}{dx_F}+\frac{1}{10}\frac{dP_{\rm icd}^{6F}}{dx_F}+\frac{1}{2}\left(\frac{1}{10}\frac{dP_{\rm ics}^{6F}}{dx_F}+\frac{1}{4}\frac{dP_{\rm ics}^{6C}}{dx_F}\right) \qquad \text{(A-22)} \\
\frac{dP_{\Xi_c^0}}{dx_F} &= \frac{1}{10}\frac{dP_{\rm ic}^{4F}}{dx_F}+\frac{1}{10}\frac{dP_{\rm icu}^{6F}}{dx_F}+\frac{1}{10}\frac{dP_{\rm icd}^{6F}}{dx_F}+\frac{1}{2}\left(\frac{1}{10}\frac{dP_{\rm ics}^{6F}}{dx_F}+\frac{1}{4}\frac{dP_{\rm ics}^{6C}}{dx_F}\right) \qquad \text{(A-23)} \\
\frac{dP_{\Xi_c^+}}{dx_F} &= \frac{1}{10}\frac{dP_{\rm ic}^{4F}}{dx_F}+\frac{1}{10}\frac{dP_{\rm icu}^{6F}}{dx_F}+\frac{1}{10}\frac{dP_{\rm icd}^{6F}}{dx_F}+\frac{1}{10}\frac{dP_{\rm ics}^{6F}}{dx_F}\ . \qquad \text{(A-24)}
\end{aligned}$$

Bibliography

[1] F. Halzen and A. Martin, *Quarks and Leptons*, Wiley and Sons (1984).

[2] R.P. Feynman, *Photon-Hadron Interactions*, Addison Wesley (1972).

[3] M. Perl, *High Energy Hadron Physics*, Wiley and Sons (1974).

[4] M. Creutz, *Quarks, Gluons, and Lattices*, Cambridge University Press (1983).

[5] R.K. Ellis, in *Physics at the 100 GeV Scale*, Proceedings of the 17$^{\text{th}}$ SLAC Summer Institute, Stanford, California, 1989, edited by E.C. Brennan (SLAC Report No. 361) 45.

[6] J. Badier *et al.* (NA3 Collab.), Z. Phys. **C20** (1983) 101.

[7] J. Badier *et al.* (NA3 Collab.), Phys. Lett. **114B** (1982) 457.

[8] J. Badier *et al.* (NA3 Collab.), Phys. Lett. **158B** (1985) 85.

[9] J.J. Aubert *et al.* (EMC Collab.), Phys. Lett. **110B** (1982) 73.

[10] C. Akerlof *et al.* (E537 Collab.), Phys. Rev. **D48** (1993) 5067.

[11] M.I. Adamovich *et al.* (WA82 Collab.), Phys. Lett. **B305** (1993) 402.

[12] G.A. Alves *et al.* (E769 Collab.), Phys. Rev. Lett. **72** (1994) 812.

[13] R. Werding (WA89 Collab.), in Proceedings of *ICHEP94*, 27$^{\text{th}}$ International Conference on High Energy Physics, Glasgow, Scotland (1994).

[14] M.I. Adamovich *et al.* (WA89 Collab.), Eur. Phys. J. **C8** (1999) 593.

[15] E. Ramberg in *Hyperons, Charm and Beauty Hadrons*, Proceedings of the 2$^{\text{nd}}$ International Conference on Hyperons, Charm and Beauty Hadrons, Montreal, Canada, 1996, edited by C.S. Kalman *et al.*, Nucl. Phys. **B** (Proc. Suppl.) **55A** (1997) 173.

[16] S.J. Brodsky, J.F. Gunion and D.E. Soper, Phys. Rev. **D36** (1987) 2710.

[17] S.J. Brodsky, P. Hoyer, C. Peterson and N. Sakai, Phys. Lett. **B93** (1980) 451; S. J. Brodsky, C. Peterson and N. Sakai, Phys. Rev. **D23** (1981) 2745.

[18] S.J. Brodsky, P. Hoyer, A.H. Mueller and W.-K. Tang, Nucl. Phys. **B369** (1992) 519.

[19] W.-K. Tang, Invited talk at Workshop on the Future of High Sensitivity Charm Experiments: CHARM2000, Batavia, IL, p. 251 (hep-ph/9408372).

[20] P. Hoyer, Acta Phys. Polon. **B23** (1992) 1145.

[21] G.P. Lepage, S.J. Brodsky, Phys. Rev. **D22** (1980) 2157.

[22] R. Vogt and S.J. Brodsky, Nucl. Phys. **B438** (1995) 261.

[23] G. R. Farrar, Phys. Rev. Lett. **51** (1995) 3904; *ibid.* **76** (1996) 4111.

[24] G. R. Farrar, Nucl. Phys. **B** (Proc. Suppl.) **62** (1998) 485.

[25] A. Alavi-Harati *et al.* (KTeV Collab.), Phys. Rev. Lett. **B3** (1999) 2128.

[26] J. Adams *et al.* (KTeV Collab.), Phys. Rev. Lett. **79** (1997) 4083.

[27] I.F. Albuquerque *et al.* (E761 Collab.), Phys. Rev. Lett. **78** (1997) 3252.

[28] L. Clavelli, UA-HEP-99-4, hep-ph/9908342.

[29] T. Gutierrez and R. Vogt, Nucl. Phys. **B539** (1999) 189.

[30] T.D. Gutierrez, R. Vogt, J.F. Gunion, LBNL-45042, UCD-2000-06, hep-ph/0002046.

[31] E.M. Aitala *et al.* (E791 Collab.), Phys. Lett. **B371** (1996) 157.

[32] M. Aguilar-Benitez *et al.* (LEBC-EHS Collab.), Phys. Lett. **161B** (1985) 400; Z. Phys. **C31** (1986) 491.

[33] S. Barlag *et al.* (ACCMOR Collab.), Z. Phys. **C49** (1991) 555.

[34] J.C. Collins, D.E. Soper and G. Sterman, *Perturbative QCD*, ed. A. H. Mueller (World Scientific, Singapore, 1989). G. Bodwin, Phys. Rev. **D31** (1985) 2616, **D34** (1986) 3932. J. Qiu and G. Sterman, Nucl. Phys. **B353** (1991) 105,137.

[35] E.M. Aitala *et al.* (E791 Collab.), Phys. Lett. **B411** (1997) 230.

[36] R. Vogt and S.J. Brodsky, Nucl. Phys. **B478** (1996) 311.

[37] R. Vogt, S.J. Brodsky and P. Hoyer, Nucl. Phys. **B360** (1991) 67.

[38] R. Vogt, S.J. Brodsky and P. Hoyer, Nucl. Phys. **B383** (1992) 643.

[39] T. Sjöstrand, Comput. Phys. Commun. **82** (1994) 74. Program updates and documentation can be found at *http://www.thep.lu.se/tf2/staff/torbjorn/Pythia.html.*

[40] R.C. Hwa, Phys. Rev. **D27** (1983) 653; Phys. Rev. **D51** (1995) 85.

[41] V. A. Bednyakov, Dubna preprint JINR E2-94-79 (1994), Mod. Phys. Lett. **A10** (1995) 61; V.G. Kartvelishvili, A.K. Likhoded, and S.R. Slobospitskii, Sov. J. Nucl. Phys. **33**(3) (1981) 434 [Yad. Fiz. **33** (1981) 832].

[42] R. Vogt, Z. Phys. **C71** (1996) 475.

[43] S. Frixione, M.L. Mangano, P. Nason, and G. Ridolfi, Nucl. Phys. **B431** (1994) 453.

[44] M. Glück, E. Reya, A. Vogt, Z. Phys. **C67** (1995) 433.

[45] A.D. Martin, R.G. Roberts and W.J. Stirling, Phys. Lett. **B306** (1993) 145.

[46] C. Peterson, D. Schlatter, I. Schmitt, and P. Zerwas, Phys. Rev. **D27** (1983) 105.

[47] J. Chirn, in proceedings of the 'International Symposium on the Production and Decay of Heavy Flavors', Stanford, CA, edited by E. Bloom and A. Fridman, (1987) 131.

[48] M. Aguilar-Benitez *et al.* (LEBC-EHS Collab.), Phys. Lett. **B189** (1987) 476.

[49] S. Barlag *et al.* (ACCMOR Collab.), Phys. Lett. **B247** (1990) 113.

[50] M. Glück, E. Reya, and A. Vogt, Z. Phys. **C53** (1992) 651.

[51] P.J. Sutton, A.D. Martin, R.G. Roberts and W.J. Stirling, Phys. Rev. **D45** (1992) 2349.

[52] T. Sjöstrand, private communication.

[53] P. Hoyer and S.J. Brodsky, in proceedings of the 'Topical Conference on Particle Production Near Threshold', Nashville, TN, edited by H. Hann and E.J. Stephenson (1990) 238.

[54] E. Hoffmann and R. Moore, Z. Phys. **C20** (1983) 71.

[55] B.W. Harris, J. Smith, and R. Vogt, Nucl. Phys. **B461** (1996) 181.

[56] R. Vogt and S.J. Brodsky, Phys. Lett. **B349** (1995) 569.

[57] R. Vogt, Nucl. Phys. **B446**, (1995) 159.

[58] M.I. Adamovich *et al.* (BEATRICE Collab.), Nucl. Phys. **B495** (1997) 3.

[59] B.-Q. Ma and S.J. Brodsky, in proceedings of the ICTP Conference on Perspectives in Hadronic Physics, Trieste, 1997, hep-ph/9707408.

[60] S. Paiva *et al.*, Mod. Phys. Lett. **A13** (1998) 2715.

[61] C.H. Chen, M. Drees, and J.F. Gunion, Phys. Rev. **D55** (1997) 330.

[62] S. Raby, Phys. Rev. **D56** (1997) 2852; Phys. Lett. **B422** (1998) 158.

[63] P.M. Tuts *et al.* Phys. Lett. **B186** (1987) 233.

[64] F. Csikor and Z. Fodor, Phys. Rev. Lett. **78** (1997) 4335; *idem* *Jerusalem 1997, High energy physics* p. 883 [hep-ph/9712269]; Z. Nagy and Z. Trocsanyi, hep-ph/9708343; P. Abreu *et al.* (DELPHI Collab.), Phys. Lett. **B414** (1997) 410; R. Barate *et al.* (ALEPH Collab.), Z. Phys. **C96** (1997) 1.

[65] H. Baer, K. Cheung, and J.F. Gunion, Phys. Rev. **D59** (1999) 075002.

[66] D.M. Alde *et al.* (E772 Collab.), Phys. Rev. Lett. **66** 133, (1991); M.J. Leitch *et al.* (E866 Collab.), nucl-ex/9909007, Phys. Rev. Lett. in press.

[67] S. Dawson, E. Eichten, C. Quigg, Phys. Rev. **D31** (1985) 1581.

[68] The factor of $1/z$ associated with the fragmentation function was left out in Refs. [22, 29, 36, 38]. However, the factor was included in computing the numerical results given in these papers.

[69] J.A. Appel, Ann. Rev. Nucl. Part. Sci. **42** (1992) 367.